Department of Physics

Singlet-Mediated Triplet Exciton Transport

Vasil Vasilev

Supervisor:
Prof. Spiros S. Skourtis

May 2025

Abstract

Exciton transport in molecular wires underpins the performance of organic optoelectronic devices, yet the impact of intersystem crossing (ISC) and loss pathways on transport speed remains uncertain. This thesis develops a kinetic framework that couples singlet and triplet manifolds through spin-orbit–induced ISC while explicitly including exciton loss to the ground state. A $2N \times 2N$ transition–rate matrix is constructed for an N-site wire and its eigen-spectrum governs population evolution via the master equation.

It is shown that acceleration is maximised when (i) singlet hopping significantly exceeds triplet hopping and (ii) the singlet–triplet gap $\Delta E_{S_1T_1}$ is minimised, resulting in a higher reverse ISC rate. When the ISC rate equals or exceeds the singlet-to-singlet rate, further increases in ISC does not significantly reduce the transition time. Including loss channels introduces a pronounced N-dependence in longer wires as they suffer greater exciton loss to the ground singlet state S_0.

Complementary TD-DFT calculations on metal complexes were performed to evaluate the SOC-to-gap ratios. Strategies to push this ratio toward the targeted 0.1—via heavier metal centres and charge-transfer character—are proposed.

Overall, the work quantifies how singlet mediation, loss mechanisms, and molecular design parameters conspire to accelerate exciton delivery, providing design rules for molecular monomers.

Acknowledgements

This thesis would not have been possible without the guidance and support of several special individuals. I would like to express my deep gratitude to my thesis advisor, Professor Spiros Skourtis, for his invaluable guidance, insightful advice, and unwavering patience throughout the course of this project. I also thank all of my professors for their expertise and enthusiasm, which continually inspired me and shaped my understanding of physics.

I owe a heartfelt thanks to my family and friends, whose constant encouragement gave me the confidence to pursue my goals. Last but not least, I wish to thank a very special person for always being by my side.

Thank you all for making this journey challenging yet so beautiful.

Contents

Chapter 1

Introduction

1.1 Electron Transfer in Molecules

The electron transport process can be regarded as the spontaneous electron transition from an initial state to a final state of a molecular system. The initial and final states are spatially localized at the donor and acceptor parts of the system, respectively. In this section the basic concepts of molecular electron transfer reactions will be presented along with theories of the corresponding transfer rates.

1.1.1 Molecular Hamiltonian

We now examine a system consisting of N_{nuc} nuclei atoms and N_e electrons. The molecular Hamiltonian operator is given by:

$$\hat{H}_{\text{mol}} = \hat{T}_{\text{el}} + \hat{T}_{\text{nuc}} + \hat{V} \tag{1.1}$$

where, $\hat{T}_{\text{el}}$ describes the kinetic energy of the electrons, $\hat{T}_{\text{nuc}}$ describes the nuclear kinetic energy and $\hat{V}$ is the potential of the system.The kinetic energy of the electrons and the nuclei are given by:

$$\hat{T}_{\text{el}} = \sum_{i=1}^{Ne} \frac{p_i^2}{2m_e} \tag{1.2}$$

$$\hat{T}_{\text{nuc}} = \sum_{i=1}^{N\text{nuc}} \frac{P_i^2}{2M_i} \tag{1.3}$$

where, m_e is the mass of the electron and M_i is the mass of the i-th nucleus. The cartesian coordinates and momenta of the electrons and the nuclei are denoted by $(\vec{r}, \vec{p})$ and $(\vec{R}, \vec{P})$, respectively. The potential energy $\hat{V}$ describes the repulsion between electrons and between protons, as well as the Coulomb attraction between electrons and protons of the nuclei. It is therefore given by:

$$\begin{aligned} \hat{V} &= \hat{V}_{el-el} + \hat{V}_{n-n} + \hat{V}_{el-n} \\ \hat{V} &= \frac{1}{2}\sum_{i\neq j}^{N_e} \frac{e^2}{4\pi\epsilon_0 \mid \vec{r_i} - \vec{r_j} \mid} + \frac{1}{2}\sum_{i\neq j}^{N_{\text{nuc}}} \frac{Z_i Z_j\, e^2}{4\pi\epsilon_0 \mid \vec{R_i} - \vec{R_j} \mid} - \sum_{i}^{N_e}\sum_{j}^{N_{\text{nuc}}} \frac{Z_j\, e^2}{4\pi\epsilon_0 \mid \vec{r_i} - \vec{R_j} \mid} \end{aligned} \tag{1.4}$$

Z_i denotes the atomic number of the i-th nucleus.

Having constructed the molecular Hamiltonian $\hat{H}_{\text{mol}}$ we can write the Shrödinger equation of the multi-particle wavefunction $\Psi(\vec{r};\vec{R})$ as :

$$\hat{H}_{\text{mol}}\Psi(\vec{r};\vec{R}) = E\Psi(\vec{r};\vec{R}) \tag{1.5}$$

where, E is the energy of the system. The vectors $\vec{r} = (\vec{r}_1, \vec{r}_2, \cdots, \vec{r}_{N_e})$ and $\vec{R} = (\vec{R}_1, \vec{R}_2, \cdots, \vec{R}_{N_{\text{nuc}}})$ denote the Cartesian coordinates of the N_e electrons and N_{nuc}, respectively.

1.1.2 Born-Oppenheimer Approximation

Analytical solution of the Schrödinger equation is limited to one-electron system such as the hydrogen atom H, the helium ion He^+ or the hydrogen molecule ion H_2^+. Therefore, equation 1.5 cannot be solved for real molecules and approximations are required. The nuclei are much heavier than the orbiting electrons ($M_{\text{nuc}} \geq 2000\, m_e$) and therefore are much slower than the corresponding electrons. The Born-Oppenheimer approximation regards the nuclei as nearly static and we are left with solving the Schrödinger equation for the electrons. In this approximation the wavefunction $\Psi(\vec{r}; \vec{R})$ can be separated into two components:

$$\Psi^{\text{BO}} = \psi_e(\vec{r}; \vec{R})\psi_{\text{vib}}(\vec{R}) \tag{1.6}$$

where, $\psi_e(\vec{r}; \vec{R})$ is the electronic wavefunction for a given nuclear geometry and $\psi_{\text{vib}}(\vec{R})$ is the nuclear wavefunction.

Because of the slow motion of the nuclei compared to the electrons, we can ignore the nuclear kinetic energy operator. The Born-Oppenheimer Hamiltonian is therefore defined as:

$$\hat{H}^{\text{BO}}(\vec{r}; \vec{R}) = \hat{H}^{el}(\vec{r}; \vec{R}) + \hat{V}_{n-n} \tag{1.7}$$

where $\hat{H}^{el}$ is the electronic Hamiltonian defined as:

$$\hat{H}^{el}(\vec{r}; \vec{R}) = \hat{T}_{el} + \hat{V}_{el-n} + \hat{V}_{el-el} \tag{1.8}$$

The Born-Oppenheimer Hamiltonian $\hat{H}^{\text{BO}}$ consists of the electronic Hamiltonian $\hat{H}^{el}$ and the operator $\hat{V}_{n-n}$ describing the repulsion between nucleons. The electronic Hamiltonian describes the kinetic energy of the electrons, the Coulomb attraction between electrons and nuclei, and the Coulomb repulsion between electrons. Both, the Born-Oppenheimer and the electronic Hamiltonian, depend parametrically on the nuclear geometry $\vec{R}$.

Within the Born-Oppenheimer approximation the solution of the Schrödinger equation takes the following form:

$$\hat{H}^{\text{BO}}\Psi^{\text{BO}}(\vec{r}; \vec{R}) = E^{\text{BO}}\Psi^{\text{BO}}(\vec{r}; \vec{R}) \tag{1.9}$$

where, $E^{\text{BO}}(\vec{R})$ are the energies corresponding to the Born-Oppenheimer Hamiltonian for a given nuclear geometry.

Because of the slow motion of the nuclei relative to the electrons, we can consider the nuclei as classical particles whose motion is described by Newton's second law of motion. The Born-Oppenheimer energy E^{BO} defines a potential energy surface in the space of nuclear coordinates $\vec{R}$. Therefore, the total force exerted on the i-th nucleus from the N_e electrons and the remaining N_{nuc} nuclei atoms is:

$$\vec{F}_i = -\vec{\nabla}_{R_i} E^{\text{BO}}(\vec{R}) \tag{1.10}$$

1.2 Energy Transfer in Molecules

Energy transfer in contrast to singlet electron or hole transfer, requires both the transfer of an electron and a hole from an initial to a final electronic state. In energy transfer reactions, the initial excitation of the donor state forms a bound electron-hole pair called an exciton. This exciton is then transferred to a different location within the same molecule or to another molecule, forming the acceptor exciton.

We now consider a donor (D) and acceptor (A) molecule in immediate vicinity. The donor molecule is initially excited by an external laser pulse while the acceptor molecule remains in its ground electronic state. Through

electronic interactions between the donor and acceptor molecules an exciton is transfer from D to A. The Hamiltonian of the system is given by Equation (1.8).

1.2.1 Computing Donor–Acceptor Exciton Matrix Elements

We now consider a four-electron system that consists of donor and acceptor excitons. Each molecule is now described by two orbitals, the highest occupied molecular orbital (HOMO) denoted by ψ_D and ψ_A for the donor and acceptor excitons, respectively. Similarly, the lowest unoccupied molecular orbital (LUMO) is denoted by ψ_{D^*} and ψ_{A^*}.

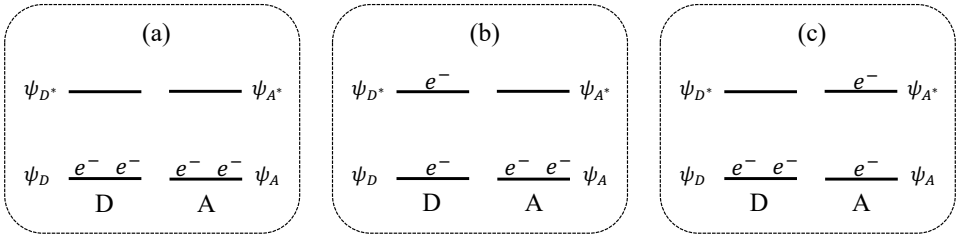

Figure 1.1: Schematic diagram of the electronic structures of a four-electron donor-acceptor exciton system. The wavefunctions of the donor exciton are denoted by ψ_D and ψ_{D^*} for the HOMO and LUMO orbitals, respectively. Similarly, the acceptor's exciton wavefunctions are denoted by ψ_A and ψ_{A^*}. (a) Illustrates the ground state configuration of the four-electron donor-acceptor system. (b) The donor molecule is in its excited state and the acceptor molecule in the ground electronic state. (c) Energy is transferred from D to A through electronic interactions, which results in the donor exciton to be in the ground state the acceptor one in its excited state.

The ground state configuration is illustrated in Figure 1.1. Moreover when the donor molecule is excited by an external laser pulse, an electron transitions from the HOMO (ψ_D) to the LUMO (ψ_{D^*}). Additionally, electronic interactions between the donor and acceptor molecules enable energy transfer from donor to acceptor, which results in the de-excitation of the donor molecule to its ground state the excitation of the corresponding acceptor molecule.

Due to electrons being fermions the wavefunction of the four-electron states has to be computed with the use of Slater determinants. The ground state Ψ_0 is computed using a singlet Slater determinant that is the anti-symmetric product of four spin orbitals. Each spin orbital is a product of a spatial orbital ψ and a spin function. The spin function is denoted by α if the electron has spin up, and β if it has spin down. As a results the ground electronic state is given by:

$$|\Psi_0\rangle = |\psi_D\alpha, \psi_D\beta, \psi_A\alpha, \psi_A\beta\rangle \tag{1.11}$$

The system illustrated in Figure 1.1b in which the exciton of the donor molecule is in its excited state is described by two possible Slater determinants. Each spatial orbital ψ_D and ψ_{D^*} can a either spin up or spin down and therefore the two possible excited states of this system are given by:

$$|\Psi_{D_1}\rangle = |\psi_D\alpha, \psi_{D^*}\beta, \psi_A\alpha, \psi_A\beta\rangle \tag{1.12a}$$
$$|\Psi_{D_2}\rangle = |\psi_{D^*}\alpha, \psi_D\beta, \psi_A\alpha, \psi_A\beta\rangle \tag{1.12b}$$

Similarly, when energy transfer takes place and the acceptor exciton is excited to ψ_{A^*} the two possible excited states of the system are given by:

$$|\Psi_{A_1}\rangle = |\psi_D\alpha, \psi_D\beta, \psi_A\alpha, \psi_{A^*}\beta\rangle \tag{1.13a}$$
$$|\Psi_{A_2}\rangle = |\psi_D\alpha, \psi_D\beta, \psi_{A^*}\alpha, \psi_A\beta\rangle \tag{1.13b}$$

The singlet and triplet states are computed by taking the appropriate linear combinations of these determiants. Specifically, the singlet states of the donor and acceptor molecules are given by:

$$|^1\Psi_D\rangle = \frac{1}{\sqrt{2}}\left(|\Psi_{D_1}\rangle + |\Psi_{D_2}\rangle\right) \tag{1.14}$$
$$|^1\Psi_A\rangle = \frac{1}{\sqrt{2}}\left(|\Psi_{A_1}\rangle + |\Psi_{A_2}\rangle\right) \tag{1.15}$$

and the triplet states:

$$|^3\Psi_D\rangle = \frac{1}{\sqrt{2}}\left(|\Psi_{D_1}\rangle - |\Psi_{D_2}\rangle\right) \tag{1.16}$$
$$|^3\Psi_A\rangle = \frac{1}{\sqrt{2}}\left(|\Psi_{A_1}\rangle - |\Psi_{A_2}\rangle\right) \tag{1.17}$$

Having defined the donor and acceptor singlet and triplet states of the four-electron system, we can proceed to the computation of the Hamiltonian matrix elements. Before we begin, it is useful to define the Hamiltonian $\hat{H}$ as:

$$\hat{H} = \hat{h}^{(1e)} + \hat{V}^{(2e)} \tag{1.18}$$

where, $\hat{h}^{(1e)}$ is the Hamiltonian describing the kinetic energy of the electrons $\hat{T}_{el}$ and the Coulomb attraction between the electrons and the nuclei $\hat{V}_{el-n}$. Subsequently, $\hat{V}^{(2e)}$ describes the repulsion between electrons. For obvious reasons, $\hat{h}^{(1e)}$ is called the one-electron operator and $\hat{V}^{(2e)}$ the two-electron operator.

By invoking the orthonormality of the spin and Slater rules for the singlet case we obtain the following matrix elements:

$$\langle^1\Psi_D|\,\hat{H}\,|^1\Psi_A\rangle = \langle^1\Psi_D|\,\hat{h}^{(1e)}\,|^1\Psi_A\rangle + \langle^1\Psi_D|\,\hat{V}^{(2e)}\,|^1\Psi_A\rangle\,, \tag{1.19a}$$
$$\langle^1\Psi_D|\,\hat{h}^{(1e)}\,|^1\Psi_A\rangle = V^e_{D^*A^*}S_{DA} - V^h_{DA}S_{D^*A^*}, \tag{1.19b}$$
$$\langle^1\Psi_D|\,\hat{V}^{(2e)}\,|^1\Psi_A\rangle = 2\,(\psi_D\psi_{D^*} \mid \psi_A\psi_{A^*}) - (\psi_{D^*}\psi_{A^*} \mid \psi_D\psi_A) \tag{1.19c}$$

and for the triplet case:

$$\langle^1\Psi_D|\,\hat{H}\,|^1\Psi_A\rangle = \langle^1\Psi_D|\,\hat{h}^{(1e)}\,|^1\Psi_A\rangle + \langle^1\Psi_D|\,\hat{V}^{(2e)}\,|^1\Psi_A\rangle\,, \tag{1.20a}$$
$$\langle^1\Psi_D|\,\hat{h}^{(1e)}\,|^1\Psi_A\rangle = V^e_{D^*A^*}S_{DA} - V^h_{DA}S_{D^*A^*}, \tag{1.20b}$$
$$\langle^1\Psi_D|\,\hat{V}^{(2e)}\,|^1\Psi_A\rangle = -\,(\psi_{D^*}\psi_{A^*} \mid \psi_D\psi_A) \tag{1.20c}$$

where, $V^e_{D^*A*}$ is the electron transfer (ET) coupling matrix element between the excited donor and acceptor molecules ψ_{D^*} and ψ_{A^*}, respectively. V^h_{DA} is the corresponding hole transfer matrix element between the ground ψ_D and ψ_A orbitals. $S_{D^*A^*}$ and S_{DA} are the overlap matrix elements between the LUMO and HOMO orbitals, respectively. The Coulomb matrix elements is expressed by the following two electron integrals:

$$(\psi_D\psi_{D^*} \mid \psi_A\psi_{A^*}) = \frac{1}{4\pi\epsilon_0}\int d^3r_1 d^3r_2\ \psi_D(\vec{r}_1)\psi_{D^*}(\vec{r}_1)\frac{1}{\mid \vec{r}_1 - \vec{r}_2 \mid}\psi_A(\vec{r}_2)\psi_{A^*}(\vec{r}_2) \tag{1.21a}$$
$$(\psi_{D^*}\psi_{A^*} \mid \psi_D\psi_A) = \frac{1}{4\pi\epsilon_0}\int d^3r_1 d^3r_2\ \psi_{D^*}(\vec{r}_1)\psi_{A^*}(\vec{r}_1)\frac{1}{\mid \vec{r}_1 - \vec{r}_2 \mid}\psi_D(\vec{r}_2)\psi_A(\vec{r}_2) \tag{1.21b}$$

The first two-electron integral expressed by Equation (1.21a) describes the classical Coulomb repulsion between charge densities localized at the donor and acceptor molecules, respectively. The second two-electron integral described by Equation (1.29) expresses the exchange integral and cannot be explain classically. The term $\psi_{D^*}(\vec{r}_1)\psi_{A^*}(\vec{r}_1)$ is the overlap density between the LUMO of the donor and acceptor molecular orbitals. Similarly, $\psi_D(\vec{r}_2)\psi_A(\vec{r}_2)$ is the overlap density of the HOMO for the donor and acceptor molecular orbitals.

The matrix element corresponding to the one-electron Hamiltonian $\hat{h}^{(1e)}$ is the same for both singlet and triplet states. In contrast, the contribution from the Coulomb repulsion is absent for the triplet case and as a result the two-electron contribution differs for singlet and triplet states. In Equation (1.19c), the dominant contribution is due to the Coulomb interaction which is characteristic of Förster energy transfer mechanism for singlet states. On the other hand, for the triplet case only the exchange contribution is present and this is historically associated with the energy transfer coupling of the Dexter mechanism.

1.2.2 Distance Dependence of the Two-Electron Integrals

The Förster and Dexter energy transfer mechanisms can be derived by examining the corresponding distance dependence of the Coulomb and exchange integrals. More precisely, since the Förster EnT mechanism is associated with the dominant Coulomb interaction integral of the two-electron singlet matrix element $\langle {}^1\Psi_D | \hat{V}^{(2e)} | {}^1\Psi_A \rangle$, one can derive the distance dependence from the Coulomb integral. Similarly, by examining the exchange integral that is associated with the Dexter EnT mechanism, we can derive the Dexter distance dependence.

The one-electron contributions, that are the same for both the singlet and triplet states, demonstrate an exponential donor-acceptor distance (R_{DA}) decay behavior.

We now consider the Coulomb integral $(\psi_D\psi_{D^*} \mid \psi_A\psi_{A^*})$ that is only present in the singlet case. We can define the donor and acceptor charge densities as $\rho_{DD^*}(\vec{r}_1) = -e\psi_D(\vec{r}_1)\psi_{D^*}(\vec{r}_1)$ and $\rho_{AA^*}(\vec{r}_2) = -e\psi_A(\vec{r}_2)\psi_{A^*}(\vec{r}_2)$, respectively. Therefore the Coulomb integral can be written as:

$$(\psi_D\psi_{D^*} \mid \psi_A\psi_{A^*}) = \frac{1}{4\pi\epsilon_0}\int d^3r_1 d^3r_2 \; \rho_{DD^*}(\vec{r}_1)\frac{1}{\mid \vec{r}_1 - \vec{r}_2 \mid}\rho_{AA^*}(\vec{r}_2) \tag{1.22}$$

If the spatial extent of the donor and acceptor charge densities is much smaller than the D-A separation we can expand the Coulomb interaction described by Equation (1.22), in a multipole series with respect to the center of mass displacements. The center of mass for the donor molecule is defined as $\delta\vec{r}_D = \vec{r}_1 - \vec{R}_D$, and for the acceptor molecule as $\delta\vec{r}_A = \vec{r}_2 - \vec{R}_A$. Additionally, the center of mass for the donor-acceptor molecules is $\vec{R}_{DA} = \vec{R}_A - \vec{R}_D$. Moreover, we define the donor and acceptor transition dipole moments matrix elements as:

$$\vec{\mu}_{DD^*} = \int d^3r_1 \rho_{DD^*}(\vec{r}_1)\delta\vec{r}_D \tag{1.23a}$$

$$\vec{\mu}_{AA^*} = \int d^3r_2 \rho_{AA^*}(\vec{r}_2)\delta\vec{r}_A \tag{1.23b}$$

The relative distance $\vec{r}_{12}$ between the charge densities localized at the donor and acceptor molecule can be written as:

$$\begin{aligned} \vec{r}_{12} \; &= \mid \vec{r}_2 - \vec{r}_1 \mid \; = \mid \delta\vec{r}_A + \vec{R}_A - \delta\vec{r}_D - \vec{R}_D \mid \\ &\Rightarrow \vec{r}_{12} = \mid \delta\vec{r}_A + \vec{R}_{DA} - \delta\vec{r}_b \mid \end{aligned} \tag{1.24}$$

where, $\mid \delta\vec{r}_D \mid$ and $\mid \delta\vec{r}_D \mid$ are much smaller than $\mid \vec{R}_{DA} \mid$. If we perform a Taylor expansion for $\mid \delta\vec{r}_D \mid / \mid \vec{R}_{DA} \mid \ll 1$, the term $1/r_{12}$ becomes:

$$\frac{1}{r_{12}} = \frac{1}{\mid \delta\vec{r}_A + \vec{R}_{DA} - \delta\vec{r}_b \mid} \approx \frac{1}{\mid \delta\vec{r}_A + \vec{R}_A \mid} + \frac{\left(\delta\vec{r}_A + \vec{R}_A\right)}{\mid \delta\vec{r}_A + \vec{R}_A \mid^3} \cdot \delta\vec{r}_D \tag{1.25}$$

Subsequently, by performing a Taylor expansion for $\mid \delta\vec{r}_A \mid / \mid \vec{R}_{DA} \mid \ll 1$, on the components of Equation (1.25) we get:

$$\frac{1}{\mid \delta\vec{r}_A + \vec{R}_A \mid} \approx \frac{1}{\mid \vec{R}_{DA} \mid} - \frac{\vec{R}_{DA} \cdot \delta\vec{r}_A}{\mid \vec{R}_{DA} \mid^3}, \tag{1.26a}$$

$$\frac{\left(\delta\vec{r}_A + \vec{R}_{DA}\right)}{|\delta\vec{r}_A + \vec{R}_{DA}|^3} \cdot \delta\vec{r}_D \;\approx\; \frac{\vec{R}_{DA}\cdot\delta\vec{r}_D}{|\vec{R}_{DA}|^3} \;+\; \frac{\delta\vec{r}_D\cdot\delta\vec{r}_A}{|\vec{R}_{DA}|^3} \;-\; 3\,\frac{\left(\vec{R}_{DA}\cdot\delta\vec{r}_D\right)\left(\vec{R}_{DA}\cdot\delta\vec{r}_A\right)}{|\vec{R}_{DA}|^5} \tag{1.26b}$$

Finally, the $1/r_{12}$ term becomes:

$$\frac{1}{r_{12}} \approx \frac{1}{\mid \vec{R}_{DA} \mid} - \frac{\vec{R}_{DA} \cdot \delta\vec{r}_A}{\mid \vec{R}_{DA} \mid^3} + \frac{\vec{R}_{DA}\cdot\delta\vec{r}_D}{|\vec{R}_{DA}|^3} \;+\; \frac{\delta\vec{r}_D\cdot\delta\vec{r}_A}{|\vec{R}_{DA}|^3} \;-\; 3\,\frac{\left(\vec{R}_{DA}\cdot\delta\vec{r}_D\right)\left(\vec{R}_{DA}\cdot\delta\vec{r}_A\right)}{|\vec{R}_{DA}|^5} \tag{1.27}$$

Since the molecular orbitals are orthonormal to each other, that is, $\int d^3r_1 \rho_{DD^*}(\vec{r}_1) = 0$ and $\int d^3r_2 \rho_{AA^*}(\vec{r}_2) = 0$, the first three terms of Equation (1.27) do not contribute to the overall Coulomb interaction. Therefore the final expression of the Coulomb interaction takes the following form:

$$(\psi_D\psi_{D^*} \mid \psi_A\psi_A^*) = \frac{1}{4\pi\epsilon_0}\left(\frac{\vec{\mu}_{DD^*}\;\vec{\mu}_{AA^*} - 3\left(\vec{\mu}_{DD^*}\;\hat{R}_{DA}\right)\left(\vec{\mu}_{AA^*}\;\hat{R}_{DA}\right)}{\mid \vec{R}_{DA} \mid^3}\right) \tag{1.28}$$

where $\hat{R}_{DA}$ is a unit vector along the direction of the position vector that connects the donor and acceptor molecules.

It is evident from Equation (1.28) that the Coulomb interaction integral is approximated by the dipole-dipole interaction, which is the important interaction between neutral donor and acceptor molecules. The dipole-dipole interaction decays as $1/R_{DA}^3$ and depends on the individual D and A transition dipole moments.

The exchange integral from Equation (1.29) only contributes to the energy transfer coupling for short distances between donor-acceptor separations. This short range nature arises due to the strong dependence on the overlap between the donor and acceptor molecular orbitals. Therefore, the exchange interaction may be rewritten as:

$$(\psi_{D^*}\psi_{A^*} \mid \psi_D\psi_A) = \frac{1}{4\pi\epsilon_0}\int d^3r_1 d^3r_2 \; S^e_{D^*A^*}(\vec{r}_1)\frac{1}{\mid \vec{r}_1 - \vec{r}_2 \mid}S^h_{DA}(\vec{r}_2) \tag{1.29}$$

where $S^e_{D^*A^*}(\vec{r}_1)$ is the overlap density between the LUMO of the donor and acceptor molecular orbitals. Similarly, $S^h_{DA}(\vec{r}_2)$ is the overlap density between the HOMO of the donor and acceptor molecular orbitals. The magnitude of the orbital overlap decays exponentially, that is, $S^e_{D^*A^*}(\vec{r}_1) \propto e^{-\beta_{el}R_{DA}}$ and $S^h_{DA}(\vec{r}_2) \propto e^{-\beta_{\text{hole}}R_{DA}}$ for the electrons and holes, respectively. β_{el} and β_{hole} denote the electron and hole tunneling decay constants. Because of the exponential decrease of the orbital overlap, the contribution of the exchange interaction for large distances between donor and acceptor molecules is negligible and can be ignored. Therefore, if R_{DA} is large enough only the Coulomb term $(\psi_D\psi_{D^*} \mid \psi_A\psi_{A^*})$ contributes to singlet energy transfer.

1.2.3 Förster Energy Transfer Mechanism

The Förster energy transfer mechanism refers to the singlet exciton transfer between the donor and acceptor molecules when the distance between them is sufficiently larger than their molecular sizes. Therefore physical contact between the molecules is not required for the energy transfer process to take place.

In Equations (1.19a) to (1.19c), Förster theory identifies the Coulomb interaction $2\left(\psi_D\psi_{D^*} \mid \psi_A\psi_{A^*}\right)$ as the dominant contribution. We showed previously that the Coulomb integral is approximated as a dipole-dipole interaction, therefore we can express the singlet Hamiltonian matrix element as:

$$V_S^{\text{Förster}} \equiv \langle {}^1\Psi_D | \hat{H} | {}^1\Psi_A \rangle \approx 2\left(\psi_D\psi_{D^*} \mid \psi_A\psi_{A^*}\right)$$
$$V_S^{\text{Förster}} = \frac{1}{4\pi\epsilon_0}\left(\frac{\vec{\mu}_{DD^*}\ \vec{\mu}_{AA^*} - 3\left(\vec{\mu}_{DD^*}\ \hat{R}_{DA}\right)\left(\vec{\mu}_{AA^*}\ \hat{R}_{DA}\right)}{\mid \vec{R}_{DA} \mid^3}\right) \tag{1.30}$$

Through the dipole-dipole interaction, the initial excitation energy of the donor molecule is transferred to the acceptor molecule. We can also interpret this as a singlet exciton state initially localized in the donor molecule being transferred to the acceptor molecule.

Figure 1.2 illustrates the Förster energy transfer mechanism between a donor and acceptor molecule. Initially, the donor molecule is in a singlet exciton state. Dipole-dipole Coulomb interactions trigger energy transfer between the donor and acceptor molecules. This results in the de-excitation of the donor molecule and the excitation of the acceptor one, that is also now described by a singlet exciton state.

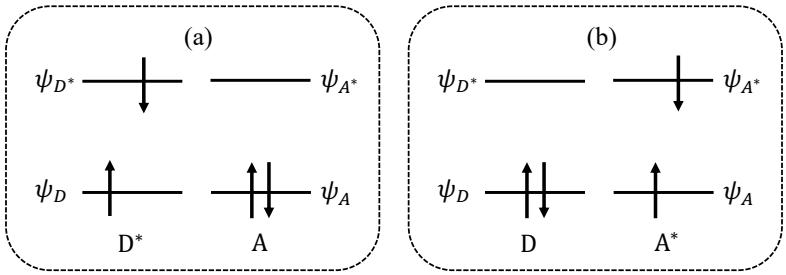

Figure 1.2: Schematic diagram of the Förster energy transfer mechanism. (a) The donor molecule is initially excited and can be described by a singlet exciton state. Dipole-dipole Coulomb interactions cause energy transfer from the donor molecule to the acceptor one. (b) After energy transfer between the donor and acceptor molecules, the donor molecule de-excites and is its ground state while the acceptor molecule is in its excited state, described again by a singlet exciton state.

The Förster energy transfer coupling $V_S^{\text{Förster}}$ in Equation (1.30) decays as $1/R_{DA}^3$. This distance dependence enables EnT to occur efficiently even in large separation distances between the donor and acceptor molecules if appropriate conditions are satisfied. More precisely, good spectral overlap and desirable energy transfer enhanced orientation of the transition dipole moments $\vec{\mu}_{DD^*}$ and $\vec{\mu}_{AA^*}$ are needed for efficient donor-acceptor energy transfer. The one-electron $\langle {}^1\Psi_D | \hat{h}^{(1e)} | {}^1\Psi_A \rangle$ contribution as well as the exchange integral $\left(\psi_{D^*}\psi_{A^*} \mid \psi_D\psi_A\right)$ are ignored by the Förster mechanism because of their exponential distance dependence.

1.2.4 Dexter Energy Transfer Mechanism

We now examine the Dexter energy transfer mechanism that describes triplet to triplet energy transfer via the two-electron exchange interaction between the donor and acceptor molecules. This is a short range mechanism that requires physical contact between the two molecules for the overlap between the donor and acceptor molecules to be significant. Alternatively, the donor and acceptor molecules can be connected through other molecules or a bond that will act as an intermediate bridge for the donor-acceptor energy transfer process to occur.

Figure 1.3 illustrates schematically the Dexter energy transfer mechanism that involves the transfer from a triplet donor state to a triplet acceptor state. The donor molecule is initially excited and described by a

triplet exciton state. The exchange interaction ($\psi_{D^*}\psi_{A^*} \mid \psi_D\psi_A$) enables the simultaneous electron transfer from the donor LUMO (ψ_{D^*}) to the acceptor LUMO (ψ_{A^*}) and hole transfer from the donor and acceptor HOMO orbitals, ψ_D and ψ_A respectively. As a result, the Dexter donor to acceptor energy transfer can be regarded as a double particle transfer initiated through the exchange interaction among particles. Therefore, the double particle exchange between HOMO and LUMO orbitals of the donor and acceptor molecules results in the transfer of the triplet exciton initially residing at the donor molecule to the acceptor one.

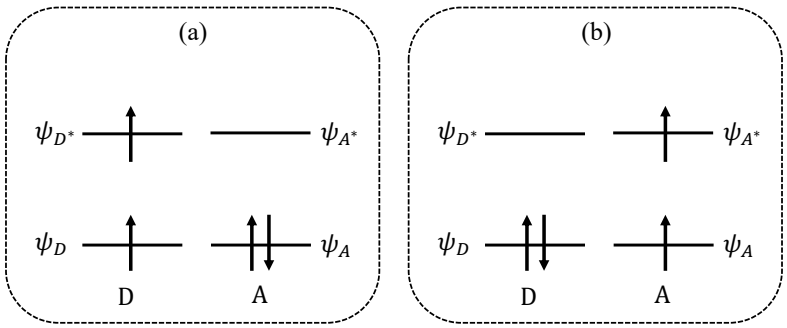

Figure 1.3: Schematic diagram of Dexter energy transfer mechanism. (a) The donor molecule is initially excited and described by a triplet exciton state. Exchange interaction between the two molecules enable energy transfer from the donor to the acceptor molecule. (b) The initial excitation energy of the donor molecule is transferred to the acceptor molecule. This leads to the de-excitation of the donor molecule to the ground state and the excitation of the acceptor molecule that is also described by a triplet exciton state.

The Dexter triplet to triplet energy transfer includes the one-electron contributions. Because the term "one-electron" might be misleading due to holes also being included, we will refer to this contribution as one-particle contribution. The coupling of the Dexter EnT is given by:

$$V_{tr}^{\text{Dexter}} \equiv \langle {}^3\Psi_D | \hat{H} | {}^3\Psi_A \rangle = \langle {}^3\Psi_D | \hat{h}^{(1e)} | {}^3\Psi_A \rangle + \langle {}^3\Psi_D | \hat{V}^{(2e)} | {}^3\Psi_A \rangle$$
$$V_{tr}^{\text{Dexter}} \approx 2\frac{(V_{D^*A^*}^e) \times \left(V_{DA}^h\right)}{\Delta E_{CT}} - (\psi_{D^*}\psi_{A^*} \mid \psi_D\psi_A) \tag{1.31}$$

where $\Delta E_{CT}$is the energy difference between the triplet donor and acceptor charge transfer configuration. In this configuration the hole occupies the ground donor or acceptor state while the electron occupies the corresponding excited state. $V_{D^*A^*}^e$ is the electron transfer coupling matrix element between the excited donor and acceptor molecular orbitals. Similarly, V_{DA}^h is the hole transfer coupling matrix element between the ground donor and acceptor orbitals. Historically, in the Dexter energy transfer mechanism only the exchange interaction was taken into consideration. However, the one-particle term can be comparable to the exchange term and therefore it must be included in the Dexter interaction.

Both the single particle coupling matrix elements ($V_{D^*A^*}^e, V_{DA}^h$), and the exchange interaction integral demonstrate an exponential dependence on the distance between the donor and acceptor molecules. Therefore, the overall Dexter triplet-to-triplet energy transfer coupling has approximately an exponential dependence on the donor-acceptor distance that is approximately equal to the sum of the electron and hole decay constants ($\beta_{el}, \beta_{\text{hole}}$). This exponential dependence of the Dexter coupling makes triplet-to-triplet energy transfer particular sensitive to the molecular structure and the energetics.

1.2.5 Energy Transfer Rate Between Donor and Acceptor Molecules

In the nonadiabatic limit, energy transfer can be described by Fermi's golden rule. In the golden rule approximation the energy transfer rate is given by:

$$k_{DA} = \frac{2\pi}{\hbar} \mid V_{DA} \mid^2 \rho_{FC} \tag{1.32}$$

where $\mid V_{DA} \mid$ is the donor-acceptor electronic coupling given by the Hamiltonian matrix elements for singlet or triplet excitons and ρ_{FC} is the Franck-Condon factor for the donor and acceptor exciton energies.

The Franck-Condon factor ρ_{FC}, can be formulated both in its classical and quantum mechanical representation. The spectral overlap of the donor emission $F_{(D^* \to D)}$ spectrum with the acceptor absorption $A_{(A \to A^*)}$ spectrum can be used to approximate the Franck-Condon factor in energy transfer reactions. Thus, we can write the Franck-Condon factor as:

$$\rho_{FC} = \int_{-\infty}^{+\infty} dE \; F_{(D^* \to D)}(E) \times A_{(A \to A^*)}(E) \tag{1.33}$$

where the emission and absorption spectrums are given by:

$$F_{(D^* \to D)}(E) = \frac{1}{\sqrt{4\pi k_B T \lambda_{D^* D}}} exp\left[- \left(E - \Delta E_{D^* D + \lambda_{D^* D}}\right)^2 / 4\lambda_{D^* D} k_B T \right] \tag{1.34a}$$

$$A_{(A \to A^*)}(E) = \frac{1}{\sqrt{4\pi k_B T \lambda_{A A^*}}} exp\left[- \left(E - \Delta E_{A A^* + \lambda_{A A^*}}\right)^2 / 4\lambda_{A A^*} k_B T \right] \tag{1.34b}$$

Equations (1.34a) and (1.34b) correlate the emission and absorption spectra, which are experimental observables, to complicated theoretical descriptions of nuclear overlap factors and nuclear reorganization energies included in the Franck-Condon factor.

1.3 Molecular Spin–Orbit Coupling Effects

While we typically picture atoms as a stationary nucleus surrounded by orbiting electrons, in the electron's rest frame, the nucleus appears to orbit the electron. The magnetic moment of an electron arises from its spin and orbital angular momentum, $\vec{\mu}_s$ and $\vec{\mu}_l$, respectively. The spin magnetic moment $\vec{\mu}_s$ of the electron is given by:

$$\vec{\mu}_s = -\frac{g_s e}{2m_e} \vec{S} \tag{1.35}$$

where g_s is the electron's spin g-factor. Similarly, the orbital magnetic moment is given by:

$$\vec{\mu}_l = -\frac{g_l e}{2m_e} \vec{L} \tag{1.36}$$

where g_l is the electron's orbital g-factor.
The spin and orbital g-factors are given approximately by:

$$g_s \approx 2 \tag{1.37a}$$

$$g_l = 1 \tag{1.37b}$$

In the electron's frame the interaction between the spin magnetic moment of the electron and the magnetic field generated by the orbiting proton is referred to as the spin-orbit coupling (SOC). Because of the mixing of the orbital angular momentum with the spin angular momentum, transition between triplet and singlet states $T_i \leftrightarrow S_i$ are allowed via intersystem crossing (ISC). When the electron is at rest, the motion of a proton gives rise to a magnetic field $\vec{B}_{\text{nuc}}$ that is given by:

$$\vec{B}_{\text{nuc}} = \frac{\vec{E}_{\text{nuc}} \times \vec{v}}{c^2} \tag{1.38}$$

where c is the speed of light in vacuum and $\vec{E}_{\text{nuc}}$ is the electric field produced by the nucleus. Using $\vec{E}_{\text{nuc}} = -\vec{\nabla} V$ and $\vec{p} = m_e \vec{v}$, Equation (1.38) can be expressed as:

$$\vec{B}_{\text{nuc}} = -\frac{1}{m_e c^2}\vec{\nabla}V \times \vec{p} \tag{1.39}$$

For this system, the spin-orbit coupling Hamiltonian is given by:

$$\hat{H}^{\text{SOC}} = -\hat{\mu}_s \cdot \hat{B}_{\text{nuc}} \tag{1.40}$$

Using Equations (1.35) and (1.39), Equation (1.40) becomes:

$$\hat{H}^{\text{SOC}} = \frac{e}{2m_e^2 c^2}\left(\vec{\nabla}V \times \vec{p}\right) \cdot \vec{S} \tag{1.41}$$

where the factor $\frac{1}{2}$ arises as a relativistic correction from the Dirac equation.

For a hydrogen-like ion with Z protons, the electric potential is $V = -\frac{Ze^2}{r}$. Its gradient is given by $\vec{\nabla}V = \frac{Ze^2}{r^3}\vec{r}$. We can thus write the SOC Hamiltonian as:

$$\hat{H}^{\text{SOC}} = \frac{Ze^2}{2m_e^2 c^2}\frac{1}{r^3}(\vec{r} \times \vec{p}) \cdot \vec{S} \Rightarrow \hat{H}^{\text{SOC}} = \frac{Ze^2}{2m_e^2 c^2}\frac{1}{r^3}\vec{L} \cdot \vec{S} \tag{1.42}$$

where $\vec{L} = \vec{r} \times \vec{p}$ is the angular momentum of the electron.

1.3.1 The spin-orbit coupling Hamiltonian in molecules

For a molecular system consisting of N atoms and N_e electrons the SOC Hamiltonian is approximately given by:

$$\hat{H}^{\text{SOC}} = \hat{H}_{1e}^{\text{SOC}} + \hat{H}_{2e}^{\text{SOC}} \tag{1.43}$$

where the one-electron term $\hat{H}_{1e}^{\text{SOC}}$ is given by:

$$\hat{H}_{1e}^{\text{SOC}} \sum_{i=1}^{N_e}\sum_{K=1}^{N} \xi(r_{iK})\vec{L}_{iK} \times \vec{S}_{iK} \tag{1.44}$$

and the two-electron term $\hat{H}_{2e}^{\text{SOC}}$ is given by:

$$\begin{aligned}\hat{H}_{2e}^{\text{SOC}} = &-\frac{1}{2m_e^2 c^2}\sum_{i=1}^{N_e}\sum_{j\neq i}^{N_e}\frac{1}{r_{ij}^3}(\vec{p}_i \times \vec{r}_{ij}) \cdot \vec{S}_i \\ &+\frac{1}{m_e^2 c^2}\sum_{i=1}^{N_e}\sum_{j\neq i}^{N_e}\frac{1}{r_{ij}^3}(\vec{p}_j \times \vec{r}_{ij}) \cdot \vec{S}_i\end{aligned} \tag{1.45}$$

The atomic center is described by the variable K, while the electrons are described by the variables i and j. The one-electron term describes interactions between the spin magnetic moment of the i-th electron with the orbital magnetic moment arising from its orbit motion inside the field of the nucleus K. The i-th electron can either belong to the atom K or to a different atom. The two-electron contribution describes two types of interactions. Firstly, interaction related to the coupling between the spin magnetic moment and the orbital magnetic moment of the i-th electron caused by the electric field generated by the electrons j. Secondly, it describes interactions related to the coupling between the spin magnetic moment of the i-th electron and the orbital magnetic moment of the j-th electron caused by magnetic fields that arise because of the relative orbital motion of the two electrons. The one-electron term is proportional to Z^4.

Chapter 2

Exciton Transport

2.1 System Model

The system under study consists of N molecules arranged in a linear molecular wire (see Figure 2.1). Each molecule can exist in one of two possible excited states: a triplet state T_i with energy E_T, or a singlet state S_i with energy E_S. For convenience, we set the reference energy level such that $E_T = 0$. The exciton can move along the wire via transitions between adjacent triplet states ($T_i \leftrightarrow T_{i+1}$) and adjacent singlet states ($S_i \leftrightarrow S_{i+1}$), as well as through intersystem crossing (ISC) between singlet and triplet states at the same molecular site ($S_i \leftrightarrow T_i$). The exciton moves in discrete steps along the wire, and transitions occur according to well-defined forward and reverse rates. We define forward transition rates as those describing exciton transport in the rightward direction, from molecule i to molecule $i+1$, while reverse transition rates correspond to transitions in the opposite direction, from $i+1$ to i. Forward transition rates between adjacent triplet states are denoted by $K_{T_i,\, T_{i\pm1}}$, indicating a transition from triplet state T_i to one of the neighboring triplet state T_{i+1} or T_{i-1}. Similarly, transition rates between adjacent singlet states are denoted by $K_{S_i,\, S_{i\pm1}}$ describing a transition from the singlet state S_i to one of the singlet states S_{i-1} or S_{i+1}. We define the forward ISC rate, K_{S_i,T_i}, as the rate of transitions from the excited singlet state S_i to the corresponding triplet state T_i of the same molecule. The reverse ISC rate (rISC), K_{T_i,S_i}, describes the rate of transitions from $T_i \rightarrow S_i$.

Although it may seem intuitive, we explicitly impose boundary conditions on the system to ensure that the first molecule's excited triplet and singlet states, (T_1, S_1), can only transition to states belonging to the second molecule, (T_2, S_2), since there is no molecule to their left. Similarly, the excited states of the last molecule, (T_N, S_N), can only transition to states of the preceding molecule, (T_{N-1}, S_{N-1}).

One can think of the molecular wire as a system with two distinct energy levels, E_S and E_T, in thermal contact with a much larger reservoir at a well-defined temperature T. Each excited singlet or triplet state corresponds to a microstate of the system. Since each energy level consists of N microstates, the total number of microstates is $2N$.

If we isolate the triplet channel from the rest of the system, the triplet states T_i (all with energy $E_T = 0$) would be equally probable. Now, however, we consider the interaction between triplet and singlet states, where all $2N$ microstates are in contact with a thermal reservoir at a fixed temperature T. Assuming thermal equilibrium, we aim to determine the probability distribution over the $2N$ microstates, describing the likelihood of the exciton occupying a particular triplet or singlet excited state.

Each excited triplet or singlet state is not an isolated system, but the excited states and the reservoir together do make an isolated system, and the probability of finding this combined system in one of its microstates depends on the energy of that particular microstate.

The probability then, of the system being in state i is given by [5]

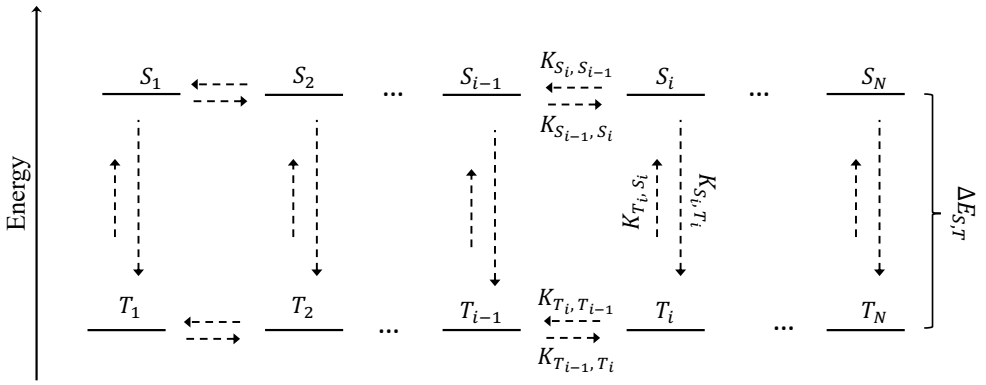

Figure 2.1: Schematic diagram of the molecular wire consisting of N excited singlet and triplet states. Transition rates between excited states are represented by dashed arrows. When two opposing arrows differ in length, it indicates that the forward and reverse transition rates are unequal. In contrast, equal-length arrows signify that the corresponding transition rates are equal.

$$P_i = \frac{1}{Z}\, e^{-E_i/k_B T} \tag{2.1}$$

where, E_i is the energy of the state i, k_B is the Boltzmann constant, and T is the temperature of the given state. $k_B T$ has dimensions of energy and is often referred to as thermal energy. In statistical mechanics Equation (2.1) is sometimes called the Boltzmann distribution or the canonical distribution and is regarded as the most useful formula in all of statistical mechanics. The exponential factor is called a Boltzmann factor, and the constant $1/Z$ is just a constant of proportionality that converts a Boltzmann factor into a probability.

If we examine the excited triplet states T_i, all of which have energy of $E_T = 0$ we can see from Equation (2.1) that the probability of finding the exciton in one of these states T_i is just $1/Z$, and it the same for all the other triplet states. Moreover, if we examine the excited singlet states, which have positive energy ($E_S \geq 0$), we can clearly see that if the singlet states have energy much greater than the thermal energy ($E_S \gg k_B T$) the probability of the exciton occupying one of these states will be negligible due to the exponential Boltzmann factor. If on the other hand $E_S \leq k_B T$, the probability will be closer to $1/Z$.

The partition function Z is determined by ensuring that the total probability of the system being in one of the $2N$ microstates sums to unity.

$$1 = \sum_i P_i = \sum_i \frac{1}{Z} e^{-E_i/k_B T} = \frac{1}{Z} \sum_i e^{-E_i/k_B T} \tag{2.2}$$

Solving for Z therefore gives

$$Z = \sum_i e^{-E_i/k_B T} \tag{2.3}$$

The quantity Z is called the partition function, and is nothing more than the sum of all the Boltzmann factors.

Since our system is composed of $2N$ microstates distributed evenly on two distinct energy levels $E_T = 0$ and E_S, an alternate definition to Equation (2.3) where the sum is over the energy levels rather than states would be more appropriate. In this alternate definition, the partition function then becomes [1]

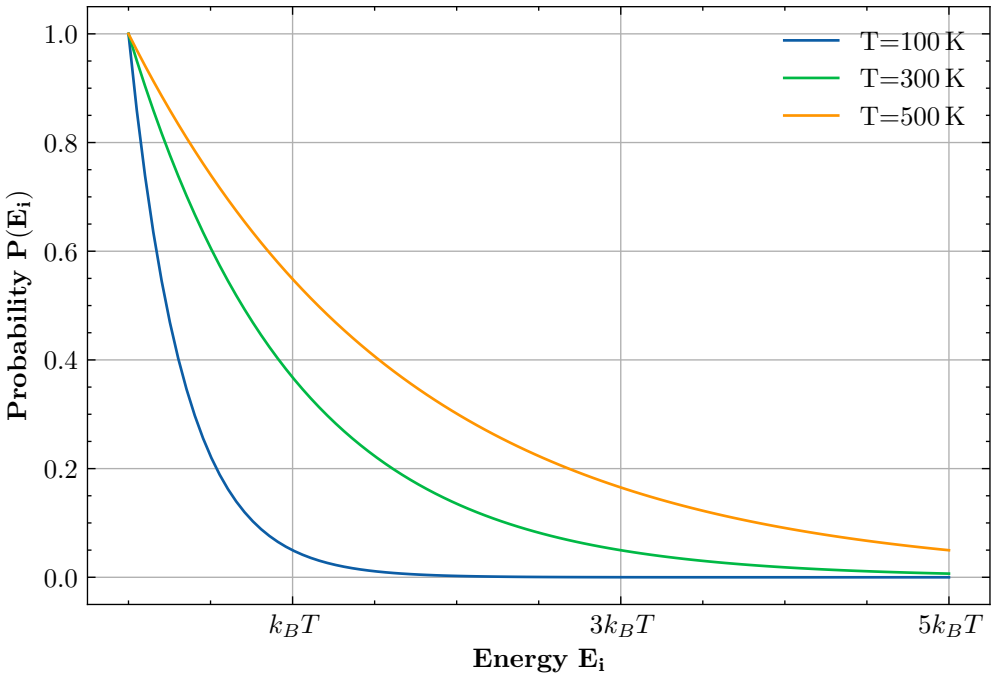

Figure 2.2: Probability distribution $P(E_i)$ of an exciton occupying a state with energy E_i, shown for three different values of temperature. As expected from the Boltzmann distribution, higher temperatures increase the probability of occupying higher-energy states.

$$Z = \sum_{E_i} g(E_i)\ e^{-\beta E_i} \tag{2.4}$$

where $g(E_i)$ is the degeneracy of the energy level and we have substituted the thermal energy for the thermodynamic beta $\beta = \frac{1}{k_B T}$ for simplicity. There are N excited triplet states all with energy equal to E_T, and similarly N excited singlet states with energy E_S. Thus, the degeneracy is equal to N for both energy levels and since it is independent of the energy, $g(E_i)$ can be taken out of the sum. Equation (2.4) then becomes

$$Z = N \sum_{E_i} e^{-\beta E_i} \tag{2.5}$$

When the reference energy level is such that $E_T = 0$, Equation (2.5) is further simplified and is given by:

$$Z = N\ (1 + e^{-E_S/k_B T}) \tag{2.6}$$

With $E_T = 0$, the partition function Z depends only on the energy of the excited singlet states E_S, the temperature T, and the number of molecules N.

Referring to the partition function as a proportionality constant might be misleading. It is a "constant" in the sense that it does not depend on any particular state i, but it does depend on temperature. To understand the temperature dependence further, let's consider again the probability of locating the exciton in one of the excited triplet states. The Boltzmann factors of all the triplet states is equal to 1, and the Boltzmann factors for states with energy $E_i \geq 0$ are less than 1, by a little or a lot, depending on the probabilities of the associated states. At very low temperatures, $Z \approx N$, since all the excited singlet states have very small Boltzmann factors. At higher temperatures Z will be much larger due to the non negligible contribution of the excited singlet states.

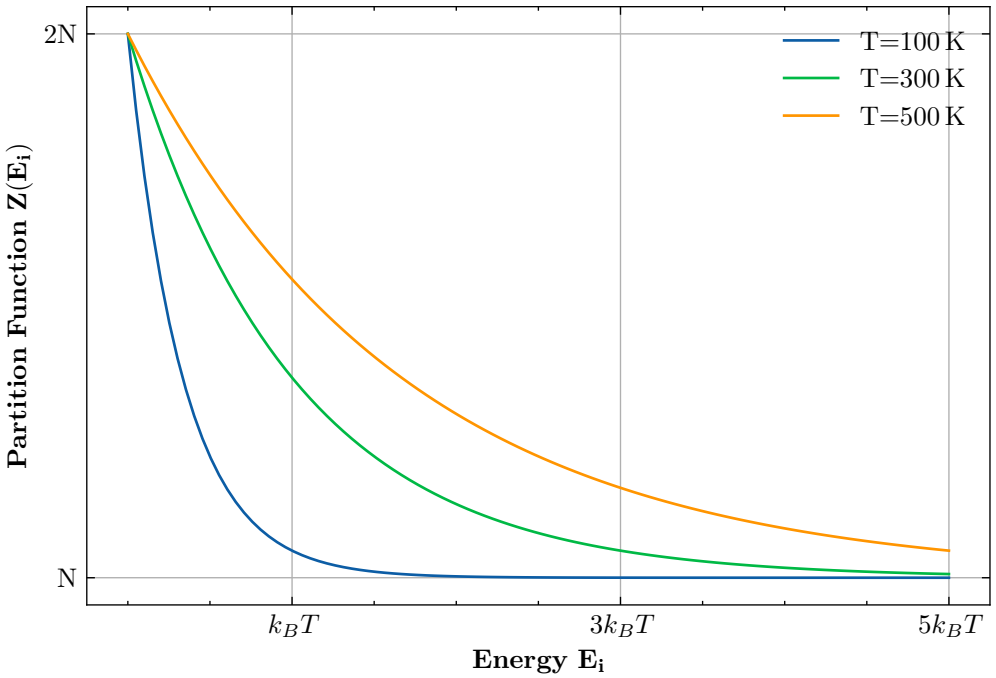

Figure 2.3: Partition function $Z(E_i)$ of the $2N$ excited singlet and triplet states as a function of the energies of the states E_i. At higher temperatures, Z becomes larger as predicted by Eq. (2.5).

Since the probability of a state is only dependent on its energy, we can express the relative likelihood of two states in equilibrium as the ratio of their Boltzmann factors. The ratio of probabilities will be just the ratio of the respective Boltzmann factors, so

$$\frac{P_i}{P_j} = \frac{e^{-E_i/k_BT}}{e^{-E_j/k_BT}} = e^{-(E_i-E_j)/k_BT} \tag{2.7}$$

For a fixed temperature the ratio of probabilities depends only on the energy difference between the two states since the partition function is the same for both states. The usefulness of this result will become clear later on.

Up to this point, we have assumed that the system's states are in equilibrium with each other and with the reservoir at temperature T. However, this assumption raises an important question: are the states in equilibrium from the beginning? If not, what mechanisms govern their evolution toward equilibrium? To answer this, we now examine how state transitions follow a Markov process and how these processes drive the system toward equilibrium over time.

We assume that, at $t = 0$, the exciton is located in the first excited triplet state T_1 of the molecular wire. Thus, the probability $P_{T_1}(t = 0) = 1$. As we mentioned previously, transitions between states are allowed and are described by their corresponding transition rates but the exciton can occupy only a single state at any given moment. We also assume that exciton transitions occur instantaneously, meaning that the exciton does not spend any finite time in an intermediate state during the transition process. The transitions of the exciton are considered as a discrete-time Markov chain which is a type of Markov process where the various states of the system are discrete and are analyzed over a discrete set of times. According to [7] a discrete-time Markov chain must satisfy the so-called "Markov property", which for a discrete-time Markov chain is given by

$$\text{Prob}\{x_{n+1}|x_0, x_1, \cdots, x_n\} = \text{Prob}\{x_{n+1}|x_n\} \tag{2.8}$$

The Markov property states that the transition to the next state x_{n+1} at time t_{n+1} depends only on the current state x_n at time t_n and not on any prior states. In other words, the history of past transitions does

not influence the future evolution of the system—only the present state determines the next state.

The conditional probabilities $\text{Prob}\{x_{n+1}|x_n\}$ are the transition probabilities of the Markov chain. Given that the exciton is in state x_n at time t_n, these probabilities represent the likelihood that it will transition to state x_{n+1} at time t_{n+1}. Transitions between states are examined at a time interval of dt and the transition probability will be denoted by

$$p_{i,j} = \text{Prob}\{x_{t+dt} = j|x_t = i\} \tag{2.9}$$

Equation (2.9) represents the probability that the exciton transitions from state i to state j in a small time interval dt, given that it was initially in state i at time t. At time t, the probability of finding the exciton in state i is given by $P_i(t)$, while the probability of it occupying state j is $P_j(t)$. $K_{i,j}$ denotes the transition rate from i to j and the reverse rate is denoted by $K_{j,i}$. The principle of detailed balance is a key property of physical systems and of certain Markov Chains that allows equilibrium to be approached. For the transitions between the states i and j, it is defined as:

$$P_i(t)K_{i,j} = P_j(t)K_{j,i} \ , \ \forall i, j \tag{2.10}$$

If Equation (2.10) holds, it means that the probability that flows from $i \to j$ in one time step is the same as the probability that flows from $j \to i$. If the forward transition rate $K_{i,j}$ is known, the reverse rate $K_{j,i}$ can be computed directly using the Boltzmann distribution and the principle of detailed balance. This relation ensures that the system obeys equilibrium constraints imposed by statistical mechanics.

$$K_{j,i} = K_{i,j} \ \frac{P_i(t)}{P_j(t)} \Rightarrow K_{j,i} = K_{i,j} \ e^{-(E_i - E_j)/k_B T} \tag{2.11}$$

The reverse rate is proportional to an exponential function of the energy difference between the two states. If the energy of the state from which the exciton transitions E_i is greater than the energy of the state it transitions to E_j, the reverse rate $K_{j,i}$ will be slower than the rate $K_{i,j}$.

Equation (2.11) is particularly important as it allows for the calculation of the reverse transition rate when the forward rate and the energy difference between the two states are known. In our molecular wire, all singlet states share the same energy E_S, while all triplet states have energy E_T. Consequently, the reverse transition rates between adjacent singlet states, K_{S_{i+1},S_i}, and adjacent triplet states, K_{T_{i+1},T_i}, are equal to their respective forward transition rates, $K_{S_i,S_{i+1}}$ and $K_{T_i,T_{i+1}}$.

We now extend our discussion to intersystem crossing rates (ISC) between the singlet state S_i and the triplet state T_i. Unlike transitions within the same energy level, these transitions involve energy differences, which directly affect the transition rates. Consequently, the intersystem rates K_{S_i,T_i} and K_{T_i,S_i} will generally not be equal.

$$K_{T_i,S_i} = K_{S_i,T_i} \ e^{-(E_S - \cancelto{0}{E_T})/k_B T} \Rightarrow K_{T_i,S_i} = K_{S_i,T_i} \ e^{-E_S/k_B T} \tag{2.12}$$

Because the singlet states have a higher energy than the triplet states the reverse intersystem crossing rate K_{T_i,S_i} will be slower than the respective forward ISC rate K_{S_i,T_i}.

2.2 Transition-Rate Matrix, Eigenvalues, and Exciton Dynamics

After introducing what our molecular wire consists of, its boundary conditions and the constraints imposed by statistical mechanics and Markov processes perhaps its time to turn our attention to the time evolution of the probability distribution of the $2N$ excited states. For each state i, the probability $P_i(t)$ will change over time according to the rates at which the system transitions into and out of state i. As shown by Reif Reif1985, the time-evolution of each state probability obeys

$$\frac{d}{dt}P_i(t) = -P_i(t)\sum_{j\neq i} K_{i,j} + \sum_{j\neq i} P_j(t)K_{j,i}\,. \tag{2.13}$$

The negative sign in the first term of Equation (2.13) indicates that the probability $P_i(t)$ decreases due to transitions from state i to all other possible states j. This term accounts for the probability flux leaving state i. The second term represents the probability gained by state i, which results from transitions originating from other states j.

Since there are $2N$ possible states that the exciton can transition to, there will be $2N$ equations similar to Equation (2.13), each one describing the evolution of the probability of finding the exciton in a given state at time t. We can collectively express the rate equations in a compact matrix form. To achieve this, we first define the probability vector at time t as:

$$\overrightarrow{P}(t) = \begin{pmatrix} P_{T_1}(t) \\ \vdots \\ P_{T_N}(t) \\ P_{S_1}(t) \\ \vdots \\ P_{S_N}(t) \end{pmatrix} \tag{2.14}$$

$\overrightarrow{P}(t)$ is a $2N \times 1$ column vector containing the probabilities of each excited singlet or triplet state. It is also useful to define the probability vector at $t = 0$, which gives information about the system before transitions start taking place. For our case, we assume that at $t = 0$ the exciton is located at T_1 and the probability distribution is

$$\overrightarrow{P}(t=0) = \begin{pmatrix} 1 \\ 0 \\ \vdots \\ 0 \end{pmatrix} \tag{2.15}$$

Having defined the probability vector $\overrightarrow{P}(t)$, we can now rewrite the $2N$ rate equations in a more elegant way

$$\frac{d}{dt}\overrightarrow{P}(t) = \widetilde{Q}\overrightarrow{P}(t) \tag{2.16}$$

where, $\widetilde{Q}$ is a $2N \times 2N$ matrix, often referred to as the transition matrix that contains all the transition rates between states.

For the transition matrix $\widetilde{Q}$ the elements of the main diagonal are given by

$$Q_{ii} = -\sum_{j\neq i} K_{i,j} \tag{2.17}$$

And for the off-diagonal elements we have

$$Q_{ij} = \sum_{j\neq i} K_{j,i} \tag{2.18}$$

It is important to remember that the allowed transitions, governed by the transition rates $K_{i,j}$, are those between adjacent singlet states $S_i \leftrightarrow S_{i+1}$, adjacent triplet states $T_i \leftrightarrow T_{i+1}$ and between singlet and triplet states belonging to the same molecule $T_i \leftrightarrow S_i$.

Our molecular wire is considered as an isolated system and thus as we have previously mentioned the total probability at each moment t is conserved and equal to unity. This invokes the following constraint on the transition matrix $\widetilde{Q}$

$$
\begin{aligned}
P_{total}(t) = \sum_i P_i(t) \ = 1 \Rightarrow \frac{d}{dt} P_{total}(t) &= 0 \\
\Rightarrow \sum_i \frac{d}{dt} P_i(t) &= 0 \\
\Rightarrow \sum_i \sum_j Q_{ij} P_j(t) &= 0 \\
\Rightarrow \sum_j P_j(t) \sum_i Q_{ij} &= 0 \\
\text{Hence,} \qquad \sum_i Q_{ij} &= 0\,, \quad \forall\, i
\end{aligned} \tag{2.19}
$$

Equation (2.19) states that for the total probability distribution to be conserved, the sum of every column of the transition matrix must be zero.

Since the transition matrix $\widetilde{Q}$ depends only on the transition rates between states, which are time independent, Equation (2.16) is a linear differential equation with constant coefficients, thus we can attempt to solve it with the following substitution as discussed in [6]

$$\overrightarrow{P}(t) = \overrightarrow{X}\, e^{\lambda t} \tag{2.20}$$

If we insert Equation (2.20) into (2.16)

$$\widetilde{Q}\, \overrightarrow{X} = \lambda\, \overrightarrow{X} \tag{2.21}$$

Equation (2.21) is just the eigenvalue equation of the transition matrix $\widetilde{Q}$, where λ are the eigenvalues of $\widetilde{Q}$ and $\overrightarrow{X}$ are the respective eigenvectors.

The rate matrix $\widetilde{Q}$ is real but generally not symmetric, meaning that in general, $Q_{ij} \neq Q_{ji}$ for $i \neq j$. For our case, this asymmetry arises due to the energy difference between the excited singlet and triplet states, defined as $\Delta E \equiv (E_S - E_T)$. This energy difference leads to a finite difference between the forward ISC rate K_{S_i,T_i} and the reverse ISC rate K_{T_i,S_i} for every molecule i.

Although $\widetilde{Q}$ is real, since it is not symmetric, its eigenvalues may be complex and the left eigenvectors $\overrightarrow{X}^L_m$ may be different from the right ones $\overrightarrow{X}^R_m$. The left and right eigenvectors satisfy the following equations:

$$\widetilde{Q}\, \overrightarrow{X}^R_m = \lambda_m\, \overrightarrow{X}^R_m \tag{2.22}$$

$$\overrightarrow{X}^L_m\, \widetilde{Q} = \lambda_m\, \overrightarrow{X}^L_m \tag{2.23}$$

where $\overrightarrow{X}^R_m$ is a $2N \times 1$ column vector and $\overrightarrow{X}^L_m$ is a $1 \times 2N$ row vector. The orthonormality of left and right eigenvectors corresponding to different eigenvalues λ_m and $\lambda_{m'}$, is defined as:

$$\overrightarrow{X}^L_m \cdot \overrightarrow{X}^R_{m'} = \delta_{m,m'} \tag{2.24}$$

for $\lambda_m \neq \lambda_{m'}$.

The complete solution of Equation (2.16) will be a superposition of the possible special solutions it. The probability distribution at time t is thus given by:

$$\overrightarrow{P}(t) = \sum_m e^{\lambda_m t}\ \overrightarrow{X}^R_m\ \left(\overrightarrow{X}^L_m\ \cdot\ \overrightarrow{P}(0)\right) \tag{2.25}$$

Once we have calculated the $2N$ eigenvalues λ_m, and the corresponding left and right eigenvectors $\overrightarrow{X}^L_m$ and $\overrightarrow{X}^R_m$, we can use Equation (2.25) to compute the probability distribution at any time t efficiently. Once we have constructed the transition rate matrix $\widetilde{Q}$, we can compute the eigenvectors and eigenvalues computationally, see [2].

$$\overrightarrow{P}(t) = \sum_m e^{\lambda_m t}\ \overrightarrow{V}^R_m\ \left(\overrightarrow{V}^L_m\ \cdot\ \overrightarrow{P}(0)\right) \tag{2.26}$$

where,

$$\overrightarrow{V}^R_m = \frac{1}{\sqrt{\overrightarrow{X}^L_m\ \cdot\ \overrightarrow{X}^R_m}}\overrightarrow{X}^R_m \tag{2.27}$$

$$\overrightarrow{V}^L_m = \frac{1}{\sqrt{\overrightarrow{X}^L_m\ \cdot\ \overrightarrow{X}^R_m}}\overrightarrow{X}^L_m \tag{2.28}$$

$\overrightarrow{V}^L_m$, $\overrightarrow{V}^R_m$ are the normalized left and right eigenvectors respectively. These vectors must satisfy the orthonormality condition:

$$\overrightarrow{V}^L_m \cdot \overrightarrow{V}^R_{m'} = \delta_{m,m'} \tag{2.29}$$

2.3 Stability and Steady-State Probabilities

It is now time to discuss the stability of the system and how it finds itself to equilibrium. From Equation (2.26) we see that the evolution of the probability distribution with time is dictated by the exponential factor $\exp(\lambda_m t)$ in the summation. How do we, then, know that the probability of a single state $P_j(t)$ will not blow up as time increases? Before we answer this question we will examine for a moment the eigenvalues λ_m of the transition matrix as they are the ones that determine the behavior of $\overrightarrow{P}(t)$ as $t \to \infty$. We mentioned previously that due to the asymmetry of the transition matrix the eigenvalues are not guaranteed to be real and can be written as $\lambda_m = a + ib$. The exponential factors in Equation (2.26) can then be written as

$$e^{\lambda_m t} = e^{(a+ib)t} = e^{at}\left(\cos(at) + i\,\sin(bt)\right) \tag{2.30}$$

The magnitude of the exponent is thus solely determined by the real part e^{at}. The imaginary part produces sinusoidal waves which do not affect the amplitude of the probability. Furthermore, if $a > 0$ the exponential factors increase indefinitely as t increases. If on the other hand $a < 0$, the solution decays and is equal to zero when $t \to \infty$. Hence, Equation (2.26) is stable if and only if all eigenvalues have negative or zero real part $Re(\lambda_m) \leq 0$. If all the eigenvalues have a negative real part, then the probability distribution $\overrightarrow{P}(t)$ will reach zero eventually. Thus, the existence of a zero eigenvalue ($Re(\lambda_m) = 0$) is necessary if we want to ensure that there is a stationary solution such that $\sum_i P_i = 1$.

For our system, it can easily be shown that there will be a zero eigenvalue if the probability distribution is constant. We can start by writing Equation (2.2) in matrix notation

$$\big(1, 1, \cdots, 1\big)_{1\times 2N} \cdot \begin{pmatrix} Q_{1,1} & \cdots & Q_{1,2N} \\ \vdots & \ddots & \vdots \\ Q_{2N,1} & \cdots & Q_{2N,2N} \end{pmatrix} = \big(0, 0, \cdots, 0\big)_{1\times 2N} \tag{2.31}$$

We can define the row vector whose elements are all equal to one

$$\overrightarrow{1} = \begin{pmatrix} 1 \\ 1 \\ \vdots \\ 1 \end{pmatrix}_{2N\times 1} \tag{2.32}$$

Equation (2.31) can be simplified to

$$\overrightarrow{1}^T \times \widetilde{Q} = 0 \times \overrightarrow{1}^T \tag{2.33}$$

This clearly shows that $\overrightarrow{1}^T$ is a left eigenvector of the transition matrix with eigenvalue $\lambda_0 = 0$. We denote this eigenvector as:

$$\overrightarrow{X}_0^L = \overrightarrow{1}^T \tag{2.34}$$

Since we are certain that there will exist some eigenvalue λ_m whose real part is equal to zero we can proceed to the calculation of the steady-state probability distribution of our molecular wire. The steady-state probability obeys the following condition

$$\begin{aligned} &\overrightarrow{P}(t+dt) - \overrightarrow{P}(t) = 0 \\ &\Rightarrow \frac{d}{dt}\overrightarrow{P}(t) = 0 \end{aligned} \tag{2.35}$$

The steady-state probability can be thought of as the probability distribution that remains unchanged from one time step to the next. It represents the state the system naturally converges to once all time dependence from the exponential terms in Equation (2.25) vanish.

We now present a standard derivation of the steady-state probability which begins by isolating the zero eigenvalue λ_0 from the rest eigenvalues $\lambda_{m\neq 0}$. Starting from Equation (2.26) we have

$$\begin{aligned} &\overrightarrow{P}(t) = \sum_m e^{\lambda_m t}\ \overrightarrow{V}_m^R\ \left(\overrightarrow{V}_m^L\ \cdot\ \overrightarrow{P}(0)\right) \\ \Rightarrow\ &\overrightarrow{P}(t) = \overrightarrow{V}_0^R \times \left(\overrightarrow{V}_0^L\ \cdot\ \overrightarrow{P}(0)\right) + \sum_{m\neq 0} e^{\lambda_m t}\ \overrightarrow{V}_m^R\ \left(\overrightarrow{V}_m^L\ \cdot\ \overrightarrow{P}(0)\right) \end{aligned} \tag{2.36}$$

As time increases, the contribution of the summation in Equation (2.36) will decrease and when $t \to \infty$ it will vanish due to all the eigenvalues having negative real parts.

$$\begin{aligned} &\lim_{t\to\infty} \overrightarrow{P}(t) = \overrightarrow{V}_0^R \times \left(\overrightarrow{V}_0^L\ \cdot\ \overrightarrow{P}(0)\right) \\ \Rightarrow\ &\lim_{t\to\infty} \overrightarrow{P}(t) = \overrightarrow{X}_0^R \times \left(\frac{\overrightarrow{X}_0^L\ \cdot\ \overrightarrow{P}(0)}{\overrightarrow{X}_0^L\ \cdot\ \overrightarrow{X}_0^R}\right) \end{aligned}$$

The probability of finding the exciton in any of the $2N$ possible states is equal to 1 at every instant of time t. We can express this using matrix notation

$$\begin{aligned} &\sum_i P_i(t) = 1\,, \quad \forall\, t \\ &\Rightarrow \overrightarrow{1}^T\ \cdot\ \overrightarrow{P}(t) = 1 \end{aligned}$$

If we use Equation (2.34) and examine the system at the beginning ($t = 0$) we get

$$\overrightarrow{1}^T\ \cdot\ \overrightarrow{P}(0) = 1 \Rightarrow \overrightarrow{X}_0^L\ \cdot\ \overrightarrow{P}(0) = 1 \tag{2.37}$$

The steady-state probability is defined as the probability distribution at the limit $t \to \infty$ and is denoted by

$$\overrightarrow{P}^{\text{ss}} \equiv \overrightarrow{P}(t \to \infty) = \frac{1}{\overrightarrow{1}^T\ \cdot\ \overrightarrow{X}_0^R}\overrightarrow{X}_0^R \tag{2.38}$$

Conservation of probability ensures that the steady-state probability $\overrightarrow{P}^{\text{ss}}$ is independent of the initial probability distribution $\overrightarrow{P}(0)$ of the system.

What does the condition $t \to \infty$ truly mean, and how can we examine a system in this limit? We know that as $t \to \infty$, all exponential terms in Equation (2.36) vanish due to the negative eigenvalues λ_m, which act as decay coefficients. The larger the real part of an eigenvalue $\text{Re}(\lambda_m)$, the faster $e^{\lambda_m t}$ decays to zero. Thus, the probability distribution will become independent of time when the eigenvalue with the smallest real part $\min(\text{Re}(\lambda_m))$ becomes negligible. Therefore, we can define $t \to \infty$ as the time needed for the exponential term with the smallest eigenvalue to vanish, and that occurs when

$$t \gg \frac{1}{\min(\text{Re}(\lambda_m))}$$

2.4 Probability Evolution and Exciton Transition Times

Thus far, we have described our molecular wire consisting of N molecules and identified the allowed transitions between the excited singlet and triplet states. We have also explained how these transition rates define the transition rate matrix, which governs the evolution of the probability distribution for locating the exciton in different excited states. Now, we turn our attention to the time needed for an exciton, starting from an initial excited state, to transition to a particular final state. We refer to this time as the transition time, denoted by

$$\text{Transition time} = \tau_{i \to j} \tag{2.39}$$

where i represents the initial state of the exciton, and j is the final state it transitions to.

Finding the exciton in a particular state j at time t is a probabilistic event, which can not be determined with certainty. Instead, it is described by the probability vector $\overrightarrow{P}(t)$. We define the transition time $\tau_{i \to j}$ as the time required for the probability of locating the exciton in the final state $P_j(t)$ to approach the steady-state probability of that state P_j^{ss}. This will allow us to determine if the exciton has transitioned to that state, and to quantify the time it required for this transition. Equation (2.35) indicated that $\overrightarrow{P}(t)$ will approach asymptotically the steady-state probability vector $\overrightarrow{P}^{\text{ss}}$ as t increases leading to equality when $t \to \infty$. Therefore, for an arbitrary state j, we assume that the probability has reached the steady-state probability when it is within a given threshold ε of the corresponding steady-state probability P_j^{ss}, and the condition is given by

$$P_j(t) = \varepsilon P_j^{\text{ss}} \tag{2.40}$$

where ε represents the allowable deviation between $P_j(t)$ and P_j^{ss}.

We now assume that the exciton is initially located in the first excited triplet state T_1 and we investigate the time it requires to transition to the final excited triplet state T_N. The probability distribution of all the states is given by Equation (2.15) and the transition time $\tau_{T_1 \to T_N}$ is defined as the time required for Equation (2.40) to be satisfied.

Usually, the transition rates of adjacent triplet states $K_{T_i, T_{i\pm1}}$ are considered to be slower than the corresponding transition rates between adjacent singlet states $K_{S_i, S_{i\pm1}}$ by several orders of magnitude. This gives rise to an important question: If the exciton starts in the first triplet state T_1 and it needs to transition to the final triplet state T_N, will the transition time be reduced if it first undergoes a transition to the faster singlet channel? Once in a singlet state, it may complete the necessary transitions to reach the final molecule's excited singlet state S_N before transitioning back to the final triplet state T_N.

It is expected that transitioning to the faster singlet channel and undergoing the majority of transitions there will be beneficial for exciton transport. We now explore how the parameters of the system affect these results and determine the conditions under which the transition time $\tau_{T_1 \to T_N}$ is minimized. Particularly, we are interested in how the following parameters affect the system:

- The size of the system: N
- The energy difference between excited singlet and triplet states: ΔE
- The transition rates between adjacent singlet states: $K_{S_i,\, S_{i\pm1}}$
- The transition rates between adjacent triplet states: $K_{T_i,\, T_{i\pm1}}$
- The transition rate between excited singlet and triplet states of the same molecule i: $K_{S_i,\, T_i}$ and $K_{T_i,\, S_i}$

These parameters influence the rates at which transitions between two states occur and the number of transitions that are needed for the exciton to reach the final triplet state.

2.5 Simulation Methodology

To better understand the behavior of our system, we start the simulation analysis by examining the transition time when transition between triplet and singlet states is forbidden, that is, $K_{S_i \to T_i} = 0$ for all of the N molecules. Since the exciton starts in T_1, by not being allowed to transition to any of the singlet states through the rISC rate, it is forced to reach the final triplet state only by undergoing transitions between adjacent triplet states with a transition rate of $K_{T_i,\, T_{i\pm1}}$. Therefore the transition time $\tau_{T_1 \to T_N}$ is solely dependent on the transition rates within the triplet channel. Subsequently, we examine the more general case where intersystem crossing is permitted, enabling transitions between singlet and triplet states. By comparing the results of both scenarios, we aim to determine if it is beneficial to have intersystem transitions and the parameters that produce the fastest transition time.

We carried out simulations to compute the transition time ratio, defined as

$$\text{Transition Time Ratio} \equiv \frac{\tau_{\text{closed}}}{\tau_{\text{open}}} \tag{2.41}$$

where τ_{closed} is the time required for the exciton starting at T_1 to reach the final triplet state T_N when intersystem crossing is prohibited. In contrast, τ_{open} refers to the transition time when intersystem crossing is allowed.

To determine the dependence of the transition time ratio on the various parameters of the system, a simulation of the exciton's movement was performed for the following parameters:

- $N = 2,\, 10$
- $\Delta E = [6.25 \times 10^{-4}\, eV, \cdots,\, 0.1\, eV]$
- $K_{T_i,\, T_{i\pm1}} = 1\,\text{ns}^{-1};\, 0.1\,\text{ns}^{-1}$
- $K_{S_i,\, S_{i\pm1}} = 0.1\,\text{ps}^{-1};\, 0.01\,\text{ps}^{-1}$
- $K_{T_i,\, S_i} = [1\,\text{ns}^{-1},\, \cdots,\, 1\,\text{ps}^{-1}]$

These values were selected to explore the different conditions of the molecular wire and determine the parameter regions where contributions from the singlet manifold significantly improve the transitioning.

We expect that as the number of molecules (N) increases, the exciton has to complete more transitions which suggests that the transition time in both open and closed systems will increase. However, we expect that the effects of the faster singlet channel will be more pronounced for larger systems. The reverse intersystem crossing rate $K_{T_i,\, S_i}$ describes the rate with which the exciton transitions from the slower triplet manifold to the faster singlet one. Subsequently, the intersystem crossing rate $K_{S_i,\, T_i}$ indicates how rapidly the exciton transitions back to the triplet channel. Because the singlet states have higher energies than the respective triplet states, the K_{S_i,T_i} will be faster than K_{T_i,S_i}. Given a fixed ISC rate K_{S_i,T_i}, the singlet-triplet energy gap ΔE determines how much slower the reverse rate K_{T_i,S_i} is. If the energy gap is very large, the rISC rate will be negligible relative to the ISC rate. Therefore, utilizing the singlet manifold should not be beneficial to exciton transport.

2.6 Simulation Results

In this section, we present the results of the simulations performed to evaluate the transition time ratio $\tau_{\text{closed}}/\tau_{\text{open}}$ under different parameter settings. The objective is to determine how the system size, intersystem crossing rate, singlet and triplet transition rates, and the energy gap ΔE influence the efficiency of exciton transport. Contour plots are used to visualize the variation of the transition time ratio with respect to the energy gap ΔE and ISC rate K_{S_i,T_i}. For a molecular wire of N molecules characterized by the singlet and triplet transition rates $K_{S_i,S_{i\pm1}}$ and $K_{T_i,T_{i\pm1}}$, respectively, this analysis identifies the parameter regions where ISC benefits exciton transport from T_1 to T_N.

2.6.1 Effect of System Size N

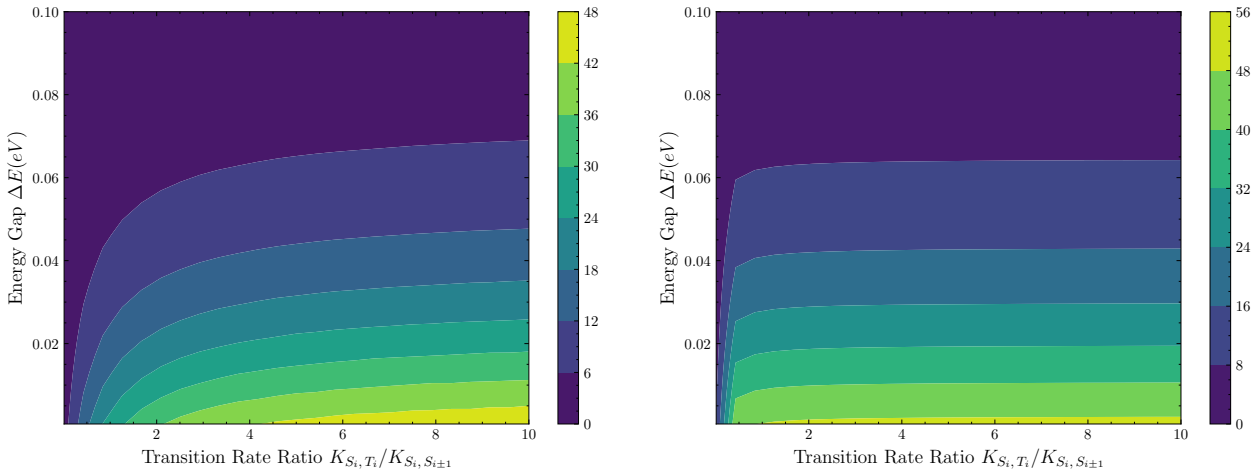

(a) $N = 2$ (b) $N = 10$

Figure 2.4: Contour plots of the transition time ratio $\tau_{\text{closed}}/\tau_{\text{open}}$ as a function of the energy gap ΔE and the rate ratio $K_{S_i,T_i}/K_{S_i,S_{i\pm1}}$. Figure 2.4a shows the results for $N = 2$, while Figure 2.4b the results when $N = 10$. The transition rate between adjacent triplet states is $K_{T_i,\,T_{i\pm1}} = 1\,\text{ns}^{-1}$ and the transition rate between adjacent singlet states is $K_{S_i,\,S_{i\pm1}} = 0.1\,\text{ps}^{-1}$.

Figure 2.4 shows the transition time ratio $\tau_{\text{closed}}/\tau_{\text{open}}$ for two different system sizes $N = 2$ and $N = 10$ as a function of the energy difference ΔE and the rate ratio $K_{S_i,\,T_i}/K_{S_i,S_{i\pm1}}$. For the x-axis, the ratio $K_{T_i,\,S_i}/K_{T_i,\,T_{i\pm1}}$ was used in order to clearly illustrate how much faster or slower the intersystem crossing rate is when compared to the singlet-to-singlet transition rate $K_{S_i,S_{i\pm1}}$. Figure **??** demonstrates that the smaller system $N = 2$ is slightly more sensitive to the ISC $K_{S_i,\,T_i}$ for small values of the ratio. However, when the ISC rate exceeds the singlet-to-singlet transition rate by a factor of two $K_{S_i,T_i}/K_{S_i,S_{i\pm1}} \geq 2$, further increases of the ISC rate do not improve $\tau_{\text{closed}}/\tau_{\text{open}}$. Similar results are observed for the larger system of $N = 10$ molecules as shown in Figure **??**. Furthermore, the effects of the energy gap ΔE on the transition time ratio are similar in both systems. The best results are achieved when the energy gap is minimal, which speeds the transitioning by increasing the rISC rate K_{T_i,S_i}, allowing the exciton to transition faster to the singlet manifold.

2.6.2 Effect of Transition Rates

For a molecular bridge consisting of N molecules, it is important to understand how the transition rates between adjacent singlet and triplet states, $K_{S_i,\,S_{i\pm1}}$ and $K_{T_i,\,T_{i\pm1}}$, influence the transition time ratio $\tau_{\text{closed}}/\tau_{\text{open}}$.

Figure 2.5 shows the transition time ratio $\tau_{\text{closed}}/\tau_{\text{closed}}$ for two different triplet-to-triplet transition rates $K_{T_i,\,T_{i\pm1}}$. The molecular wire consists of $N = 10$ molecules and singlet-to-singlet rate is $K_{S_i,\,S_{i\pm1}} = 0.01\,\text{ps}^{-1}$.

Figures 2.5a, 2.5b show similar dependence on the singlet-triplet energy gap ΔE and on the rate ratio $K_{T_i,\,S_i}/K_{T_i,\,T_{i\pm1}}$. As the singlet-triplet energy gap decreases, the time ratio increases, which means the transition time is shorter. Moreover, there is a substantial change in the transition time when the transition rate between adjacent triplet states changes. When $K_{T_i,\,T_{i\pm1}} = 1\ \mathrm{ns}^{-1}$ allowing intersystem crossing results in a reduction of the transition time of up to one order of magnitude as shown in Figure 2.5a. On the other hand, Figure 2.5b shows that when the triplet-to-triplet rate $K_{T_i,T_{i\pm1}}$ is reduced by 10 times, that is, $K_{T_i,\,S_i}/K_{T_i,\,T_{i\pm1}} = 0.01\ \mathrm{ns}^{-1}$, allowing intersystem transitions improves the transition time ratio by up to 560 times.

The dependence of $\tau_{\mathrm{closed}}/\tau_{\mathrm{open}}$ on the singlet-to-singlet transition rate $K_{S_i,\,S_{i\pm1}}$ is shown in Figure 2.6. The triplet-to-triplet transition rate is fixed at $K_{T_i,\,T_{i\pm1}} = 0.1\,\mathrm{ns}^{-1}$. In contrast to Figure 2.5, the results indicate that increasing this rate leads to significantly improved transition time ratios. For all cases, once the ISC rate $K_{S_i,\,T_i}$ exceeds the singlet-to-singlet rate $K_{S_i,S_{i\pm1}}$, the time ratio $\tau_{\mathrm{closed}}/\tau_{\mathrm{open}}$ is independent on the intersystem crossing rate.

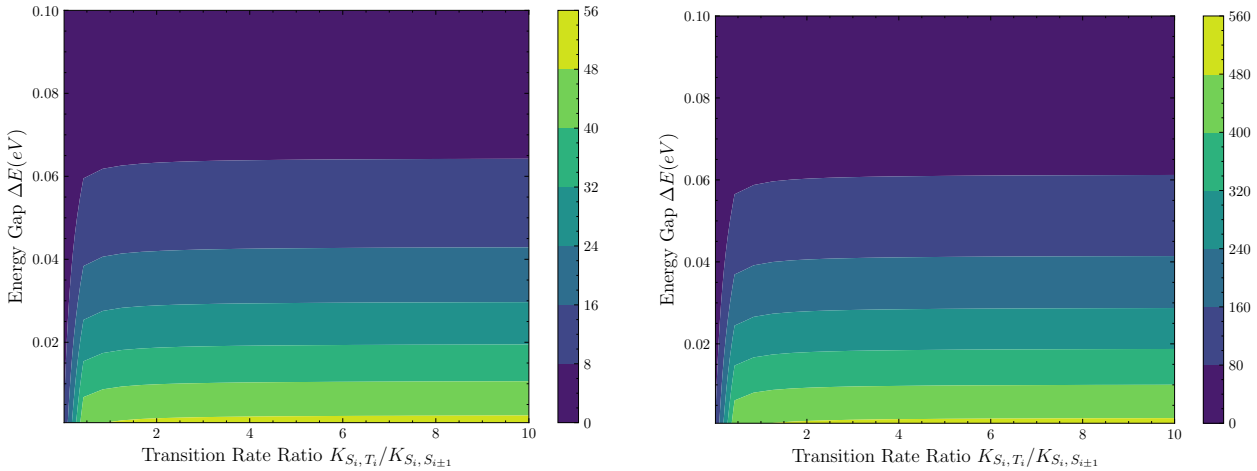

(a) $K_{T_i,\,T_{i\pm1}} = 1\,\mathrm{ns}^{-1}$

(b) $K_{T_i,\,T_{i\pm1}} = 0.1\,\mathrm{ns}^{-1}$

Figure 2.5: Contour plots of the transition time ratio $\tau_{\mathrm{closed}}/\tau_{\mathrm{open}}$ as a function of the energy gap ΔE and the rate ratio $K_{S_i,T_i}/K_{S_i,S_{i\pm1}}$. Figure 2.5a shows the results for $\tau_{\mathrm{closed}}/\tau_{\mathrm{open}}$ for a system where transitions between adjacent triplet states occur at a rate of $K_{T_i,\,T_{i\pm1}} = 1\,\mathrm{ns}^{-1}$. Figure 2.5b illustrates the results for $K_{T_i,\,T_{i\pm1}} = 0.1\,\mathrm{ns}^{-1}$. The system consists of $N = 10$ molecules and the singlet-to-singlet rate is $K_{S_i,\,S_{i\pm1}} = 0.1\,\mathrm{ps}^{-1}$.

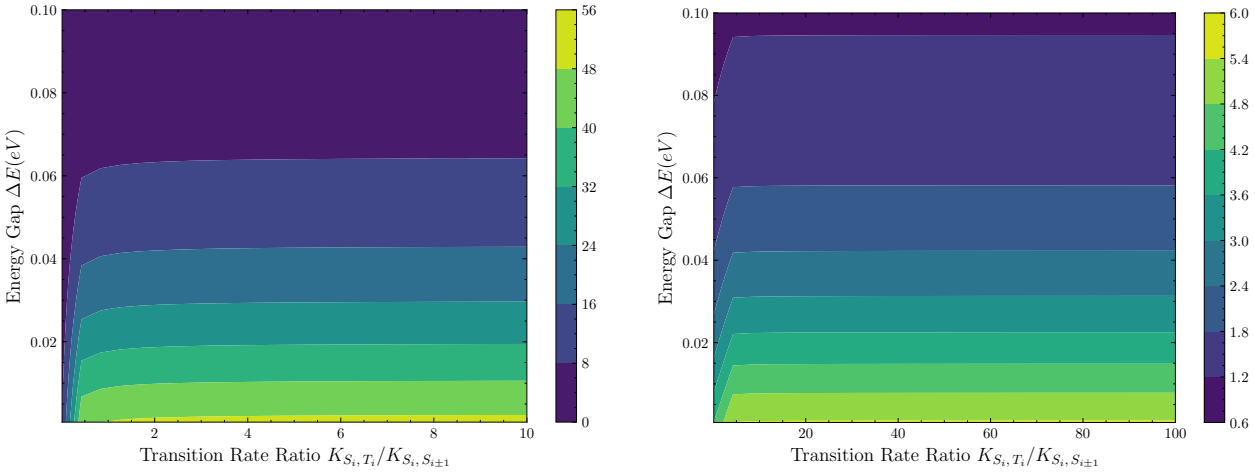

(a) $K_{S_i,\,S_{i\pm1}} = 0.1\,\mathrm{ps}^{-1}$

(b) $K_{S_i,\,S_{i\pm1}} = 0.01\,\mathrm{ps}^{-1}$

Figure 2.6: Contour plots of the transition time ratio $\tau_{\text{closed}}/\tau_{\text{open}}$ as a function of the energy gap ΔE and the rate ratio $K_{S_i,T_i}/K_{S_i,S_{i\pm1}}$ Figure 2.6a shows the results for $\tau_{\text{closed}}/\tau_{\text{open}}$ for $K_{S_i,\,S_{i\pm1}} = 0.1\,\mathrm{ps}^{-1}$ while in Figure 2.6b shows results for the slower system with $K_{S_i,\,S_{i\pm1}} = 0.01\,\mathrm{ps}^{-1}$. The system consists of $N = 10$ molecules and the triplet-to-triplet rate is $K_{T_i,\,T_{i\pm1}} = 1\,\mathrm{ns}^{-1}$.

2.7 Optimal Conditions for Rapid Exciton Transport

We examined the conditions that govern the transition time of an exciton in a closed system consisting of N molecules. Specifically, we were interested in the time required for an exciton to transition from the first excited triplet state T_1 to the final excited triplet state T_N, and to determine for which parameters of the system this transition occurs most efficiently.

Because the transitions between adjacent singlet states are significantly faster than the corresponding transitions between adjacent triplet states, we examined under what conditions the faster singlet channel can be effectively utilized to reduce the total transition time. Therefore, $\tau_{\text{closed}}/\tau_{\text{open}}$ was examined, where τ_{closed} is the transition time when intersystem crossing from the triplet channel to the singlet channel is prohibited and τ_{open} is the transition time when intersystem crossing is allowed. A ratio greater than one indicates that allowing intersystem transitions reduces the overall transition time, while a ratio close to unity suggests minimal difference between the two scenarios.

The computational results showed that the size of the system does not significantly influence the transition time ratio. Given a system of N molecules, $\tau_{\text{closed}}/\tau_{\text{open}}$ depends primarily on the energy difference ΔE between excited singlet and triplet states, as well as on the singlet-to-singlet and triplet-to-triplet transition rates. We demonstrated that allowing ISC into the singlet manifold reduced the overall transition time. The effects of ISC became more pronounced when triplet transitions slowed and singlet hopping sped up. By decreasing the energy gap, the reverse ISC rate is increased and entry into the singlet manifold is accelerated, allowing the exciton to utilize the faster singlet transitions. These results indicate that minimizing ΔE and maximizing $K_{S_i,S_{i\pm1}}$ are both necessary for fast exciton transport. In Chapter 3, we will apply these insights to study exciton transport in an open system where decay pathways to the ground singlet state S_0 are taken into consideration.

Chapter 3

Exciton Transport with Loss Mechanisms

3.1 Introduction

In the previous chapter, we examined the time required for an exciton starting in the first triplet state T_1 to transition to the final triplet state T_N of a molecular wire constructed by linearly aligning N molecules. The exciton was allowed to transition from excited triplet states to excited singlet states and vice versa in the presence of spin-orbit coupling. Furthermore, all excited triplet states had energy E_T and all the excited singlet states $E_S > E_T$.

For an exciton residing in an arbitrary triplet state T_i, transitions were allowed only to the two adjacent excited triplet states T_{i+1}, T_{i-1} and the excited singlet state S_i belonging to the same molecule i. This model allowed for the successful discovery of the parameters that allow fast exciton transport when intersystem transitions are permitted. However, this scenario ignores the existence of the ground singlet state S_0 of each molecule.

We now examine the transition time $\tau_{T_1 \to T_N}$ when the ground singlet state is taken into consideration. Transitions to the ground singlet state are possible from both excited triplet and singlet states and the system is no longer regarded as a closed system. Instead, it becomes an open system where loss mechanisms must be considered. This chapter will inspect how these loss mechanisms affect the transitioning of an exciton that is initially in the first excited triplet state T_1 and aims to reach the final excited triplet state T_N. Moreover, the transition rates between excited states along with the energy gap between the excited singlet and triplet states will be examined once again to determine if fast exciton transport is viable for this scenario.

3.2 System Model

Including the ground singlet state S_0, introduces the possibility of exciton loss, representing decay pathways that exist in real molecular systems. We refer to loss, as the irreversible transition from excited states (singlet or triplet) to the molecular ground state S_0, after which the exciton is no longer available for transition. In this model, there is a possibility that the exciton will not reach the final triplet state, and optimizing transition rates becomes even more crucial. The graphical representation of the system is shown in Figure 3.1.

Transitions to the ground singlet state are considered as loss, and the probability of the exciton being found in S_0 will not be included in the probability distribution given by Equation (2.14) of the system. The transition rates from the excited states to the ground state are denoted by γ^S_{loss} for the loss rate of the excited singlet state to the ground singlet state, and γ^T_{loss} for the loss rate of the excited triplet state to the ground singlet state. These loss rates, also referred to as decay rates, govern the rate at which probability flows from the

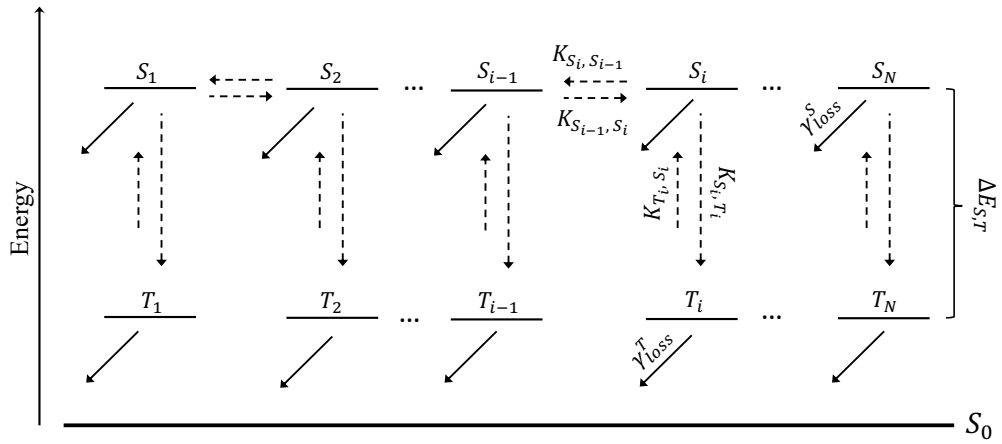

Figure 3.1: Schematic diagram of the molecular wire consisting of N excited singlet and triplet states when the ground singlet state S_0 is included. Transition rates between excited states are represented by dashed arrows and solid arrows represent the irreversible transitions from excited singlet and triplet states to the ground singlet state S_0. When two opposing arrows differ in length, it indicates that the forward and reverse transition rates are unequal. In contrast, equal-length arrows signify that the corresponding transition rates are equal.

excited-state distribution $\overrightarrow{P}(t)$ to the ground state population $P_{S_0}(t)$.

The probability of locating the exciton in one of the $2N$ excited states is no longer conserved:

$$P_{\text{total}}(t) = \sum_i P_i(t) \neq 1$$

In contrast to the previous chapter, transitions between excited triplet states are now prohibited, that is, $K_{T_i,\,T_{i\pm1}} = 0$. In the absence of spin-orbit coupling, an exciton starting in the first excited triplet state T_1 will remain in that state until it decays to the molecular ground state S_0, and will thus never reach the final destination T_N. However, in the presence of spin-orbit coupling, transitions between excited singlet and triplet states are permitted and the exciton will be able to reach the final triplet state by firstly transitioning to the singlet channel through intersystem crossing, traversing the singlet states until it reaches the final singlet state S_N, from which it will transition back to the final triplet state T_N. The time required for this full transition is denoted by $\tau_{T_1 \to T_N}$. This framework allows for a deeper understanding of the parameters that enable effective utilization of the singlet channel for exciton transport in systems where decay to the ground state S_0 is possible.

In addition, we consider the intersystem crossing rate from excited singlet states to excited triplet states $K_{S_i,\,T_i}$ to be known. Using detailed balance, the reverse intersystem crossing rate from triplet to singlet states, $K_{T_i,\,S_i}$, can be calculated as:

$$K_{T_i,\,S_i} = K_{S_i,\,T_i}\, e^{-(E_S - E_T)/k_B T} \tag{3.1}$$

As expected, since the excited singlet states lie at higher energy than the corresponding triplet states, the transition from triplet to singlet states is thermally suppressed and thus slower than the reverse process.

3.2.1 Modified Master Equation and Rate Matrix

The inclusion of loss to the ground state affects the system's dynamics by modifying the master equation previously defined in Equation (2.16). While the general form remains the same, the transition rate matrix $\widetilde{Q}$

is affected by the decay rates γ^S_{loss} and γ^T_{loss} to the ground singlet state S_0. Each excited singlet state S_i and triplet state T_i, through these loss rates, contributes an additional negative term γ^S_{loss} and γ^T_{loss}, respectively, to the diagonal of $\widetilde{Q}$. The ground state is regarded as a separate system and detailed balance is not imposed on it. As a result, there are no incoming rates to compensate for these losses, and unlike in the previous chapter, the columns of the transition rate matrix no longer sum to zero.

We showed previously, through Equation 2.19, that in order for the probability to be conserved, the columns of $\widetilde{Q}$ must sum to zero. This is no longer the case, as the loss rates γ^S_{loss} and γ^T_{loss} now determine the rate at which probability flows out of the system and into the ground singlet state.

Since the general form of the master equation remains unchanged, the probability distribution at time t is again given by Equation (2.26). However, the inclusion of the ground state and the loss rates will directly impact the eigenvalues λ_m of the transition rate matrix. Equation (2.33) showed that when the columns of $\widetilde{Q}$ sum to zero, there exists a zero eigenvalue $\lambda_0 = 0$ that ensures the system's transition to the steady-state distribution.

In the present model, the columns do not sum to zero which results in the absence of a zero eigenvalue. Therefore, in an open system, all eigenvalues λ_m will have a negative real part $\text{Re}(\lambda_m) < 0$ which will result in a continuous loss of probability until all exciton population decays into the ground singlet state.
The probability distribution as $t \to \infty$ will be given by:

$$\overrightarrow{P}(t \to \infty) = \begin{pmatrix} 0 \\ 0 \\ \vdots \\ 0 \end{pmatrix}_{2N \times 1} \tag{3.2}$$

Previously, we defined the steady-state distribution as the time-independent solution that the system approaches once all transient effects governed by the time-dependent exponential terms have decayed. In the absence of loss rates, the probability distribution will asymptotically approach the steady-state probability distribution as time increases. However, the inclusion of the ground state will prevent the probability distribution of reaching the steady-state distribution due to the loss rates from the excited states to the ground state. The effects of the loss rates on the probability distribution for locating an exciton in the final triplet state T_N are illustrated in Figure 3.2.

Throughout this chapter, we will use fixed loss rates given by:

$$\gamma^S_{\text{loss}} = 1\,\text{ns}^{-1},$$
$$\gamma^T_{\text{loss}} = 1\,\mu\text{s}^{-1}.$$

These values were chosen as they reflect typical orders of magnitude observed in real molecular systems, making them appropriate for exploring exciton transport under realistic loss conditions.

3.3 Transition Time and Effective Rate

In a closed system, the transition time $\tau_{T_1 \to T_N}$ could be defined as the time required for the probability of the final triplet state T_N to reach its steady-state value. In contrast, in an open system, the probability of the final triplet state P_N will never reach the steady-state probability P^{ss}_N because of the loss rates γ^S_{loss} and γ^T_{loss}.

This introduces an important question: When decay rates to the ground state S_0 are present, when is the exciton considered to have successfully transitioned to the final triplet state T_N ? To answer this question, a comparison with the steady-state probabilities is still needed. However, because the probability $P_N(t)$ begins to decrease at a certain point, the maximum value ($P^{\max}_N$) will from now on be used as a measurement for

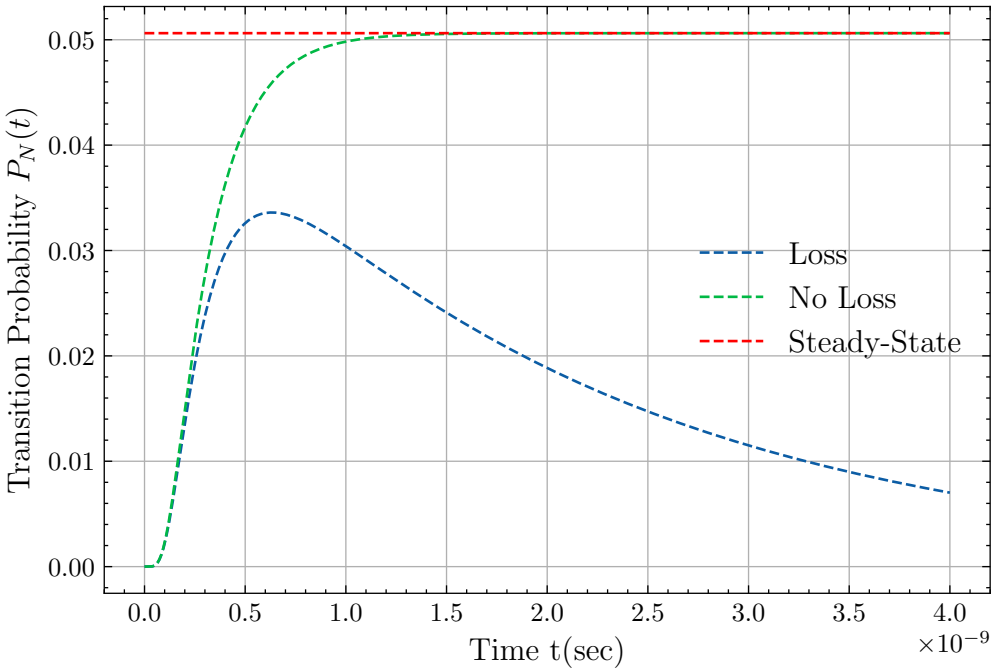

Figure 3.2: Probability $P_N(t)$ of locating an exciton in the final excited triplet state T_N as a function of time t, for a molecular wire of $N = 10$ molecules and an exciton initially located in the first excited triplet state T_1. The singlet-triplet energy gap was set to $\Delta E = 6.25 \times 10^{-4}$ eV. When loss to the ground state is not included (green dashed line), the probability approaches the steady-state distribution (red dashed line). In contrast, when decay to the ground singlet state is present (blue dashed line), the probability decreases over time, indicating that the exciton population is gradually lost before reaching the steady-state.

determining when a transition has successfully occurred.

For a successful transition to the final triplet state, it is required that $P_N(t)$ surpasses a certain threshold of the ratio $\frac{P_N^{\max}}{P_N^{ss}}$. This threshold is arbitrarily set at 0.5. If the maximum reached probability of the exciton being located in the final triplet state $P_N^{\max}$ is less than 50% of the steady-state probability P_N^{ss}, the transition from the initial triplet state T_1 to the final triplet state T_N is considered unsuccessful because of decay to the ground singlet state.

The main objective, then, is to study the transition time $\tau_{T_1 \to T_N}$, the maximum probability $P_N^{\max}$, and the probability ratio $\frac{P_N^{\max}}{P_N^{\text{ss}}}$, which compares the maximum probability of the final triplet state being occupied to its corresponding steady-state value. This analysis allows us to determine the conditions under which an exciton can successfully reach the final triplet state T_N before decaying to the ground state. Furthermore, it is important to investigate how the system parameters influence both the transition time and the probability ratio. The transition time is expected to increase, as the size of the molecular wire (N) increases because the exciton must transition through additional excited states before reaching the final triplet state. Therefore, the effects of the decay rates are expected to be more pronounced for larger systems and the maximum probability ratio $\frac{P_N^{\max}}{P_N^{\text{ss}}}$ is expected to decrease because of the increased chance of it decaying to the ground singlet state S_0 and never reaching the final triplet state. Thus, there is a molecular wire consisting of N molecules for which transitions to the final triplet state are highly unlikely to occur. Nonetheless, the probability and transition time are not solely dependent on N, but are, rather a multivariable functions depending on the transition rates between the adjacent singlet states $K_{S_i, S_{i\pm1}}$, as well as on the intersystem crossing and reverse intersystem crossing rate K_{S_i,T_i} and K_{T_i,S_i}, respectively.

Since there is no direct pathway connecting the excited triplet states T_1 and T_N, the transition must occur via the singlet channel. For this reason, we define an effective transition rate as:

$$K^{\text{eff}}_{T_1 \to T_N} = 1/\tau_{T_1 \to T_N} \tag{3.3}$$

This rate, quantifies the number of transitions that can occur within a given time frame, thereby providing useful insight into exciton transport in the system.
It would also be useful to have a measurement of how much probability is transferred during this transition. For this we define the effective probability rate as:

$$R^{\text{eff}} = \frac{\Delta P_N}{\tau_{T_1 \to T_N}} = \frac{P_N^{\max} - P_N(t=0)}{\tau_{T_1 \to T_N}} = \frac{P_N^{\max}}{\tau_{T_1 \to T_N}} \tag{3.4}$$

3.4 Results with Loss

3.4.1 Dependence on Molecular Wire Size N

We now examine how the size of the molecular wire affects both the transition probability $P_N^{\max}$ and the effective transition rate $K^{\text{eff}}_{T_1 \to T_N}$ of the exciton. Figure 3.3 shows the maximum probability of locating the exciton in the final triplet state T_N for different lengths N of molecular wires. The excited singlet and triplet states have an energy gap of $\Delta E = 0.1$ eV and the transition rates between adjacent excited singlet states and intersystem transitions are $K_{S_i, S_{i\pm1}} = 0.1$ ps^{-1} and $K_{S_i, T_i} = 0.1$ ps^{-1}, respectively. The energy gap and the transition rates used in Figure 3.3 were chosen in an attempt to mimic realistic conditions and determine the dependence of the maximum probability reached $P_N^{\max}$ on the size of the molecular wire N.

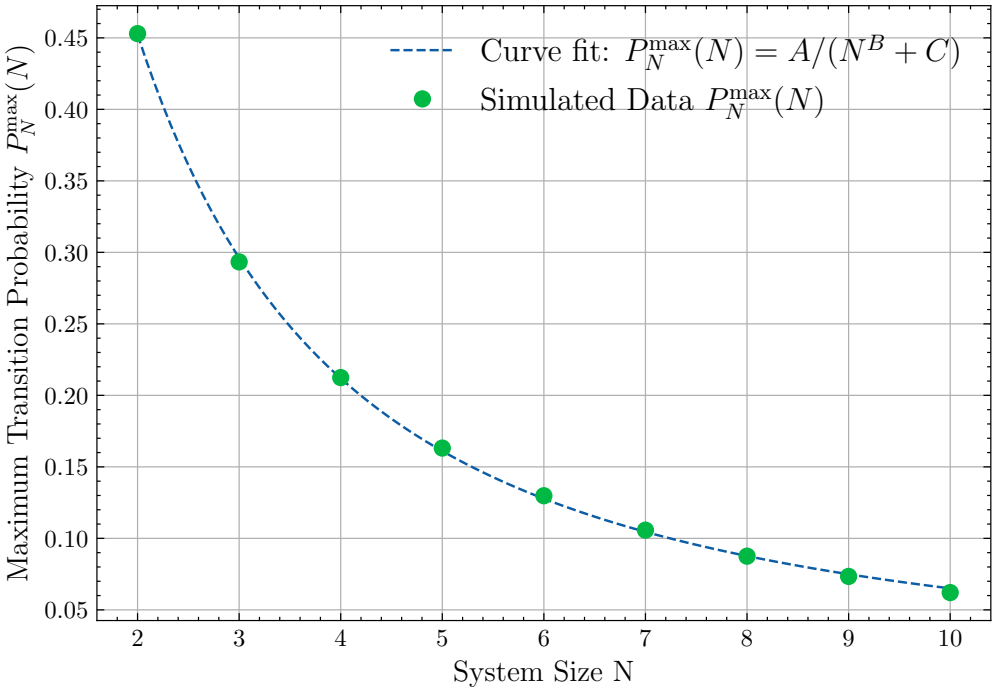

Figure 3.3: Maximum transition probability to the final triplet state $P_N^{\max}$ as a function of the molecular wire size N. The energy gap of the excited triplet and singlet state is $\Delta E = 0.1\,eV$ and the transition rates between adjacent excited singlet states and intersystem transitions are $K_{S_i, S_{i\pm1}} = 0.1$ ps^{-1} and $K_{S_i, T_i} = 0.1$ ps^{-1}, respectively. A non-linear least squares fit (blue dashed line) was performed on the simulated data to determine the dependence of $P_N^{\max}$ on N.

Based on the non-linear fit, the dependence of the maximum probability $P_N^{\max}$ on the size of the molecular system N is given by:

$$P_N^{\max}(N) = \frac{(1.772 \pm 0.128)}{N^{(1.415 \pm 0.036)} + (1.251 \pm 0.226)}$$

When the ground singlet state is included, the maximum probability $P_N^{\max}$ has a shifted power-like dependence on the size of the molecular wire N similar to the dependence observed when loss rates are absent. However, when loss rates are neglected, the probability reaches the steady-state probability and the dependence is $P_N(t \to \infty) \propto N^{-1}$. With loss rates present, the dependence on the size of the system becomes more pronounced due to the increased likelihood of decay before the exciton reaches the final triplet state.

Previously, when the loss rates were not taken into consideration, the probability of an exciton initially in the first triplet state T_1 reaching the final triplet state T_N approached the steady-state probability P_N^{ss} as $t \to \infty$. Because the steady-state probability depends only on the energies of the excited states and the size of the molecular wire, the probability of the final triplet state as $t \to \infty$ is independent of the initial probability distribution and the transition rates. In contrast, decay rates to the ground state cause the system to be sensitive to both the initial state in which the exciton resides and the rates that govern transitions between excited states. If the exciton is initially closer to the final triplet state T_N, fewer transitions are required to reach its destination which reduces the probability of decay before arriving.

The overall dependence of the effective transition rate $K_{T_1 \to T_N}^{\text{effective}}$ on the size of the molecular wire N is illustrated in Figure 3.4 and is similar to that of $P_N^{\max}$. Subsequently, the dependence on N is not constant but depends on the transition rates between excited states and on the energy gap between the excited singlet and triplet states.

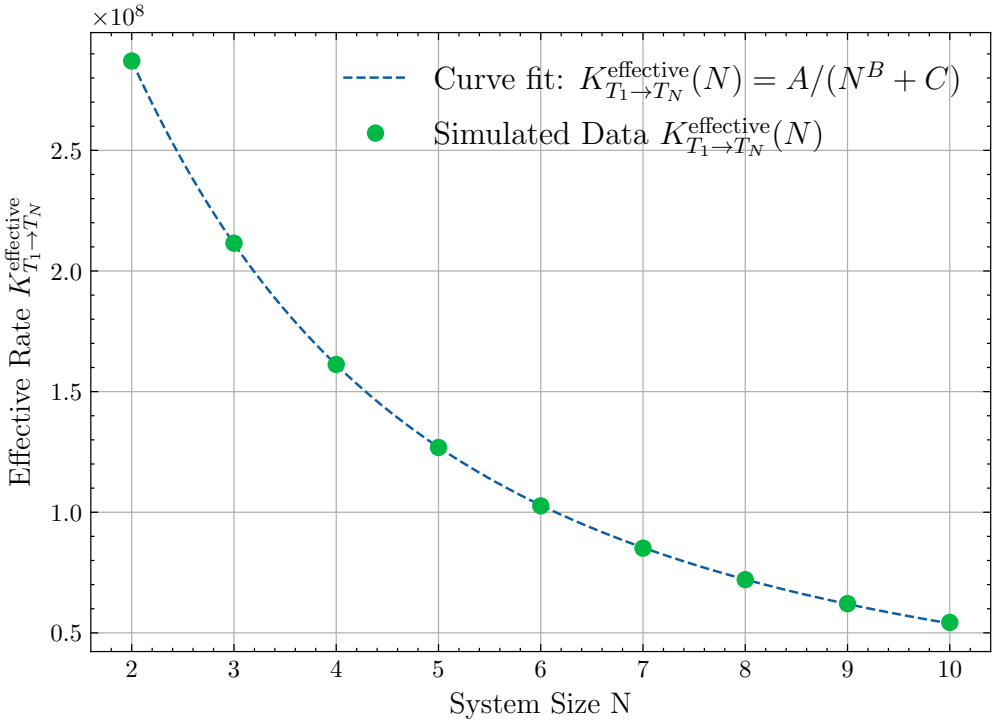

Figure 3.4: Effective transition rate to the final triplet state $K_{T_1 \to T_N}^{\text{effective}}$ as a function of the molecular wire size N. The energy gap of the excited triplet and singlet state is $\Delta E = 0.1$eV and the transition rates between adjacent excited singlet states and intersystem transitions are $K_{S_i, S_{i\pm1}} = 0.1$ ps^{-1} and $K_{S_i, T_i} = 0.1$ ps^{-1}, respectively. A non-linear least squares fit (blue dashed line) was performed on the simulated data to determine the dependence of $K_{T_1 \to T_N}^{\text{effective}}$ on N.

3.4.2 Energy Gap ΔE and Intersystem Transition Rate K_{S_i,T_i} Dependence

For a given transition intersystem crossing rate K_{S_i,T_i}, the reverse rate K_{T_i,S_i} is determined by the energy gap between the excited singlet and triplet states ΔE with the help of Equation 3.1. We now examine how the energy difference ΔE and the intersystem crossing rate from excited singlet to triplet states K_{S_i,T_i} affect the effective transition rate $K^{\text{eff}}_{T_1\to T_N}$ and the maximum probability of locating the exciton in the final triplet state $P_N^{\max}$.

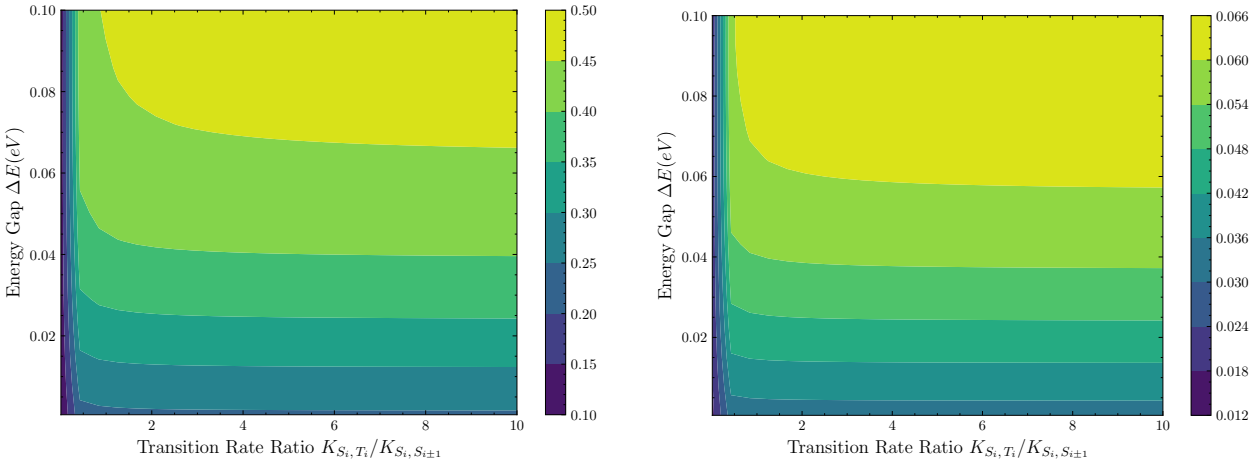

(a) Maximum Transition Probability Ratio $P_N^{\max}$ for a molecular wire consisting of $N = 2$ molecules.

(b) Maximum Transition Probability Ratio $P_N^{\max}$ for a molecular wire consisting of $N = 10$ molecules.

Figure 3.5: Contour plots of the maximum transition probability $P_N^{\max}$ for two different system sizes N. The probability $P_N^{\max}$ is plotted as a function of the singlet-triplet energy gap ΔE, and the intersystem crossing rate to the singlet-to-singlet transition rate, $K_{S_i,T_i}/K_{S_i,S_{i\pm1}}$. The singlet-to-singlet transition rate is fixed at $K_{S_i,S_{i\pm1}} = 0.1\ \text{ps}^{-1}$.

The steady-state probabilities of the excited states are governed by the Boltzmann distribution, as given by Equation (2.1). According to the distribution, a decrease in the energy of a state leads to an exponential increase in its equilibrium probability. In a closed system, where the total probability is conserved, an increase in the population of one state results in a decrease in the populations of the others. As the energy of the excited singlet states E_S decreases, thereby reducing the singlet-triplet energy gap ΔE, the steady-state probabilities of the excited singlet and triplet states are expected to increase and decrease, respectively. In an open system, where loss mechanisms are present, the probability of a particular state still tends toward its steady-state (Boltzmann) distribution, but fails to fully reach it due to population loss through decay pathways to the ground singlet state S_0. Its deviation from the Boltzmann distribution is determined by the magnitude of the decay rates. For an exciton initially in the first excited triplet state T_1, the maximum probability of transition to the final triplet state $P_N^{\max}$ is shown, for two system sizes, $N = 2$ and $N = 10$, in Figure 3.5. The probability $P_N^{\max}$ is plotted as a function of the energy difference between the singlet and triplet states ΔE, and the intersystem crossing rate to the singlet-to-singlet transition rate $K_{S_i,T_i}/K_{S_i,S_{i\pm1}}$. Figures 3.5a and 3.5b effectively illustrate that the maximum transition probability $P_N^{\max}$ of the final triplet state decreases with decreasing ΔE. Additionally, for the bigger system $N = 10$ the maximum probabilities are significantly smaller than the respective probabilities for the smaller system $N = 2$. This is attributed to the distribution of probability among the different states of the system according to their energies. These results are consistent with the expected redistribution of population away from the triplet states as the singlet-triplet energy gap ΔE decreases and the size of the system N increases. This suggests that increasing the energy gap ΔE initially leads to a higher maximum transition probability. However, a larger energy gap also results in a slower reverse intersystem crossing (ISC) rate. Beyond a certain threshold, the reverse ISC becomes so inefficient that exciton population is increasingly lost to the ground singlet state S_0, causing a decline in transport efficiency. As shown in Figure 3.6, when ΔE becomes sufficiently large, the maximum

transition probability $P_N^{\max}$ begins to decrease.

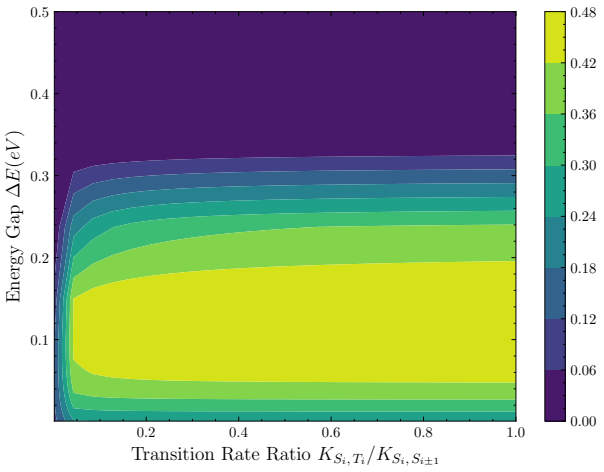

(a) Maximum Transition Probability Ratio $P_N^{\max}$ for a molecular wire consisting of $N = 2$ molecules.

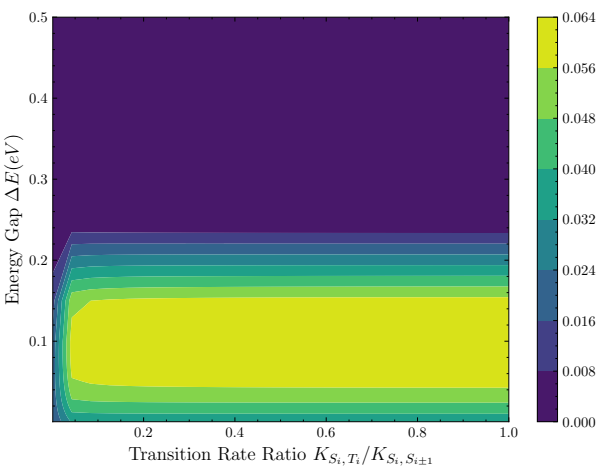

(b) Maximum Transition Probability Ratio $P_N^{\max}$ for a molecular wire consisting of $N = 10$ molecules.

Figure 3.6: Contour plots of the maximum transition probability $P_N^{\max}$ for two different system sizes N. The probability $P_N^{\max}$ is plotted for a larger range of singlet-triplet energy gap vaalues ΔE. The contour plots are also a function of the intersystem crossing rate to the singlet-to-singlet transition rate, $K_{S_i,T_i}/K_{S_i,S_{i\pm1}}$. The singlet-to-singlet transition rate is fixed at $K_{S_i,S_{i\pm1}} = 0.1$ ps^{-1}.

For a transition rate $K_{S_i,\,S_{i\pm1}} = 0.1$ ps^{-1} between adjacent singlet states in a system of $N = 10$ molecules, the maximum transition probability ratio $P_N^{\max}/P_N^{\text{ss}}$ and the effective transition rate $K_{T_1\to T_N}^{\text{effective}}$ of an exciton reaching the final triplet state are shown in Figure 3.7 for different energy gaps ΔE between excited singlet and triplet states and intersystem crossing rates $K_{S_i,\,T_i}$. Figure 3.7a illustrates that $P_N^{\max}/P_N^{\text{ss}}$ does not experience substantial changes as the energy difference decreases. This is crucial because it means that the success of a transition does not strongly depend on the energy gap between the singlet and triplet states. Moreover, in this particular case, the maximum probability ratio surpasses the defined threshold of 0.5 for all the parameter combinations, indicating successful transitions across all energy gap and intersystem crossing rate values. In contrast, the effective transition rate increases as the energy gap decreases. As ΔE decreases, the reverse intersystem crossing rate $K_{T_i,\,S_i}$ increases. This improves the transitioning as it allows excitons to quickly transition from the excited triplet states T_i to the excited singlet states S_i.

The intersystem crossing rate affects the maximum probability $P_N^{\max}$ and the effective transition rate $K_{T_1\to T_N}^{\text{eff}}$ only when the ratio of the isc rate over the singlet-to-singlet rate is smaller than 1, that is, $K_{S_i,\,T_i}/K_{S_i,\,S_{i\pm1}} \leq 1$. Figure 3.5 illustrates that independent of the size N of the system, when the intersystem crossing rate is equal to or greater than the singlet-to-singlet transition rate a saturation in the maximum probability $P_N^{\max}$ occurs. This is also true for the effective transition rate $K_{T_1\to T_N}^{\text{eff}}$ (see Figure 3.7b). Increasing the intersystem crossing rate does not significantly impact the overall exciton transition if the singlet-to-singlet transition rate is faster than the intersystem crossing rate. Intuitively, since our goal is to utilize the faster singlet channel, one might expect that the exciton will require more time to reach the final triplet state as the intersystem crossing rate becomes larger than the singlet-to-singlet transition rate because it will rapidly transition out of the singlet manifold. However, by increasing the intersystem crossing rate the reverse rate is also increased and the exciton transitions faster out of the triplet manifold and into the singlet one which aids its overall transition towards reaching the final triplet state.

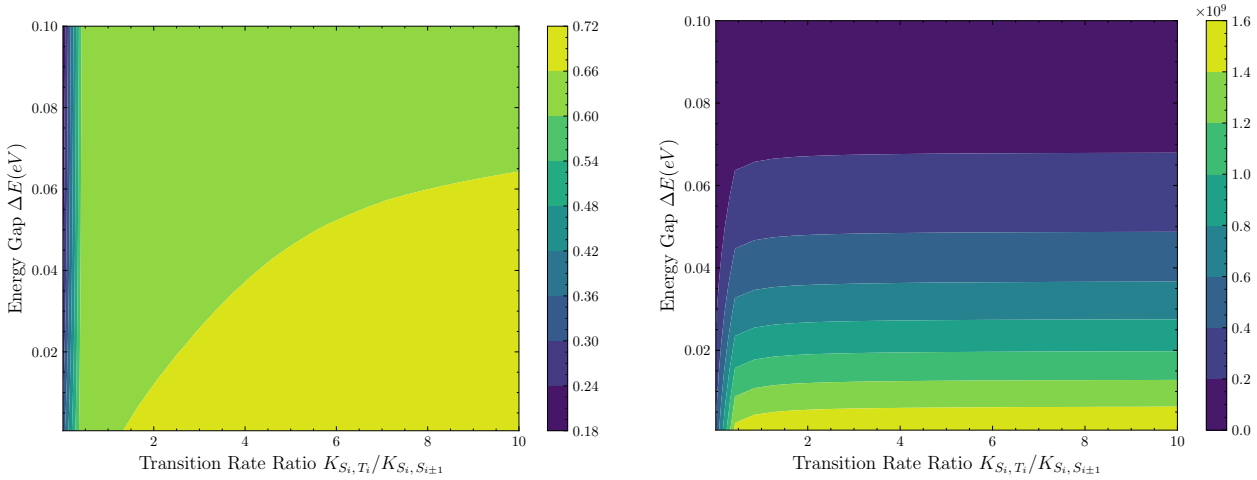

(a) Maximum Transition Probability Ratio $P_N^{\max}/P_N^{\text{ss}}$

(b) Effective Transition Rate $K_{T_1\to T_N}^{\text{effective}}$ (s^{-1})

Figure 3.7: Contour plots of the maximum probability ratio $P_N^{\max}/P_N^{\text{ss}}$ and the effective transition rate $K_{T_1\to T_N}^{\text{effective}}$ of the exciton reaching the final triplet state T_N for different energy gap values between excited triplet and singlet states ΔE along with different intersystem transition rates $K_{S_i,\,T_i}$. Figure 3.7a shows the maximum probability ratio $P_N^{\max}/P_N^{\text{ss}}$ of locating the exciton in the final triplet state T_N compared to the steady-state value when there are no decay rates to the ground singlet state. Figure 3.7b, illustrates the effective transition rate $K_{T_1\to T_N}^{\text{effective}}$. The molecular bridge consists of $N = 10$ molecules and transition rate between adjacent excited singlet states is $K_{S_i,\,S_{i\pm1}} = 0.1$ ps^{-1}.

3.4.3 Singlet-to-Singlet Transition Rate $K_{S_i,S_{i\pm1}}$ Dependence

To further understand under what conditions the use of the singlet channel improves exciton transport from T_1 to T_N, we now investigate its dependence on the transition rate between adjacent excited singlet states $K_{S_i,S_{i\pm1}}$. One might think that the answer is straightforward: The best results would be achieved for the fastest singlet-to-singlet transition rate. However, we attempt to examine if this is indeed true, and whether there exists a parameter region where optimal transitioning occurs.

To quantify the effect of the singlet channel in exciton transport, we simulated systems of size N with a fixed ISC transition rate K_{S_i,T_i}. These simulations were performed for various singlet-to-singlet transition rates $K_{S_i,S_{i\pm1}}$ to evaluate their influence on the maximum probability of transition $P_N^{\max}$ and the energy gap between singlet and triplet states ΔE.

First, we want to determine the effect that the system size N has on the transition probability $P_N^{\max}$ when the singlet-to-singlet transition rate $K_{S_i,S_{i\pm1}}$ varies. Figure 3.8 illustrates the maximum transition probability for two different system sizes $N = 2$ and $N = 10$, as a function of the energy gap ΔE and the singlet-to-singlet transition rate $K_{S_i,S_{i\pm1}}$. As we discussed previously, the intersystem crossing rate does not influence the system after a certain threshold. Therefore, the simulations were performed for a fixed ISC rate of $K_{S_i,T_i} = 1$ ps^{-1}. Figures 3.8a and 3.8b show that, as the size of the system increases, the influence of the singlet transition rate $K_{S_i,S_{i\pm1}}$ becomes more pronounced. For the smaller system ($N = 2$), the maximum probability $P_N^{\max}$ reaches a plateau as the singlet-to-singlet transition rate is increased. In this case, only four excited states exist, two triplet and two singlet states. As a result, once the exciton transitions to the singlet channel, it only needs to hop once to reach the final molecule before returning to the triplet manifold and thus reaching its destination. The best results, i.e., the highest value of $P_N^{\max}$ is achieved when the energy gap is larger than $\Delta E = 0.05$ eV, and the singlet-to-singlet rate is fastest.

To determine the influence of the singlet-to-singlet transition rate on the effective rate when loss mechanisms are taken into consideration, the larger molecular wire consisting of $N = 10$ molecules was examined. Fig-

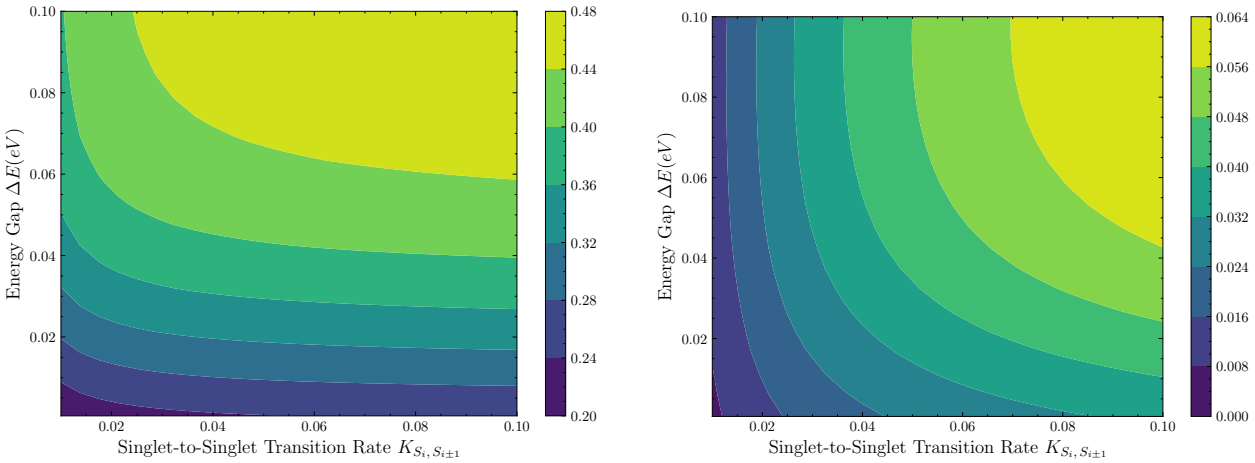

(a) Maximum Transition Probability $P_N^{\max}$ for $N = 2$

(b) Maximum Transition Probability $P_N^{\max}$ for $N = 10$

Figure 3.8: Contour plots of the maximum transition probability $P_N^{\max}$, shown as a function of the energy gap ΔE, and the singlet-to-singlet transition rate $K_{S_i,S_{i+1}}$ for two different system sizes. The intersystem crossing rate between excited singlet and triplet state is fixed at $K_{S_i,T_i} = 1$ ps^{-1}.

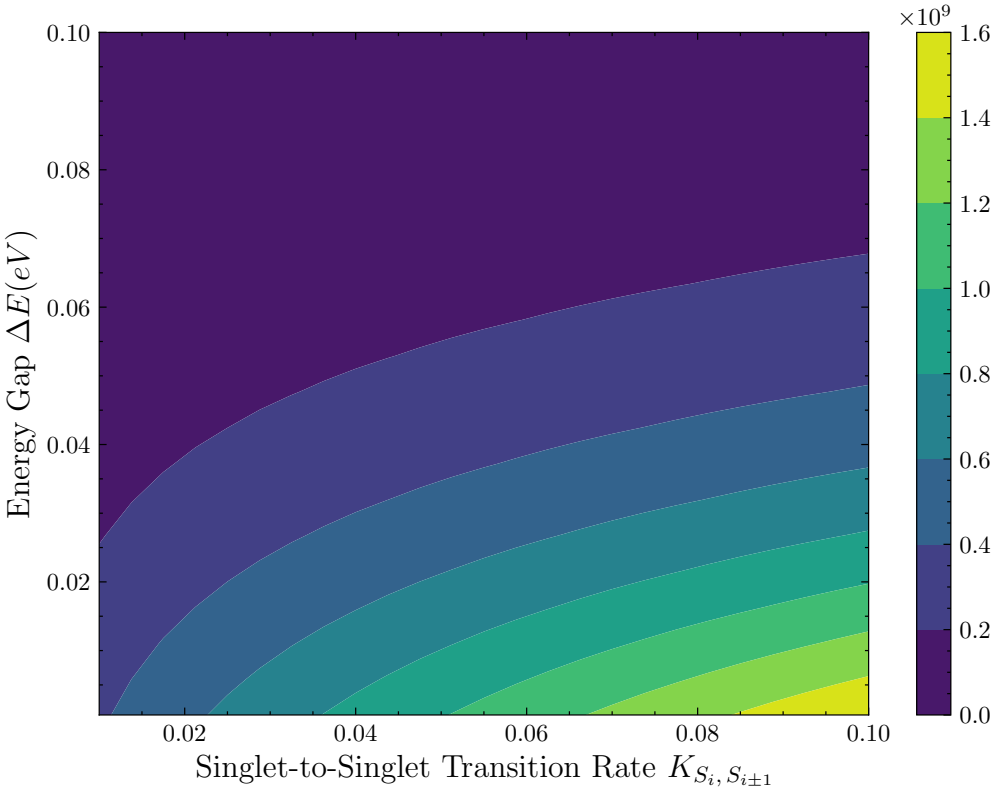

Figure 3.9: Contour plot of the effective transition rate $K^{\text{eff}}_{T_1\to T_N}(\text{s}^{-1})$ as a function of the energy gap ΔE and the singlet transition rate $K_{S_i,S_{i\pm1}}$. The system consists of $N = 10$ molecules, and the intersystem crossing rate is $K_{S_i,T_i} = 1$ ps^{-1}.

ure 3.9 illustrates the effective transition rate $K^{\text{effective}}_{T_1\to T_N}$ as a function of the energy gap ΔE between excited singlet and triplet states, and the transition rate between adjacent singlet states $K_{S_i,S_{i\pm1}}$. The intersystem

crossing rate is $K_{S_i,T_i} = 1$ ps^{-1}. For a fixed intersystem crossing rate K_{S_i,T_i}, the energy gap affects the reverse intersystem crossing rate K_{T_i,S_i}. More precisely, K_{T_i,S_i} decreases exponentially with increasing ΔE. Therefore, for large energy gaps, the exciton transitions very slowly from the triplet manifold to the singlet one and increasing the singlet-to-singlet transition rate does not seem to benefit the effective transition rate $K^{\text{eff}}_{T_1 \to T_N}$. Thus, efficient transition to the final triplet state T_N is achieved when the energy gap is smaller than the thermal energy $k_B T$ at room temperature ($\Delta E \leq 0.025$ eV) and when the transition rate $K_{S_i,S_{i\pm1}}$ is at its maximum.

3.4.4 Effective Probability Rate R^{eff}

Earlier in Equation (3.4), we defined the effective probability rate R^{eff} as the rate at which population accumulates in the final triplet state T_N during the characteristic transition time $\tau_{T_1 \to T_N}$. This measure better represents the effectiveness of a transition as it combines the maximum transition probability $P_N^{\max}$ and the effective transition time $\tau_{T_1 \to T_N}$. As such, it offers a more complete evaluation of exciton transport performance. In this section, we examine how the effective probability rate is influenced by the size of the molecular wire N, the singlet-triplet energy gap ΔE, the intersystem crossing rate K_{S_i,T_i} and the singlet-to-singlet transition rate $K_{S_i,S_{i\pm1}}$. Finally, similar to the effective transition rate, we aim to identify the parameter regions where optimal exciton transport occurs.

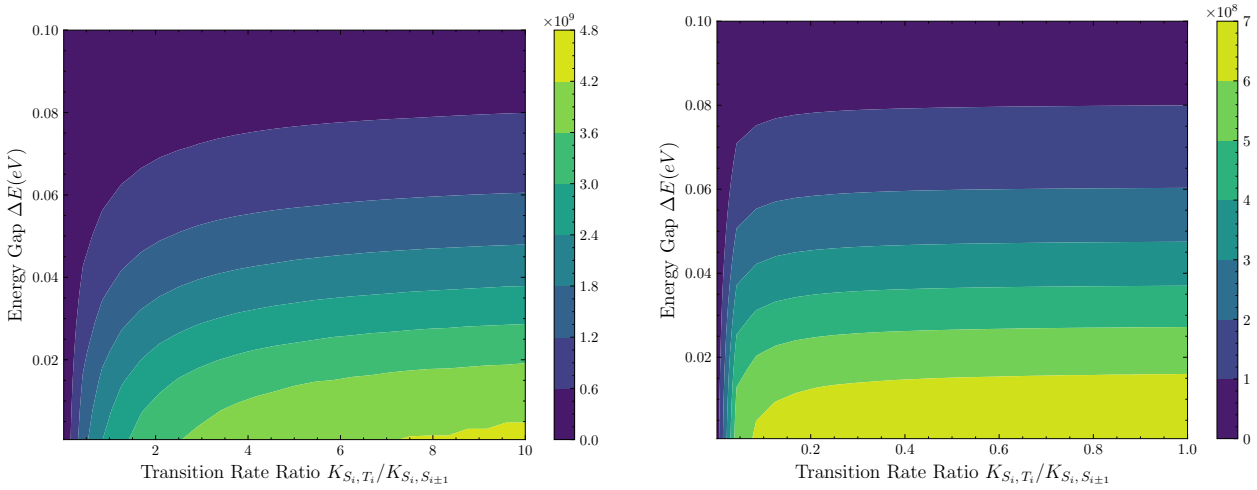

(a) Effective Probability Rate R^{eff} for singlet-to-singlet transition rate of $K_{S_i,S_{i\pm1}} = 0.1$ ps^{-1}.

(b) Effective Probability Rate R^{eff} (s^{-1}) for singlet-to-singlet transition rate of $K_{S_i,S_{i\pm1}} = 0.01$ ps^{-1}.

Figure 3.10: Contour plots showing the effective probability rate R^{eff} (s^{-1}) for a system consisting of $N = 2$ molecules with two different singlet-to-singlet transition rates $K_{S_i,S_{i\pm1}}$. The effective probability rate is a function of the energy difference ΔE between singlet and triplet states and the ratio of the intersystem crossing rate over the singlet-to-singlet transition rate $K_{S_i,T_i}/K_{S_i,S_{i\pm1}}$.

Figures 3.10 and 3.11, illustrate the effective probability rate R^{eff} at two different system sizes, $N = 2$ and $N = 10$. As a first observation, the best results for each system size are achieved when the singlet-to-singlet transition rate is fastest, that is, $K_{S_i,S_{i\pm1}} = 0.1$ ps^{-1}. Furthermore, as the size of the system is increased, a smaller fraction of the population reaches the final triplet state T_N within the transition time $\tau_{T_1 \to T_N}$. This behavior is expected, since for the larger system ($N = 10$), an exciton will need to undergo a larger number of transitions before reaching its destination, therefore increasing the probability of decay to the ground state before arriving. The probability rate seems to become largely independent of the ISC rate K_{S_i,T_i} once it exceeds a certain threshold of the singlet-to-singlet rate $K_{S_i,S_{i\pm1}}$. For the larger system $N = 10$ the saturation of R^{eff} with respect to the intersystem crossing rate occurs when $K_{S_i,T_i} \geq K_{S_i,S_{i\pm1}}$ (i.e., $K_{S_i,T_i}/K_{S_i,S_{i\pm1}} \geq 1$). However, the smaller system $N = 2$ is more sensitive to the intersystem crossing rate K_{S_i,T_i} and increasing it

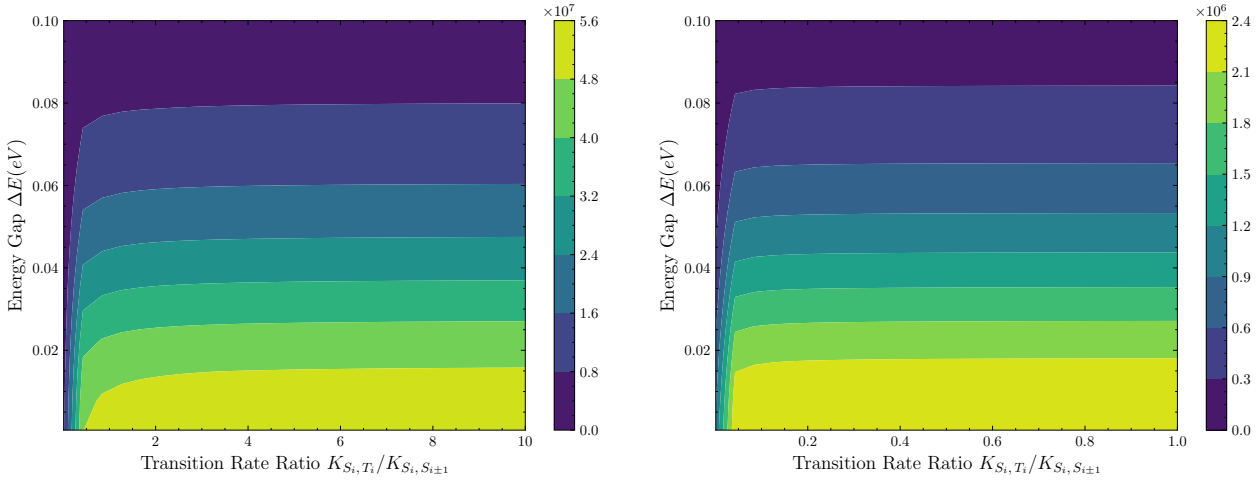

(a) Effective Probability Rate R^{eff} (s^{-1}) for singlet-to-singlet transition rate of $K_{S_i,S_{i\pm1}} = 0.1$ ps^{-1}.

(b) Effective Probability Rate R^{eff} (s^{-1}) for singlet-to-singlet transition rate of $K_{S_i,S_{i\pm1}} = 0.01$ ps^{-1}.

Figure 3.11: Contour plots showing the effective probability rate R^{eff} (s^{-1}) for a system consisting of $N = 10$ molecules with two singlet-to-singlet transition rates $K_{S_i,S_{i\pm1}}$. The effective probability rate is a function of the energy difference ΔE between singlet and triplet states and the ratio of the intersystem crossing rate over the singlet-to-singlet transition rate $K_{S_i,T_i}/K_{S_i,S_{i\pm1}}$.

leads to a slightly faster transition until $K_{S_i,T_i}/K_{S_i,S_{i\pm1}} \geq 10$. Lower singlet-triplet energy gaps ΔE reduce the steady-state probability distribution of the excited triplet states and thus result in a lower maximum transition probability $P_N^{\max}$, as shown in Figure 3.5. This would suggest a corresponding decrease in the probability rate R^{eff} as ΔE decreases. However, as ΔE decreases, the reverse intersystem crossing rate K_{T_i,S_i} increases significantly, allowing excitons that are in the triplet manifold to quickly transition to the faster singlet manifold. This accelerates the overall transfer and yields higher values of R^{eff}.

3.4.5 Inclusion of a Triplet Trap

We now examine exciton transport when the final triplet state T_N acts as a trap. More precisely, the energy of T_N is lowered by ΔE_{trap} which significantly reduces the reverse intersystem crossing rate to the final singlet state S_N, and thus, traps the flowing population. A schematic diagram for this system is shown in Figure 3.12. Loss mechanisms to the ground singlet state S_0 are included, and transitions between adjacent triplet states are forbidden. The triplet trap not only influences the reverse ISC rate, but it also impacts the steady-state probability of the final triplet state P_N^{ss}. The energy of the trap was set to $\Delta E_{\text{trap}} = 0.5$ eV, and from Equation (2.1) the steady-state probability of T_N is:

$$P_N^{ss} = \frac{1}{Z} e^{(\Delta E_{\text{trap}}/k_B T)} = \frac{e^{20}}{(N-1) + N e^{-E_S/k_B T} + e^{20}} \Rightarrow P_N^{ss} \approx 1$$

where Z is the partition function and E_S is the energy level of the excited singlet states. Since all triplet states have energy $E_T = 0$, and all excited singlet states have higher energies, the contribution of these states to the partition function is negligible. As a result, the steady-state probability of the final triplet state is approximately equal to unity.

The inclusion of a triplet trap is expected to improve exciton transport efficiency even when loss rates are included since more population is expected to flow into T_N and the accumulated population can only leave the site through decay to the ground state. In this section, we will determine if the placement of a triplet trap improves transport, if so, to quantify the resulting improvement in the effective transition rate $K_{T_1 \to T_N}^{\text{eff}}$ and the effective probability rate R^{eff}.

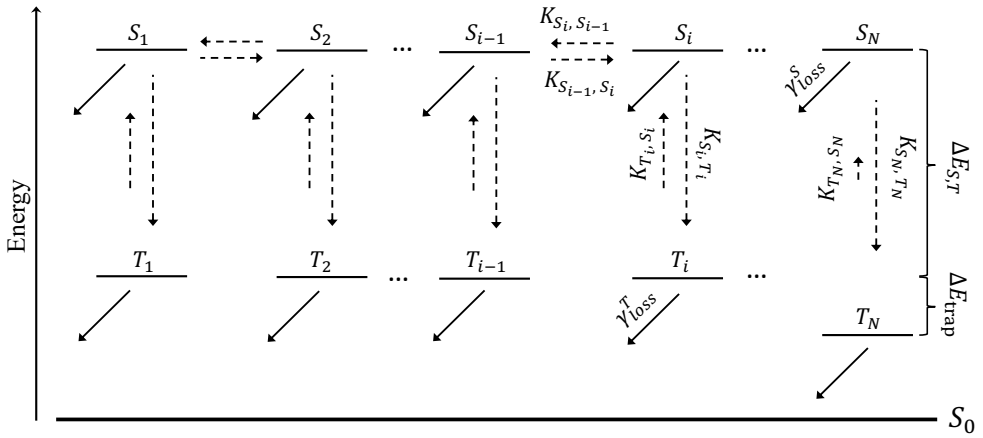

Figure 3.12: Schematic diagram of the molecular wire consisting of N excited singlet and triplet states when the ground singlet state S_0 is included. Because the final triplet state T_N lies ΔE_{trap} below the other triplet states, the reverse intersystem crossing rate is reduced, effectively trapping the exciton at T_N. Transition rates between excited states are represented by dashed arrows and solid arrows represent the irreversible transitions from excited singlet and triplet states to the ground singlet state S_0. When two opposing arrows differ in length, it indicates that the forward and reverse transition rates are unequal. In contrast, equal-length arrows signify that the corresponding transition rates are equal.

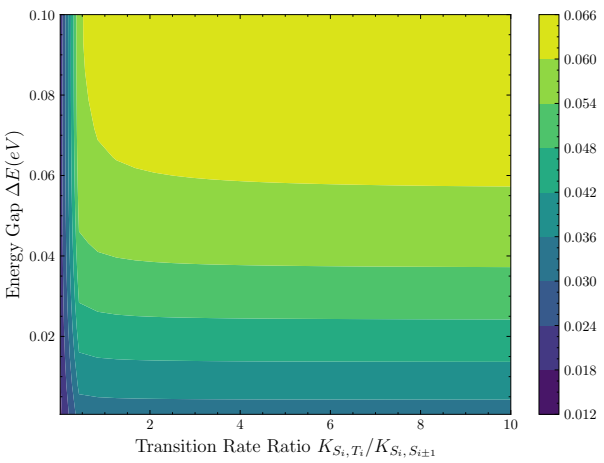

(a) Maximum Transition Probability $P_N^{\max}$ for $N = 10$ without triplet trap.

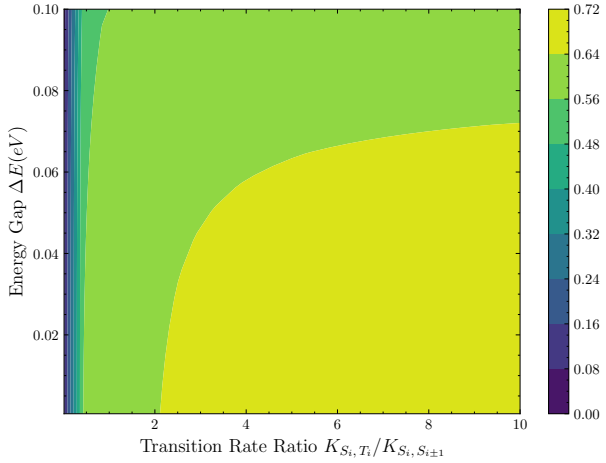

(b) Maximum Transition Probability $P_N^{\max}$ for $N = 10$ with triplet trap.

Figure 3.13: Contour plots of the maximum transition probability $P_N^{\max}$ as a function of the energy gap ΔE and the ratio $K_{S_i,T_i}/K_{S_i,S_{i+1}}$. Figure (a) shows the case without a trap, and Figure (b) includes a triplet trap on the final triplet state T_N with $\Delta E_{\text{trap}} = -0.5$ eV. In both cases, the singlet-to-singlet transition rate is $K_{S_i,S_{i\pm1}} = 0.1$ ps^{-1}

We begin by examining the maximum transition probability $P_N^{\max}$ of the exciton for a system of $N = 10$ molecules. Figure 3.13 compares the maximum probability with and without a trap on the final triplet state T_N. When the final triplet state is set as a trap, the probability reaches a significantly higher value. However, when the final triplet state has the same energy as the other triplet states, the probability distribution follows the Boltzmann distribution and therefore probability is distributed among the system according to the

energy of each state. Hence, comparing the maximum probability with the steady-state probability might provide further insight on how loss mechanisms and the placement of a trap affect transport. Figure 3.14a and Figure 3.14b show that when the maximum probability ratio $P_N^{\max}/P_N^{ss}$ is examined, the results do not improve when the final triplet state is a trap. This result indicates that the increased probability $P_N^{\max}$ for the trap case, is entirely due to the change of the steady-state probability. We showed earlier that for the trap case $P_N^{ss} \approx 1$ and therefore $P_N^{\max}/P_N^{ss} \approx P_N^{\max}$.

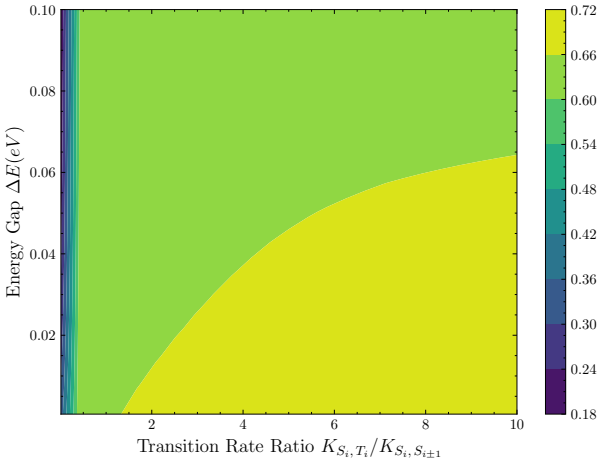

(a) Maximum Probability Ratio $P_N^{\max}/P_N^{ss}$ for $N = 10$ without triplet trap.

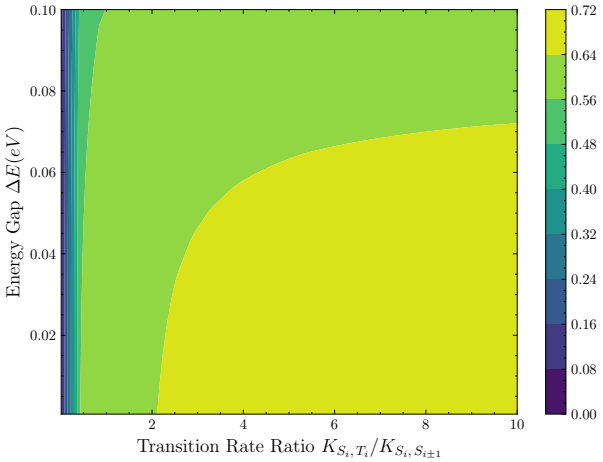

(b) Maximum Transition Probability $P_N^{\max}$ for $N = 10$ with triplet trap.

We now proceed to examine the effective transition rate $K^{\text{eff}}_{T_1 \to T_N}$ and the effective probability rate R^{eff} when a triplet trap is utilized. When a triplet trap is placed, the maximum probability $P_N^{\max}$ is ten times higher than when all the triplet states have the same energy, as illustrated in Figure 3.13. As a result, more time is required for that probability to accumulate to the final triplet state, which reduces the effective transition rate $K^{\text{eff}}_{T_1 \to T_N}$. Figure 3.14 shows that the effective transition rate is reduced by a factor of four when the final triplet state acts as a trap. Figure 3.15 shows that R^{eff} is approximately five times higher for the trap case. This is attributed to the significantly greater population that accumulates in the trap state. Thus, a triplet trap significantly increases the maximum transition probability $P_N^{\max}$ but requires a longer transition time $\tau_{T_1 \to T_N}$ to do so. However, the effective probability rate R^{eff} indicates that a triplet trap enhances transfer efficiency to T_N.

Finally, we examined a larger molecular wire consisting of $N = 20$ molecules. Figure 3.16 presents the results for the maximum transition probability $P_N^{\max}$ and the effective probability rate R^{eff}. As the system size increases, the exciton population reaching the final triplet site T_N decreases significantly. For $N = 20$, only about 20–28% of the exciton population arrives at T_N, even under favorable conditions. This trend suggests that as the number of molecular sites continues to grow, the maximum transition probability will eventually approach zero due to losses and the increased number of transitions required.

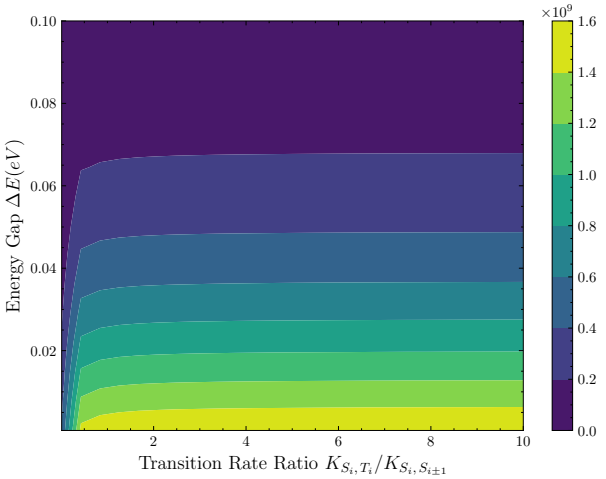

(a) Effective Transition Rate $K^{\text{eff}}_{T_1 \to T_N}$ (s^{-1}) for $N = 10$ without a triplet trap.

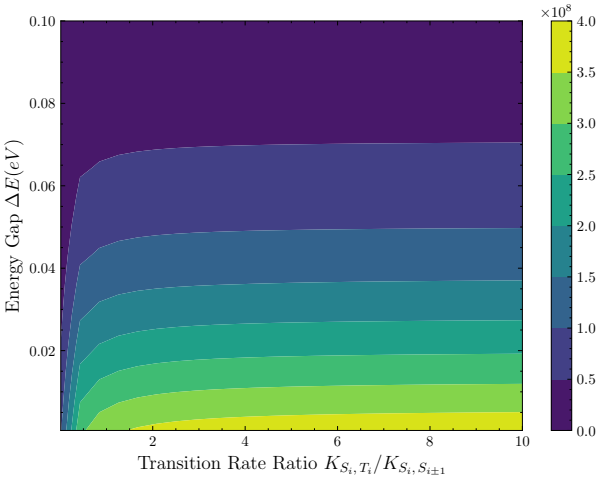

(b) Effective Transition Rate $K^{\text{eff}}_{T_1 \to T_N}$ (s^{-1}) for $N = 10$ with a triplet trap at T_N.

Figure 3.14: Contour plots of the effective probability rate R^{eff} as a function of the energy gap ΔE and the ratio $K_{S_i,T_i}/K_{S_i,S_{i\pm1}}$. Figure (a) shows the case without a trap, and Figure (b) includes a triplet trap on the final triplet state T_N with $\Delta E_{\text{trap}} = -0.5$ eV. In both cases, the singlet-to-singlet transition rate is $K_{S_i,S_{i\pm1}} = 0.1$ ps^{-1}.

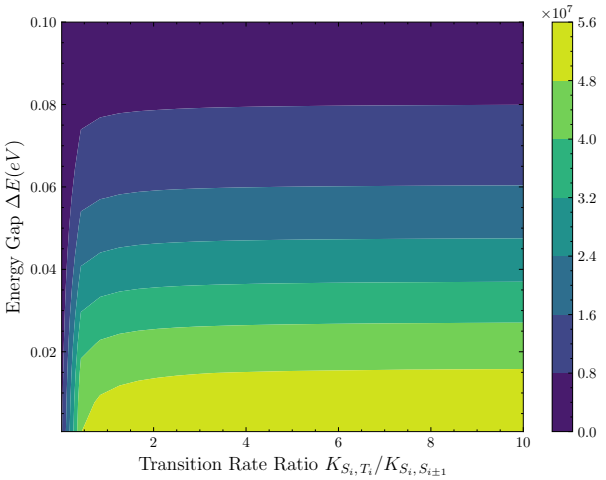

(a) Effective Probability Rate R^{eff} (s^{-1}) for $N = 10$ without a triplet trap.

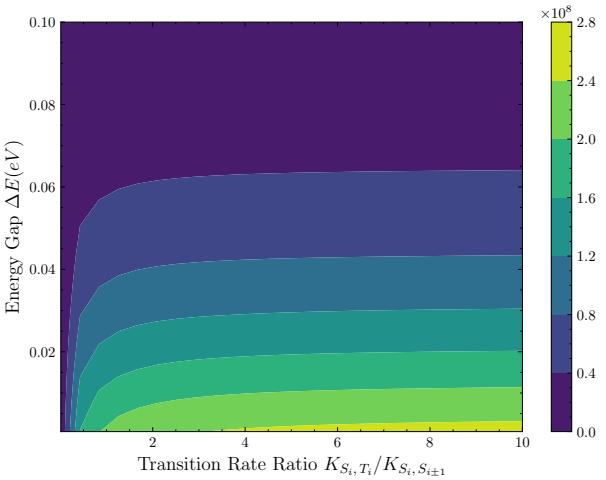

(b) Effective Probability Rate R^{eff} (s^{-1}) for $N = 10$ with a triplet trap at T_N.

Figure 3.15: Contour plots of the effective probability rate R^{eff} as a function of the energy gap ΔE and the ratio $K_{S_i,T_i}/K_{S_i,S_{i\pm1}}$. Figure (a) shows the case without a trap, and Figure (b) includes a triplet trap on the final triplet state T_N with $\Delta E_{\text{trap}} = -0.5$ eV. In both cases, the singlet-to-singlet transition rate is $K_{S_i,S_{i\pm1}} = 0.1$ ps^{-1}.

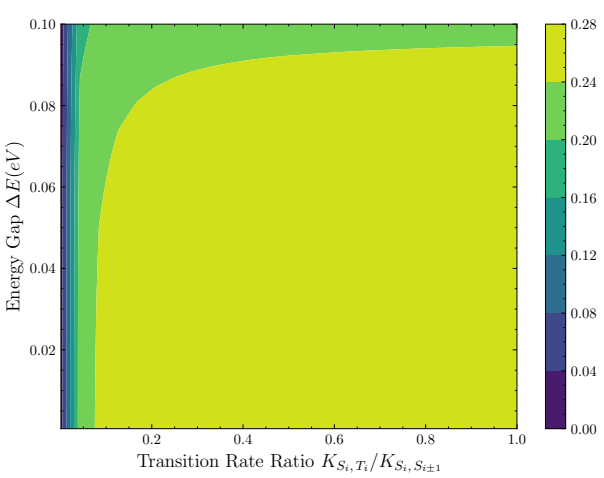

(a) Maximum Transition Probability $P_N^{\max}$ for $N = 20$ with a triplet trap at T_N.

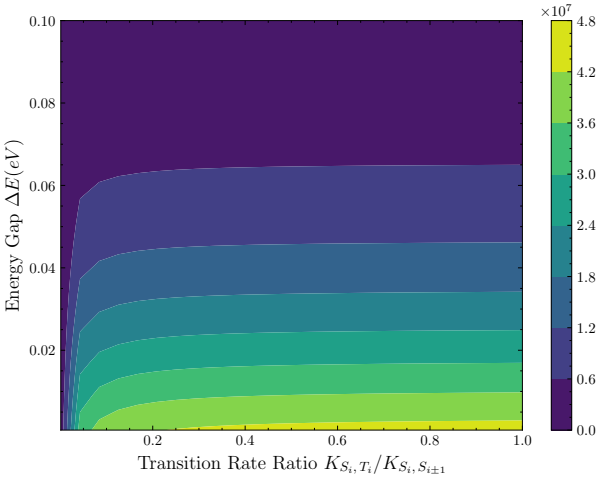

(b) Effective Probability Rate R^{eff} (s^{-1}) for $N = 20$ with a triplet trap at T_N.

Figure 3.16: Contour plots of (a) the maximum transition probability $P_N^{\max}$ and (b) the effective probability rate R^{eff} (s^{-1}) as a function of the energy gap ΔE and the ratio $K_{S_i,T_i}/K_{S_i,S_{i\pm1}}$. In both cases, the singlet-to-singlet transition rate is $K_{S_i,S_{i\pm1}} = 0.1$ ps^{-1}.

3.5 Conclusion

In this chapter, we examined exciton transport in a molecular wire consisting of N molecules with realistic loss to the ground singlet state S_0. This introduced the challenge of identifying a successful transition from T_1 to T_N. More precisely, if the molecular wire was too long, or if transition rates were slow compared to the decay rates, the exciton population fell to S_0 before arriving at T_N. To quantify the conditions for efficient transport from T_1 to T_N, we examined three metrics: the maximum probability $P_N^{\max}$; the effective transition rate $K_{T_1 \to T_N}^{\text{eff}}$; and the effective probability rate R^{eff}, which combines the first two metrics. In real molecules, loss mechanisms to the ground singlet state S_0 are always present. Therefore, it is crucial to exploit all possible techniques to enable efficient transfer of excitons from T_1 to T_N. In what follows, we summarize our results and conclusions for the case involving a triplet trap at the final triplet site.

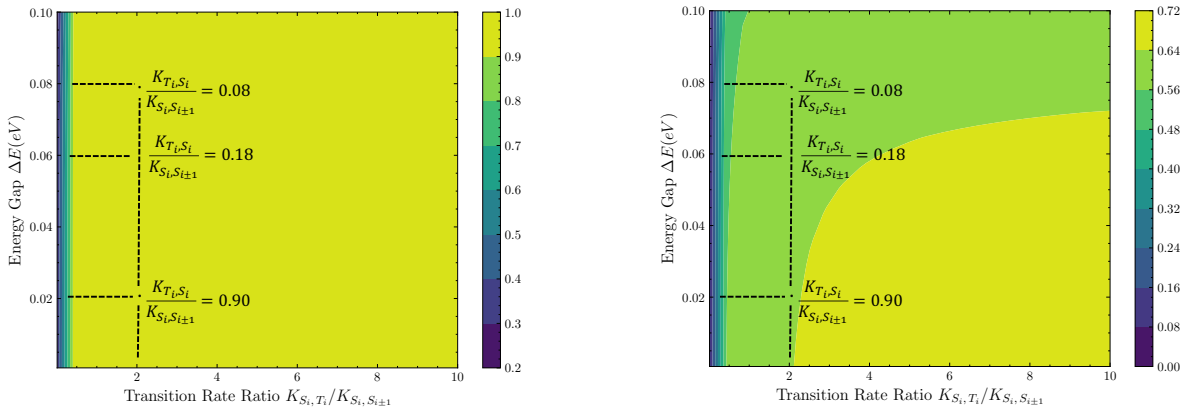

(a) Maximum Transition Probability $P_N^{\max}$ for a molecular wire consisting of $N = 2$ molecules.

(b) $P_N^{\max}$ for a molecular wire consisting of $N = 10$ molecules.

Figure 3.17: Contour plots showing the maximum transition probability $P_N^{\max}$ for molecular wires consisting of $N = 2$ (a) and $N = 10$ (b) molecules. The probability is plotted as a function of the energy difference ΔE between singlet and triplet states, and the ratio of intersystem crossing to singlet-to-singlet transfer rates, $K_{S_i,T_i}/K_{S_i,S_{i\pm1}}$. Blacked dashed lines indicate fixed values of the reverse intersystem crossing (ISC) rate K_{T_i,S_i}, shown relative to the singlet-to-singlet transition rate $K_{S_i,S_{i\pm1}}$, to illustrate how changes in ΔE affect the probability of transport to T_N. The singlet-to-singlet transition rate is $K_{S_i,S_{i\pm1}} = 0.1\ \text{ps}^{-1}$.

Figures 3.17 and 3.18 illustrate once again the maximum transition probability $P_N^{\max}$ and the effective probability rate R^{eff} for $N = 2$ and $N = 10$. In this case, black and white dashed lines have been added to show how the reverse intersystem crossing (ISC) rate K_{T_i,S_i} varies with changes in the energy gap ΔE. For a fixed forward rate ratio of $K_{S_i,T_i}/K_{S_i,S_{i\pm1}} = 2$, we observe that the reverse rate ratio $K_{T_i,S_i}/K_{S_i,S_{i\pm1}}$ decreases by approximately one order of magnitude as the energy gap increases from $\Delta E = 0.02\,\text{eV}$ to $\Delta E = 0.08\,\text{eV}$. This demonstrates that as the energy gap increases, the rate at which excitons transition from the triplet to the singlet manifold is significantly reduced, resulting in a lower effective probability rate R^{eff}.

The maximum transition probability $P_N^{\max}$, however, is less affected by the reverse ISC rate, as it primarily influences the transition time rather than the final arrival probability. Moreover, when the exciton resides in the triplet manifold, its decay to the ground state is governed by the phosphorescence rate γ_{loss}^T, which is significantly slower than the fluorescence rate γ_{loss}^S. As a result, population loss to the ground singlet state S_0 occurs more slowly from the triplet manifold.

A system consisting of just two molecules ($N = 2$) is considered very small. Therefore, we now turn our

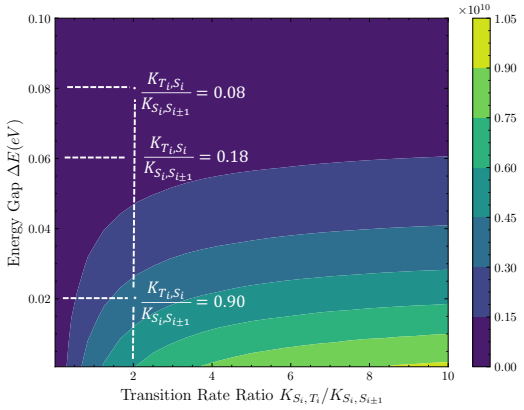

(a) Effective Probability Rate R^{eff} (ps^{-1}) for a molecular wire consisting of $N = 2$ molecules.

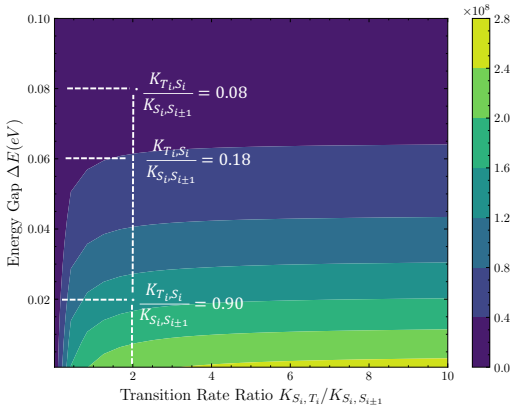

(b) Effective Probability Rate R^{eff} (ps^{-1}) for a molecular wire consisting of $N = 10$ molecules.

Figure 3.18: Contour plots showing the effective probability rate R^{eff} (s^{-1}) for molecular wires consisting of $N = 2$ (a) and $N = 10$ (b) molecules. The rate is plotted as a function of the energy difference ΔE between singlet and triplet states, and the ratio of intersystem crossing to singlet-to-singlet transfer rates, $K_{S_i,T_i}/K_{S_i,S_{i\pm1}}$. White dashed lines indicate fixed values of the reverse intersystem crossing (ISC) rate K_{T_i,S_i}, shown relative to the singlet-to-singlet transition rate $K_{S_i,S_{i\pm1}}$, to illustrate how changes in ΔE affect the effective transport. The singlet-to-singlet transition rate is $K_{S_i,S_{i\pm1}} = 0.1\ \text{ps}^{-1}$.

attention only to the larger system ($N = 10$) to examine how the maximum transition probability and the transition time are influenced by the singlet-to-singlet transition rate and the intersystem crossing (ISC) rate. For this analysis, we consider a reasonable energy gap of $\Delta E = 0.025\,\text{eV}$ between the excited singlet and triplet states. Table 3.1 shows the results for $P_N^{\max}$ and $\tau_{T_1 \to T_N}$ for four different cases. We consider both slow and fast singlet-to-singlet transition rates, with $K_{S_i,S_{i\pm1}} = 0.01\,\text{ps}^{-1}$ and $K_{S_i,S_{i\pm1}} = 0.1\,\text{ps}^{-1}$, respectively. Similarly, two intersystem crossing (ISC) rates are examined: a slow rate of $K_{S_i,T_i} = 0.1\,\text{ps}^{-1}$ and a fast rate of $K_{S_i,T_i} = 1.0\,\text{ps}^{-1}$. These rate values were chosen to illustrate how the transition probability and time change when one of the corresponding rates is varied by a factor of 10.

For the slower singlet-to-singlet transition rate of $K_{S_i,S_{i\pm1}} = 0.01\,\text{ps}^{-1}$, approximately 10% of the exciton population reaches T_N within 13.3 ns. However, when the singlet-to-singlet rate is increased by a factor of 10 to $K_{S_i,S_{i\pm1}} = 0.1\,\text{ps}^{-1}$, approximately 60–65% of the population reaches the final triplet site within 4–5 ns, indicating significantly improved transport.

For both values of the singlet-to-singlet transition rate, increasing the ISC rate does not substantially reduce the transition time, nor does it consistently improve the population arrival at T_N. This suggests that the singlet-to-singlet rate is the primary factor governing exciton transport efficiency in the system under consideration. This independence or plateau in response to the ISC rate can also be observed in Figure 3.18b for the effective probability rate.

In summary, for a system consisting of $N = 10$ molecules, efficient exciton transport to T_N is achieved by minimizing the energy gap ΔE, which facilitates faster transitions from the triplet manifold to the singlet manifold. Additionally, a rapid singlet-to-singlet transition rate is essential to fully exploit the faster dynamics of the singlet manifold. Finally, the intersystem crossing (ISC) rate should be equal to or greater than the singlet-to-singlet rate to avoid becoming a limiting factor in the overall transport process. If these conditions are met, the system can achieve an effective exciton arrival rate of approximately $10^8\,\text{s}^{-1}$.

Larger molecular wires can be constructed, as previously shown for $N = 20$, but as N increases, the exciton

$K_{S_i,S_{i\pm1}}$ (ps^{-1})	K_{S_i,T_i} (ps^{-1})	$P_N^{\max}$	$\tau_{T_1\to T_N}$ (s)
0.01	0.1	0.09	1.33×10^{-8}
0.01	1.0	0.10	1.32×10^{-8}
0.1	0.1	0.61	4.93×10^{-9}
0.1	1.0	0.65	4.30×10^{-9}

Table 3.1: Summary of maximum transition probability $P_N^{\max}$ and transition time $\tau_{T_1\to T_N}$ for a molecular wire of $N = 10$ and $\Delta E = 0.025\,\mathrm{eV}$, across various singlet–singlet and intersystem transition rates.

must undergo more transitions to reach T_N, increasing the likelihood of decay to the ground singlet state S_0. Consequently, the transport efficiency exhibits a stronger dependence on N when loss mechanisms are included.

Chapter 4

Spin Orbit Coupling

4.1 Computational Methodology

We tried building different materials in an attempt to find the ones that support fast exciton transport in molecular wires. Materials with high SOC values and low energy gaps between excited states were targeted because they allow for fast and efficient intersystem crossing between singlet and triplet states. The spin-orbit coupling constant $\xi(r)$ increases substantially with the increase of the atomic number Z of the atom ($\xi \propto Z^4$). Therefore, it is expected that monomers that contain heavy atoms will exhibit strong spin-orbit coupling.

The computational study presented in this chapter was carried out in three main stages: the construction of molecular monomers, the optimization of their geometries, and the calculation of excitation energies along with spin–orbit coupling between singlet and triplet excited states. Molecular structures were first built using ADF's graphical user interface and the coordinates of the atoms were exported in .xyz format. These monomers were then optimized using DFT methods in ORCA and finally TDDFT calculations were performed to extract the excitation energies of the singlet and triplet states and to compute the SOC matrix elements. Each step of this process is detailed below.

Due to its user-friendly graphical interface, we used ADF to build the molecular structures. Although initial structures were based on known geometries from literature, the monomers were built manually and in several cases specific customizations such as changes to ligands and removal of atoms were made to experiment with new structures. No constraints were imposed on these structures and the coordinates were exported in .xyz files. Although ADF allows for geometry optimization and DFT/TDDFT calculations of the systems, ORCA was used due to its flexibility when it comes to choosing functionals and basis sets.

Geometry optimization was performed in ORCA for each monomer to find the lowest-energy three-dimensional structure, i.e., the equilibrium state. All future calculations required a good ground-state geometry. For the functional PBE0 was used which is a hybrid functional combining PBE exchange-correlation with 25% exact exchange. For the light atoms of the monomer the 6-31G* basis set was used. It is an efficient and reliable split-valence double-zeta polarized basis set that applies to atoms H through Kr. For heavy atoms the LANL2DZ basis set was used along with the Hay-Wadt effective core potential (ECP). To improve numerical precision the default SCF convergence was changed from NormalSCF to TightSCF to reduce noise in the gradients. For the optimization 16 CPU cores were used with 2500 MB of RAM allocated to each core and without imposing any symmetry restrictions.

Time-dependent density functional theory (TDDFT) was used to compute the excitation energies of singlet and triplet states, and spin-orbit coupling matrix elements. In total 10 singlet and 10 triplet excited states were computed and the Tamm–Dancoff Approximation (TDA) was used for numerical stability. Similar to the geometry optimization, a PBE0 functional was used. As for the basis sets, when metal complexes containing a heavy atom at the core were constructed, the SARC-ZORA-TZVP basis was used for the heavy

atom and for the remaining atoms the ZORA-def2-SVP basis set was utilized. In the absence of heavy atoms ZORA-def2-TZVP was used as the default basis set. The 0th regular approximation (ZORA) along with the one-center approximation for SOC integrals were used to cover relativistic effects. 16 CPU cores were utilized for parallel processing and 2500 MB RAM were allocated to each core. Furthermore, no symmetry constraints were imposed on the monomers and all electrons were treated explicitly by not employing frozen cores.

4.2 Results

4.2.1 Zn-1 Inspired Complex

The design of this structure was motivated by the Zn-1 metal complex that was originally studied by Sakai et al. [4]. It was later reviewed by Li et al. as a representative metal complex exhibiting TADF with both fluorescence and delayed fluorescence (DF). Using TD-DFT, the energy gap between the first excited singlet state S_1 and the first excited triplet state T_1 was found to be approximately 0.025 eV. Additionally, the spin-orbit coupling matrix elements $V^{\mathrm{SOC}}_{S_1,T_1}$ and $V^{\mathrm{SOC}}_{S_1,T_2}$ were found to be relatively low due to the absence of a heavy atom at the core, which results in a weak SOC. Zinc belongs to Group 12 of the periodic table and as such shares similar characteristics with the other elements of the group. Because of this, we investigated the Zn-1 structure with different metals at the core. Cadmium (Cd), which is approximately 1.7 times heavier than zinc, was chosen as the central atom in the Zn-1 metal complex. Finally, two ligands were removed from the original structure in an attempt to make the monomer flatter. This monomer, denoted by Zn-1*, would allow for the creation of dimers or trimers, ultimately enabling efficient exciton transport. The results for the energy gap and the spin-orbit coupling matrix element between the excited singlet state S_1 and the excited triplet states T_1, T_2 are shown in Table 4.1. For the complete metal complex with zinc and cadmium, the energy gaps are in the range $0.019 - 0.050$ eV. However, both metals do not exhibit strong enough spin-orbit coupling resulting in small SOC-to-gap $V^{\mathrm{SOC}}_{S,T}/\Delta E_{S,T}$ ratios. Moreover, when two ligands were removed from the complex the the excited states are delocalized from each other which results in very large energy gaps. Summarizing the weak spin-orbit coupling that this complex exhibits limits its ISC and TADF potential.

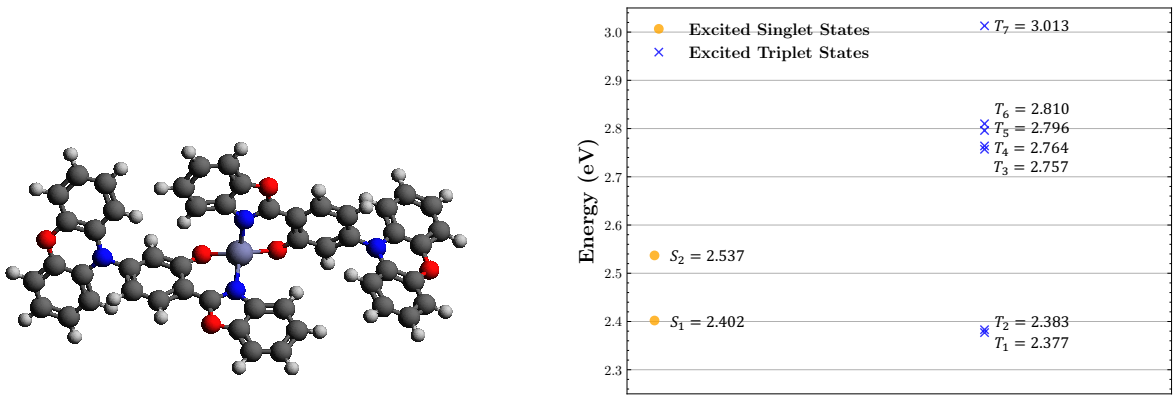

(a) Molecular structure of **Zn-1** monomer.

(b) Excitation energies of the **Zn-1** monomer.

Figure 4.1: Molecular structure (left) and TD-DFT-calculated excitation energies (right) of the **Zn-1** monomer. Orange and blue markers correspond to singlet and triplet excited states, respectively.

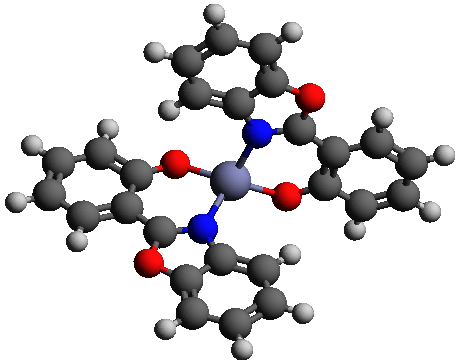

(a) Molecular structure of **Zn-1** monomer.

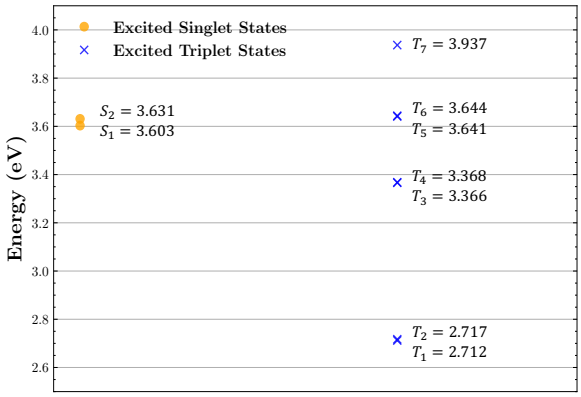

(b) Excitation energies of the **Zn-1** monomer.

Figure 4.2: Molecular structure (left) and TD-DFT-calculated excitation energies (right) of the **Zn-1*** monomer. Orange and blue markers correspond to singlet and triplet excited states, respectively.

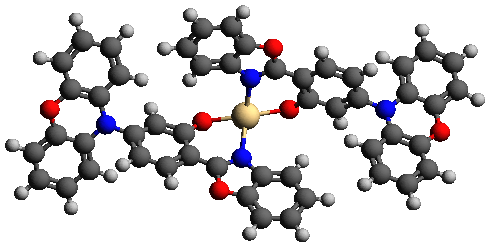

(a) Molecular structure of **Cd** monomer.

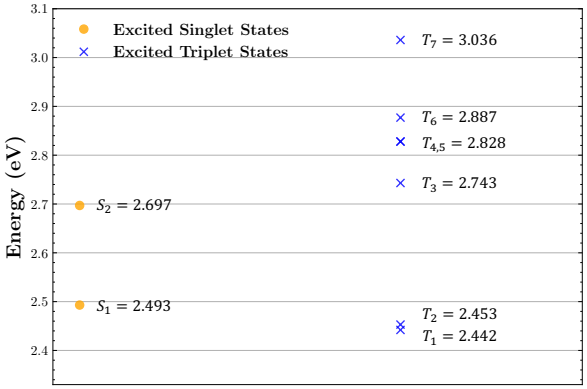

(b) Excitation energies of the **Cd** monomer.

Figure 4.3: Molecular structure (left) and TD-DFT-calculated excitation energies (right) of the **Cd** monomer. Orange and blue markers correspond to singlet and triplet excited states, respectively.

Structure	$\Delta E_{S_1,T_1}$ (eV)	$\Delta E_{S_1,T_2}$ (eV)	$V^{\mathrm{SOC}}_{S_1,T_1}$ (eV)	$V^{\mathrm{SOC}}_{S_1,T_2}$ (eV)	$V^{\mathrm{SOC}}_{S_1,T_1}/\Delta E_{S_1,T_1}$	$V^{\mathrm{SOC}}_{S_1,T_2}/\Delta E_{S_1,T_2}$
Zn-1	0.025	0.019	1.26×10^{-5}	7.38×10^{-6}	4.78×10^{-5}	3.88×10^{-5}
Cd	0.050	0.040	2.31×10^{-5}	6.90×10^{-5}	4.53×10^{-4}	1.72×10^{-4}
Zn-1 *	0.891	0.886	6.65×10^{-5}	6.42×10^{-5}	7.47×10^{-5}	7.25×10^{-5}

Table 4.1: Spin-orbit coupling values and corresponding singlet–triplet energy gaps for the **Zn-1** monomers and the **Cd** monomer inspired from the **Zn-1** metal complex.

4.2.2 Au(III) Acetylide Metal Complex

This structure consists of an Au(III) acetylide metal complex with a para-diphenylamino substituent designed by Zhou et al.[8] to have donor-acceptor frameworks that promote TADF. The gold atom at the center of the metal complex has an oxidation state of +3 relative to its neutral atomic state. The electron rich donor (diphenylamino) along with the electron deficient metal center create a strong intramolecular charge transfer (ICT) axis that promotes a lower energy gap between excited singlet and triplet states. Furthermore, the

use of Au(III), which is a heavy atom, enhances intersystem crossing (ISC) because of the strong intrinsic spin–orbit coupling due to relativistic effects of gold. The results for the energy gaps $\Delta E_{S,T}$ between the excited singlet state S_1 and the excited triplet states T_1 and T_2 along with the corresponding spin-orbit coupling matrix elements $V_{S,T}^{\mathrm{SOC}}$ are illustrated in Table 4.2. While the energy gap between S_1 and T_1 is smaller than that between S_1 and T_2, the SOC is significantly stronger in the latter case. The SOC-to-gap ratio for transitions through T_2 is an order of magnitude higher than that for T_1 indicating that intersystem crossing and TADF are likely to proceed mainly through the T_2 pathway.

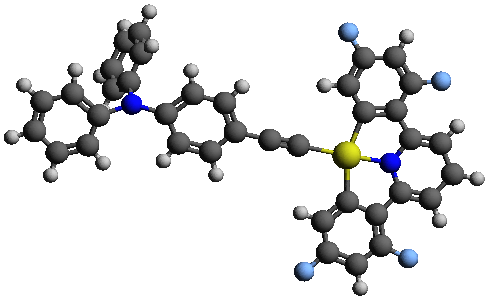

(a) Molecular structure of **Au** monomer.

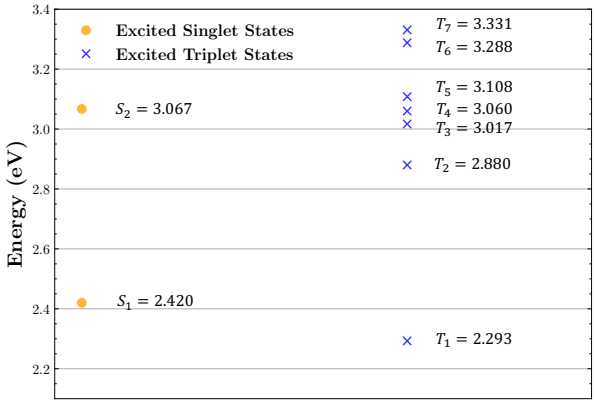

(b) Excitation energies of the **Au** monomer.

Figure 4.4: Molecular structure (left) and TDDFT-calculated excitation energies (right) of the **Au** monomer. Orange and blue markers correspond to singlet and triplet excited states, respectively.

$\Delta E_{S_1,T_1}$ (eV)	$\Delta E_{S_1,T_2}$ (eV)	$V_{S_1,T_1}^{\mathrm{SOC}}$ (eV)	$V_{S_1,T_2}^{\mathrm{SOC}}$ (eV)	$V_{S_1,T_1}^{\mathrm{SOC}}/\Delta E_{S_1,T_1}$	$V_{S_1,T_2}^{\mathrm{SOC}}/\Delta E_{S_1,T_2}$
0.127	0.460	2.47×10^{-4}	5.95×10^{-3}	1.94×10^{-3}	0.0124

Table 4.2: Spin-orbit coupling values and corresponding singlet–triplet energy gaps for the **Au** monomer.

4.2.3 Two-Coordinate Gold Complexes

After observing the results for the Au(III) metal complex in the previous section we decided to further explore metal complexes containing gold at the center. For this, we explored two structures initially synthesized by Schaab et al.[3]. Both structures consist of a linear gold(I) carbene–amide complex featuring a Au(I) at the center which has an N-heterocyclic carbene (NHC) as ligand 1 and amide-based aryl as ligand 2. Furthermore, both structures have a cyano group (CN) attached to aryl amide ligand that enhances ICT, stabilizes the excited states and reduces the singlet-triplet energy gap $\Delta E_{S,T}$. The difference between the two structures, is that one uses a methyl (Me) as the substituent on the N-heterocyclic carbene ligand, positioned adjacent to the carbonyl group on the carbene ring while the other uses a phenyl (Ph) and is denoted by Ph-Au$^{\mathrm{CN}}$. The first structure will be denoted by Me-Au$^{\mathrm{CN}}$ while the second by Ph-Au$^{\mathrm{CN}}$. The results for the excitation energies and the SOC matrix elements between the first excited singlet state S_1 and the excited triplet states T_1 and T_2 are shown in Table 4.3. Both Me-Au$^{\mathrm{CN}}$ and Ph-Au$^{\mathrm{CN}}$ exhibit strong spin-orbit coupling and high SOC-to-gap ratios, indicating efficient ISC and promising TADF behavior. Ph-Au$^{\mathrm{CN}}$ exhibits a significantly smaller $\Delta E_{S_1,T_1}$ and since $V_{S_1,T_1}^{\mathrm{SOC}}$ is approximately the same for both materials, the SOC-to-gap ratio for $S_1 \leftrightarrow T_1$ transitions for Ph-Au$^{\mathrm{CN}}$ is considerably higher. On the other hand, for transitions between $S_1 \leftrightarrow T_2$ the spin-orbit coupling is stronger and the energy gap is smaller for the Me-Au$^{\mathrm{CN}}$ structure resulting in a higher SOC-to-gap ratio. This suggests that Ph-Au$^{\mathrm{CN}}$ may favor ISC via T_1, but Me-Au$^{\mathrm{CN}}$ provides an efficient pathway through T_2 .

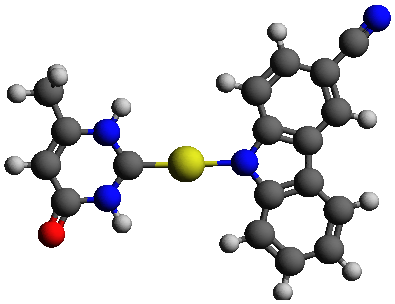

(a) Molecular structure of **MeAu^{CN}** monomer.

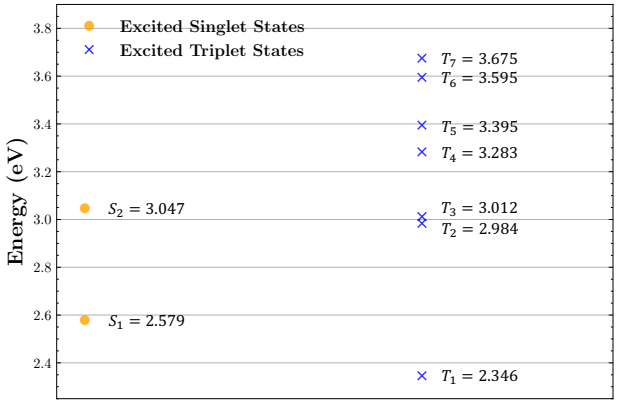

(b) Excitation energies of the **MeAu^{CN}** monomer.

Figure 4.5: Molecular structure (left) and TDDFT-calculated excitation energies (right) of the **MeAu^{CN}** monomer. Orange and blue markers correspond to singlet and triplet excited states, respectively.

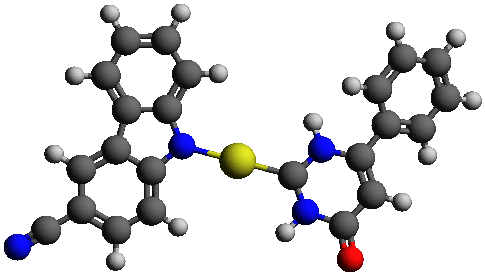

(a) Molecular structure of **PhAu^{CN}** monomer.

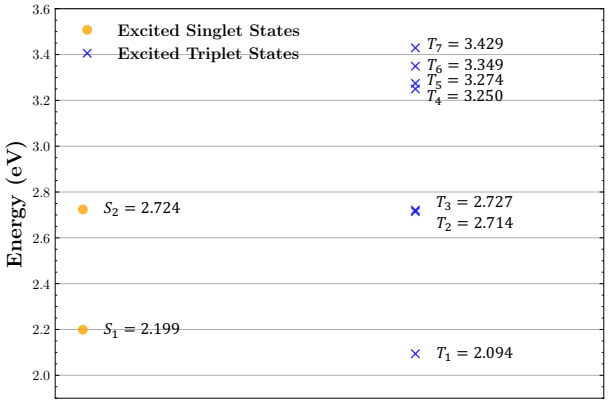

(b) Excitation energies of the **PhAu^{CN}** monomer.

Figure 4.6: Molecular structure (left) and TDDFT-calculated excitation energies (right) of the **PhAu^{CN}** monomer. Orange and blue markers correspond to singlet and triplet excited states, respectively.

Structure	$\Delta E_{S_1,T_1}$ (eV)	$\Delta E_{S_1,T_2}$ (eV)	$V^{SOC}_{S_1,T_1}$ (eV)	$V^{SOC}_{S_1,T_2}$ (eV)	$V^{SOC}_{S_1,T_1}/\Delta E_{S_1,T_1}$	$V^{SOC}_{S_1,T_2}/\Delta E_{S_1,T_2}$
Me-Au^{CN}	0.233	0.405	3.43×10^{-4}	2.35×10^{-3}	1.47×10^{-3}	5.79×10^{-3}
Ph-Au^{CN}	0.105	0.515	3.34×10^{-4}	8.48×10^{-4}	3.18×10^{-3}	1.65×10^{-3}

Table 4.3: Spin-orbit coupling values and corresponding singlet–triplet energy gaps for the **Ph-Au^{CN}** and **Me-Au^{CN}** metal complexes.

4.3 Summary of Spin–Orbit Coupling Performance

From the four different materials tested, the Zn-1 based monomer was found to be the least favorable candidate due to its low SOC-to-gap ratio compared to the gold-containing metal complexes. Moreover, the Au(III) acetylide metal complex exhibited the highest SOC-to-gap ratio of when the T_2 pathway is utilized, with a value of 1.24×10^{-2}. The results for the two-coordinate Au(I) carbene-amide structures were also promising. The Me-Au^{CN} complex had a SOC-to-gap ratio of 5.79×10^{-3} for $S_1 \leftrightarrow T_2$ transitions and for

the Ph-Au^{CN} complex, the SOC-to-gap ratio was found to be 3.18×10^{-3} along the T_1 channel. Since the SOC-to-gap ratios for all the gold-containing metal complexes were in the range 10^{-2} to 10^{-3}, these materials are regarded as promising materials for exhibiting efficient ISC and TADF behavior.

Chapter 5

Conclusion

This thesis examined exciton transport dynamics in excited singlet and triplet manifolds, both with and without ground-state loss mechanisms, and analyzes real molecular TADF systems by calculating their excited-state energy gaps and spin–orbit coupling matrix elements. We first examined the effectiveness of intersystem crossing from triplet to singlet states to determine whether the faster singlet manifold can accelerate exciton transport from T_1 to T_N. For a ten-site molecular wire, we observed that the transition time $\tau_{T_1 \to T_N}$ decreased by a factor of approximately 560. Increasing the singlet-to-singlet transition rate and decreasing the singlet-triplet energy gap both enhance exciton transport from T_1 to T_N.

When decay rates were included, transitions between adjacent triplet states were forbidden and the exciton could only reach the final triplet state via ISC to the singlet manifold. Including loss rates resulted in a stronger $N-$dependence because longer wires increase the probability of an exciton decaying to the singlet ground state. Furthermore, we found that the effective probability rate R^{eff} was the most reliable metric for quantifying transport efficiency. Finally, in the open-system model, we introduced a trap at T_N to enhance exciton capture there and prevent any back-transfer via ISC.

Using the ADF molecular builder, we constructed several metal complexes and computed their excited-state energies and singlet–triplet spin–orbit couplings to test whether real TADF structures exhibit the parameters that enable rapid exciton transport via the singlet manifold. The highest SOC-to-gap ratio (1.94×10^{-3}) between T_1 and S_1 was found in the Au(III) acetylide metal complex. To further enhance exciton transport, we aim to identify materials with smaller singlet-triplet energy gap $\Delta E_{S_1,T_1}$ and a larger spin-orbit coupling $V^{\text{SOC}}_{S_1,T_1}$, targeting an SOC-to-gap ratio of at least 0.1.

Appendix A: Exciton Transport Scripts

```python
def calculate_backward_rates(energies, forward_rates, T):
    '''
    Given a transition rate, it computes the reverse (backwards) rate through detailed
    balance.
    '''
    N = energies.shape[0]   # Total number of singlet/triplet states
    backward_rates = np.zeros(N)
    kbT300 = 0.025                              # Thermal energy at 300K in eV
    kbT = kbT300*(T/300)                        # Thermal energy for temperature T
    for i in range(1,N):
        dE = energies[i-1]-energies[i]
        backward_rates[i] = forward_rates[i-1]*np.exp(-(dE)/kbT)
    return backward_rates
```

Listing 1: Function that computes the reverse singlet-to-singlet or triplet-to-triplet rates with detailed balance.

```python
def calculate_reverse_intersystem_rates(energies_singlet, energies_triplet,
    forward_singlet_triplet_rate, kbT, N):
    '''
    Given an ISC rate, the reverse ISC rate is computed using detailed balance.
    '''
    backward_singlet_triplet_rate = np.zeros(N)
    for i in range(N):
        dE = energies_singlet[i] - energies_triplet[i] # Energy difference between singlet(
    higher energy state) and triplet(lower energy state) state.
        backward_singlet_triplet_rate[i] = forward_singlet_triplet_rate[i]*np.exp(-dE/kbT)
    return backward_singlet_triplet_rate
```

Listing 2: Function that computes the reverse intersystem crossing rates with detailed balance.

```python
def get_eval_evec(K):
    '''
    Function that computes the eigenvalues of a square matrix
    along with the right and left eigen vectors.
    '''
    eval, vl, vr = scipy.linalg.eig(K, left=True, right=True)
    left_evec = [vl[:,i] for i in range(len(vl))]
    # The left and right eigenvectors are computed by taking each column from the result of
    # scipy.linalg.eig i.e vl[:,i]
    right_evec = [vr[:,i] for i in range(len(vr))]
    return eval, np.array(left_evec), np.array(right_evec)
```

Listing 3: Function that computes the eigen values along with the left and right eigenvectors of the square transition rate matrix using scipy.linalg.eig from the SciPy library.

```python
def construct_rate_matrix_without_isc(backward_triplet_rates, forward_triplet_rates, N):
    K = np.zeros((N, N))
    for i in range(N):
```

```
        K[i, i] = -(forward_triplet_rates[i] + backward_triplet_rates[i])
        for j in range(N):
            if j == i+1:
                K[i, j] = backward_triplet_rates[j]
            elif j == i-1:
                K[i, j] = forward_triplet_rates[j]
    return K
```

Listing 4: Function that constructs the transition rate matrix K

```
def construct_rate_matrix(backward_singlet_rates, backward_triplet_rates,
    forward_singlet_rates, forward_triplet_rates, singlet_triplet_backward_rates,
    singlet_triplet_forward_rates, singlet_loss_rate, triplet_loss_rate):
    '''
    Construct the 2Nx2N transition-rate matrix K for an N-site singlet-triplet system.
    '''
    N = backward_singlet_rates.shape[0]
    K = np.zeros((2*N, 2*N))
    for i in range(2*N):
        # Singlet manifold: indices 0, ..., N-1
        if i < N:
            # Main diagonal elements for the singlet states.
            K[i,i] = -(forward_singlet_rates[i] + backward_singlet_rates[i] +
    singlet_triplet_forward_rates[i]) - singlet_loss_rate[i]
            # Off diagonal elements for the singlet states.
            for j in range(N):
                if j == i+1:
                    K[i, j] = backward_singlet_rates[j]
                elif j == i-1:
                    K[i, j] = forward_singlet_rates[j]
            K[i, i+N] = singlet_triplet_backward_rates[i]
        # Triplet manifold: indices N, ..., 2N-1
        if i >= N:
            # Main diagonal elements for the triplet states.
            K[i,i] = -(forward_triplet_rates[i-N] + backward_triplet_rates[i-N] +
    singlet_triplet_backward_rates[i-N]) - triplet_loss_rate[i-N]
            # Off diagonal elements for the triplet states.
            for j in range(N, 2*N):
                if j == i+1:
                    K[i, j] = backward_triplet_rates[j-N]
                elif j == i-1:
                    K[i, j] = forward_triplet_rates[j-N]
            K[i,i-N] = singlet_triplet_forward_rates[i-N]
    return K
```

Listing 5: Function that constructs the transition rate matrix K

```
def check_eval_evec(eigenvalues, left_evec, right_evec, K):
    '''
    Checks if each eigen vector (left or right) corresponds to the correct eigen value
    '''
    for i in range(K.shape[0]):
        if not(np.allclose(K.dot(right_evec[i]),eigenvalues[i]*right_evec[i])):
            print(f"Right eigenvector {i+1} does not correspond to eigenvalue {i+1}")
            print(K.dot(right_evec[i]))
            print(eigenvalues[i]*right_evec[i])

        if not(np.allclose(left_evec[i].dot(K),eigenvalues[i]*left_evec[i])):
            print(f"Left eigenvector {i+1} does not correspond to eigenvalue {i+1}")
            print(left_evec[i].dot(K))
            print(eigenvalues[i]*left_evec[i])
```

Listing 6: Function that prints error statements if the eigenvectors do not correspond to the respective eigenvalues of the rate matrix.

```
def get_initial_probabilities(N, s_or_t):
    '''
```

```
    Function that asks the user if the system is initially in a triplet or singlet state, and then
    calculates the initial probabilities vector. Indices from 0-(N-1) correspond to singlet states. While indices from (N-(2N-1) correspond to triplet states.
    '''
    initial_probabilities = np.zeros(2*N)
    while s_or_t != "triplet" and s_or_t != "singlet":
        print("Wrong input!")
        s_or_t = input("Type Triplet or Singlet: ").lower()
    initial_state = int(input("In which state is the system at t = 0: "))   # Initial state should be from 0-(N-1)
    if s_or_t == "triplet":
        initial_probabilities[initial_state + N] = 1
    elif s_or_t == "singlet":
        initial_probabilities[initial_state] = 1
    return initial_probabilities
```

Listing 7: Function that constructs the probability vector for t

```
def get_steady_state(left_eigenvectors, right_eigenvectors, eigen_values, initial_probabilities, tolerance=1e-10):
    '''
    Computes the steady-state probabilities using the left and right eigenvectors that correspond to the zero eigenvalue of the transition rate matrix K.
    '''
    # Finds the index for which the eigen value is close to zero
    zero_eigenvalue_index = np.where(np.abs(eigen_values) < tolerance)[0][0]
    # Computing the steady state probabilities
    ss = right_eigenvectors[zero_eigenvalue_index]*(np.dot(left_eigenvectors[zero_eigenvalue_index],initial_probabilities))
    # Normalization factor for the left and right eigenvector.
    norm = np.dot(left_eigenvectors[zero_eigenvalue_index],right_eigenvectors[zero_eigenvalue_index])
    ss = ss/norm
    return ss
```

Listing 8: Function that computes the steady-state probability distribution using the left and right eigenvectors corresponding to the zero eigenvalue.

```
def get_probabilities(left_eigenvector, right_eigenvector, eigen_values, time, initial_probabilities):
    '''
    Computes the probabilities for all the energy states for a given time array using the eigenvalues and the left and right eigen vectors of the
    transition rate matrix K.
    '''
    probability_list = []
    for t in time:
        probabilities = 0
        for i in range(len(left_eigenvector)):
            norm = np.dot(left_eigenvector[i], right_eigenvector[i])
            probabilities += np.exp(eigen_values[i]*t)*right_eigenvector[i]*(np.dot(left_eigenvector[i],initial_probabilities))/norm
        probability_list.append(np.real(probabilities))
    probability_list = np.array(probability_list)
    # Each row contains every probability for a given time t, in order to get P1(t) we have to slice through the first column [:,0]
    return probability_list
```

Listing 9: Function that computes the probability vector for a given time period using the left and right eigenvectors

```
def get_probabilities_convergence_without_loss(left_eigenvector, right_eigenvector, eigen_values, time_step, initial_probabilities, steady_state_probabilities, threshold):
    # Initialize the probability list, which will contain the probabilities for various # values of time t.
    probability_list = []
```

```
    t = 0   # Initial time.
    time = []
    while True:
        probabilities = np.zeros(left_eigenvector.shape[0], dtype=complex) # Initialize all
    probabilities as zero, to compute the sum.
        for i in range(left_eigenvector.shape[0]):
            norm = np.dot(left_eigenvector[i], right_eigenvector[i])
            probabilities += np.exp(eigen_values[i]*t)*right_eigenvector[i]*(np.dot(
    left_eigenvector[i],initial_probabilities))/norm
        probability_list.append(np.real(probabilities))
        time.append(t)
        if probabilities[-1] >= threshold*steady_state_probabilities[-1]:
            probability_list = np.array(probability_list)
            return probability_list, np.array(time)
        t += time_step
```

Listing 10: Function that computes and returns the probability vector along with the time required for the probability of the last triplet state P_N to exceeds the threshold value of the steady-state probability ϵP_N^{ss} of the final triplet state.

Appendix B: Calculation Input Files

B.1 Geometry Optimization Script

```
! PBE0 D3BJ 6-31G* HayWadt TightSCF Opt
! NoUseSym
! PAL16

%MaxCore 4000
%basis
  newgto heavy_atom_used "LANL2DZ"
end
%scf
  ConvForced 1
end

* xyzfile 0 1 Coordinates_to_be_optimized.xyz
```

Listing 11: ORCA input script for geometry optimization of monomers containing a heavy atom is used at the core.

```
!PBE0 ZORA ZORA-def2-SVP SARC/J TightSCF SlowConv
!PAL16
!NoFrozenCore
!NoUseSym

%maxcore 2500

%basis
  NewGTO heavy_atom_used "SARC-ZORA-TZVP" end
  end

%rel
   method ZORA
   OneCenter true
   picturechange true
   end

%scf
   ConvForced 1
   Convergence Loose
   MaxIter 200
   end

%output Print[P_Basis]2
        Print[P_MOs]1
        end

%tddft NRoots 10
       TDA true
       triplets true
       dosoc true
       printlevel 4
       end

```

```
* xyzfile 0 1 Optimized_coordinates.xyz
```

Listing 12: ORCA input file for the TDDFT calculation of excitation energies and spin–orbit coupling between excited singlet and triplet states of the monomers containing a heavy atom at the core.

```
!PBE0 ZORA ZORA-def2-TZVP TightSCF SlowConv
!PAL16
!NoFrozenCore
!NoUseSym

%maxcore 2500

%rel
   method ZORA
   OneCenter true
   picturechange true
   end

%scf
   ConvForced 1
   Convergence Loose
   MaxIter 200
   end

%output Print[P_Basis]2
        Print[P_MOs]1
        end

%tddft NRoots 10
       TDA true
       triplets true
       dosoc true
       printlevel 4
       end
* xyzfile 0 1 Optimized_coordinates.xyz
```

Listing 13: ORCA input file for the TDDFT calculation of excitation energies and spin–orbit coupling between excited singlet and triplet states of the monomers that do not contain a heavy atom at the core.

Bibliography

[1] Stephen R. Addison. *The Canonical Ensemble*. Retrieved from Academia.edu. 2003.

[2] SciPy Developers. *scipy.linalg.eig*. 2025. URL: https://docs.scipy.org/doc/scipy/reference/generated/scipy.linalg.eig.html.

[3] Tian-yi Li et al. "Toward rational design of TADF two-coordinate coinage metal complexes: understanding the relationship between natural transition orbital overlap and photophysical properties". In: *Journal of Materials Chemistry C* 10 (2022), pp. 4674–4683. DOI: 10.1039/d2c00163b.

[4] Yumi Sakai et al. "Zinc complexes exhibiting highly efficient thermally activated delayed fluorescence and their application to organic light-emitting diodes". In: *Chemical Communications* 51.16 (2015), pp. 3181–3184. DOI: 10.1039/c4cc09403d.

[5] Daniel V. Schroeder. *An Introduction to Thermal Physics*. San Francisco, CA: Addison Wesley, 2000. ISBN: 978-0201380279.

[6] Murray R. Spiegel. *Applied Differential Equations*. 3rd. Prentice Hall, 1980. Chap. 11, Part II.

[7] William J. Stewart. *Introduction to the Numerical Solution of Markov Chains*. Princeton, NJ: Princeton University Press, 1994. ISBN: 978-0691036991.

[8] Dongling Zhou et al. "Thermally stable donor–acceptor type (alkynyl)gold(III) TADF emitters achieved EQEs and luminance of up to 23.4% and 70 300 cd/m^2 in vacuum-deposited OLEDs". In: *Advanced Science* 6.9 (2019), p. 1802257. DOI: 10.1002/advs.201802297.